

DOCTORAL THESIS

CONVERSION FROM IMPERFECTION-SENSITIVE
INTO IMPERFECTION-INSENSITIVE
ELASTIC STRUCTURES

DISSERTATION

UMWANDLUNG VON IMPERFEKTIONSSENSITIVEN
IN IMPERFEKTIONSINSENSITIVE
ELASTISCHE STRUKTUREN

ausgeführt zum Zwecke der Erlangung des akademischen
Grades eines Doktors der technischen Wissenschaften

eingereicht an der Technischen Universität Wien
Fakultät für Bauingenieurwesen

von

Dipl.-Ing. Christian Schranz, M.Sc.

Matrikelnummer: 93 26 027

Dempschergasse 9, 1180 Wien, Österreich

Referent: O. Univ.-Prof. Dipl.-Ing. Dr. techn. Dr. h.c. mult. Herbert Mang, Ph.D.
Institut für Mechanik der Werkstoffe und Strukturen,
Technische Universität Wien,
Karlsplatz 13/202, 1040 Wien, Österreich

Koreferent: O. Univ.-Prof. Dipl.-Ing. Dr. techn. Dr. h.c. Hans Troger
Institut für Mechanik und Mechatronik,
Technische Universität Wien,
Wiedner Hauptstr. 8/325, 1040 Wien, Österreich

Wien, im Februar 2005

Christian Schranz

Diese Dissertation haben begutachtet:

Herbert Mang

H. Troger

Danksagung

Um ein Leben nach eigenen Vorstellungen zu gestalten, bedarf es der Unterstützung und Geduld anderer. Bei der Erstellung einer Dissertation verhält es sich genauso. Um der Gefahr zu entgehen, einen Dank zu wenig auszusprechen, möchte ich mich gleich zu Beginn bei all jenen bedanken, die wissen oder meinen, dass sie einen Beitrag bei der Erstellung dieser Arbeit geleistet haben.

An dieser Stelle möchte ich mich besonders bei Herrn o.Univ.-Prof. Dipl.-Ing. Dr.techn. Dr.h.c.mult. Herbert Mang, Ph.D., für seinen außerordentlichen Einsatz bei der Betreuung dieser Arbeit bedanken. Er fand selbst in Zeiten, da seine Aufgabe als (zuerst) Generalsekretär und (dann) Präsident der Österreichischen Akademie der Wissenschaften weit überdurchschnittliche Leistungen von ihm verlangte, noch die Zeit und Energie sich wissenschaftlichen Diskussionen zu widmen.

Herrn o.Univ.-Prof. Dipl.-Ing. Dr.techn. Dr.h.c. Hans Troger danke ich recht herzlich für die Übernahme des Koreferats der Dissertation sowie seinem Entgegenkommen und Einsatz angesichts der knappen Termine bei der Fertigstellung dieser Arbeit.

Speziell danken möchte ich auch Herrn o.Univ.-Prof. Dipl.-Ing. Dr.techn. Josef Eberhardsteiner, der mir in seiner Funktion als "Fund raiser" und Berater erst die Möglichkeit für die Absolvierung dieser Arbeit gab.

Dank gebührt auch den Herren Prof. Dipl.-Ing. Dr.techn. Peter Mackenzie-Helnwein und Dipl.-Ing. Burkhard Krenn für die Vielzahl an wissenschaftlichen Diskussionen sowie die Unterstützung bei dieser Arbeit.

Den Herren Dipl.-Ing. Paul Torzicky und Dipl.-Ing. Dr.techn. Thomas Huemer danke ich für die Geduld bei der Beantwortung vieler Fragen betreffend der Administration der Computer am Institut für Mechanik der Werkstoffe und Strukturen. Ohne ihre Unterstützung wäre die Zusatzaufgabe der Systemadministration nicht machbar gewesen.

Meinen Kollegen und Freunden Dipl.-Ing. Christoph Kohlhauser und Dipl.-Ing. Dr.techn. Karin Hofstetter danke ich für die Unterstützung, die sie mir auch in Momenten der Frustration zukommen ließen. Weiters bedanke ich mich bei meinen Institutskolleginnen und -kollegen, im Speziellen bei Dipl.-Ing. Dr.techn. Bernhard Pichler, Dipl.-Ing. Martin Fleischmann, Dipl.-Ing. Christian Pichler, Dipl.-Ing. Andreas Jäger, für das stets gute und freundschaftliche Klima am Institut. Bei Frau Martina Pöll, der Seele des Instituts, bedanke ich mich für ihre ausgezeichnete Unterstützung in allen administrativen Angelegenheiten.

Ein ganz besonderer Dank gilt meiner Mutter Erika sowie ihrem Lebensgefährten Karl für ihre selbstlose Unterstützung während der Erstellung dieser Arbeit.

Kurzfassung

Die vorliegende Dissertation besteht aus einem zweiteiligen Aufsatz, der von der Fachzeitschrift *Computer Methods in Applied Mechanics and Engineering* zur Veröffentlichung angenommen wurde.

Bei Stabilitätsverlust in Form von symmetrischem Verzweigen lässt sich eine qualitative Verbesserung des Nachbeulverhaltens einer ursprünglich imperfektionssensitiven Struktur durch Umwandlung in eine imperfektionsinsensitive Struktur durch Modifikation der ursprünglichen Struktur erzielen. Die Klassifikation einer Struktur als imperfektionssensitiv oder imperfektionsinsensitiv hängt vom initialen Nachbeulverhalten ab, das oftmals für das gesamte Nachbeulverhalten relevant ist. Die Erforschung von Versteifungsformen, welche die vorgenannte Umwandlung ermöglichen, ist sowohl von wissenschaftlichem als auch technischem Interesse.

Koitors initiale Nachbeulanalyse wird im Rahmen der Finiten Element Methode (FEM) zur Herleitung mathematischer Beziehungen benutzt, die eine Differenzierung zwischen verschiedenen Formen der Umwandlung von Imperfektionssensitivität in Imperfektionsinsensitivität gestatten. Diese Analyse dient zur Herleitung theoretischer Resultate, welche die Verifikation spezieller numerischer Resultate erlauben. Der Großteil der in dieser Arbeit beschriebenen numerischen Berechnungen wurde mittels der FEM durchgeführt, ohne dabei jedoch auf Koitors initiale Nachbeulanalyse zurückzugreifen.

In der Arbeit werden neue mathematische Bedingungen für symmetrisches Verzweigen bei nichtlinearen Vorbeulpfaden präsentiert. Für den Spezialfall linearer Vorbeulpfade sind diese Bedingungen trivial erfüllt. Es wird gezeigt, dass die Menge jener Lösungen von Koitors initialer Nachbeulanalyse, die durch das Verschwinden eines speziellen Lastparameters gekennzeichnet ist, vollständig ist. Dieses Verschwinden stellt eine notwendige, nicht aber hinreichende Bedingung für den Übergang von Imperfektionssensitivität zu Imperfektionsinsensitivität dar. Versuche zur Realisierung dieses Überganges beinhalten die Vergrößerung der Dicke der Struktur, die Erhöhung der Steifigkeit einer geeignet angebrachten, ursprünglich nicht vorhandenen Feder und die Verminderung des Stiches der Struktur. Die Resultate dieser Untersuchung beziehen sich auf verschiedene Arten der Umwandlung von imperfektionssensitiven in imperfektionsinsensitive Strukturen sowie auch das Fehlschlagen des Versuches einer solchen Umwandlung.

Ein wichtiger Bestandteil der numerischen Untersuchung sind begleitende lineare Eigenwertanalysen. Sie beruhen auf dem sogenannten konsistent linearisierten Eigenwertproblem. Zumeist weisen die resultierenden Eigenwertkurven beim Übergang von Imperfektionssensitivität zu Imperfektionsinsensitivität besondere geometrische Eigenschaften (Sattelpunkte oder Flachpunkte) im Verzweigungspunkt auf.

Eine der Schlussfolgerungen besteht darin, dass eine gleichförmige Vergrößerung der Dicke der Struktur nicht geeignet ist, den Übergang von Imperfektionssensitivität zu Imperfektionsinsensitivität zu bewerkstelligen. Als weitere Schlussfolgerung ist anzuführen, dass eine Verminderung des ursprünglichen Stiches der imperfektionssensitiven Struktur zum Übergang von Verzweigungsbeulen zu einer Situation ohne Stabilitätsverlust führt. Diese Reduktion ist allerdings mit einer starken Abnahme der Stabilitätsgrenze verbunden. Hingegen führt eine Erhöhung der Steifigkeit einer an der Struktur geeignet angebrachten elastischen Feder in der Regel zur Umwandlung einer imperfektionssensitiven in eine imperfektionsinsensitive Struktur. Zusätzliche Stützen bei ursprünglich imperfektionssensitiven Strukturen scheinen daher geeignet zu sein, die gewünschte Umwandlung zu erzielen.

Abstract

This doctoral thesis consists of the two parts of a paper accepted for publication in the journal *Computer Methods in Applied Mechanics and Engineering*, denoted as (I) Theory and (II) Numerical Investigation.

In case of loss of stability by means of symmetric bifurcation, a qualitative improvement of the postbuckling behavior of originally imperfection-sensitive elastic structures is their conversion into imperfection-insensitive structures by means of modifications of the original design. Such a conversion is restricted to symmetric bifurcation. Designation of a structure as either imperfection sensitive or insensitive depends on the initial postbuckling behavior which often is relevant to the entire postbuckling response. The search for specific modes of stiffening that result in the aforementioned conversion is of fundamental as well as of practical importance.

Koiter's initial postbuckling analysis is applied in the framework of the Finite Element Method (FEM) to deduce mathematical relations associated with the transition from imperfection sensitivity to insensitivity. This mode of analysis primarily serves the purpose of deducing important theoretical results which facilitate the verification of specific numerical results. Most of the structural analyses reported in this work are performed by means of the FEM, but without regard for Koiter's initial postbuckling analysis.

New mathematical conditions for symmetric bifurcation from nonlinear prebuckling paths are presented. For the special case of linear prebuckling paths, these conditions are satisfied trivially. In the framework of sensitivity analyses also topics such as hilltop bifurcation and transition from bifurcation buckling to no loss of stability are addressed. The completeness of the set of solutions from Koiter's initial postbuckling analysis that involve the vanishing of a specific load parameter as a necessary (but not sufficient) condition for the transition from imperfection sensitivity to imperfection insensitivity is demonstrated.

Attempts to achieve the aforementioned conversion include the increase of the thickness of the structure and of the stiffness of a spring attached to the structure, respectively, and the reduction of the rise of the undeformed structure. The results of this investigation include different modes of conversion from imperfection-sensitive into imperfection-insensitive structures as well as failure to achieve such a conversion.

An important ingredient of the numerical investigation are accompanying linear eigenvalue analyses based on the so-called consistently linearized eigenproblem. At the transition from imperfection sensitivity to insensitivity, the resulting eigenvalue curve, in general, has specific geometric properties (saddle points or planar points) at the bifurcation point.

One of the conclusions is that increasing the stiffness of a structure by means of a uniform increase of its thickness does not result in the conversion from imperfection sensitivity into insensitivity. Another one is that reducing the initial rise of an imperfection-sensitive structure eventually results in the transition from bifurcation buckling to no loss of stability. Unfortunately, such a reduction is associated with a decrease of the stability limit. Increasing the stiffness of an elastic spring, suitably attached to the structure, however, usually enables its conversion from an imperfection-sensitive into an imperfection-insensitive structure. Hence, additional supports of a structure may be effective means to achieve the desired conversion.

Conversion from imperfection-sensitive into imperfection-insensitive elastic structures

Part I: Theory	1
1 Introduction	1
2 Koiter's initial postbuckling analysis in the context of the FEM	3
3 Symmetric bifurcation	7
4 Triples of values λ_4, a_1, a_1^* for $\lambda_2 = 0$	10
5 General case: nonlinear prebuckling paths	13
5.1 Sensitivity analysis	13
5.2 Discussion of Figs. 4(a)-4(h)	16
6 Special case: linear prebuckling paths	21
7 Completeness of solutions from Koiter's initial postbuckling analysis, containing $\lambda_2 = 0$	23
8 Conclusions	25
Appendices	
A Coefficient tensors for Koiter's postbuckling analysis in the context of the FEM	28
B Coefficient vectors of $\eta^1, \eta^2, \eta^3, \eta^4, \eta^5$, and η^6	31
C Coefficients $e_1^*, \hat{f}_1, \bar{e}_1$ and b_2, d_3, b_4	33
D Mathematical properties of the consistently linearized eigenproblem	34
Part II: Numerical Investigation	46
1 Introduction	46
2 Numerical investigation	48
2.1 Example 1: Pin-jointed bar with two degrees of freedom	48
2.2 Example 2: von Mises truss	52
2.3 Example 3: Shallow cylindrical shell	56
2.4 Example 4: Pin-jointed bar with linear prebuckling paths	63
3 Conclusions	68

Conversion from Imperfection-Sensitive into Imperfection-Insensitive Elastic Structures I: Theory ^{*}

Herbert A. Mang ^{a,*}, Christian Schranz ^a, Peter Mackenzie-Helnwein ^b

^a*Institute for Mechanics of Materials and Structures, Vienna University of Technology,
Karlsplatz 13, A-1040 Vienna, Austria*

^b*Dept. of Civil and Environmental Engineering, University of Washington, 12D More Hall,
Seattle, WA 98195-2700, USA*

Abstract

A qualitative improvement of the initial postbuckling behavior of imperfection-sensitive elastic structures is their conversion into imperfection-insensitive structures by means of modifications of the original design. Such a conversion is restricted to symmetric bifurcation. Koiter's initial postbuckling analysis is applied in the framework of the FEM to deduce mathematical relations for the transition from imperfection sensitivity to insensitivity, which may be achieved by additional supports of the structure. This conclusion as well as several other conclusions from the theoretical investigation reported in Part I of this paper are corroborated by the results from a comprehensive numerical investigation documented in Part II of this work.

Key words: symmetric bifurcation buckling, imperfection sensitivity, conversion into imperfection insensitivity, Koiter's initial postbuckling analysis, finite element method

1 Introduction

"This Euler column is imperfection insensitive" and "that cylindrical shell is imperfection sensitive" ... students of structural engineering all over the world have heard such statements in the classroom, and practicing structural engineers from all parts of the globe have read them in the technical literature. Some of them may have come to the conclusion that the unfavorable mechanical diagnosis of imperfection sensitivity must be accepted as it is.

* Dedicated to Prof. Thomas J.R. Hughes on the occasion of his 60th birthday

* Corresponding author.

Email addresses: Herbert.Mang@tuwien.ac.at (Herbert A. Mang),
Christian.Schranz@tuwien.ac.at (Christian Schranz), pmackenz@u.washington.edu (Peter Mackenzie-Helnwein).

In the opinion of the writers, however, the acceptance of such a diagnosis would ignore the existence of remedies. An obvious remedy is the conversion of imperfection-sensitive into imperfection-insensitive structures by means of modifications of the original design. It leads to a qualitative improvement of the initial postbuckling behavior of the structures, which often has a strong influence on the entire postbuckling structural response. The title of the present paper refers to such a conversion which is the objective of this work.

One of several topics treated in this paper is design sensitivity analysis of the initial postbuckling behavior of elastic structures. It plays a great role in the state-of-the-art. In a paper on design sensitivity analysis of “non-linear structures”, Mróz and Haftka [9] also discussed the postbuckling behavior. The first analytical work on design sensitivity analysis of the postbuckling behavior was presented by Godoy [4]. It is restricted to consideration of the first non-vanishing term in a series expansion for the load parameter. In an extension of [9], Mróz and Piekarski [10] included imperfection insensitivity as a constraint condition for optimization of the structural behavior. Bochenek and Kruzelecki [2] proposed an approach to optimize the postbuckling behavior, which is based on determination of the maximum buckling load under the constraint that the structure is just no longer imperfection sensitive. In a paper on structural optimization of the postbuckling behavior, Bochenek [1] mentioned the necessity to introduce constraints assuring symmetric bifurcation, which is obviously needed for the conversion of an imperfection-sensitive into an imperfection-insensitive structure.

The present paper consists of two parts: (I) Theory and (II) Numerical Investigation.

Section 2 of Part I deals with Koiter’s initial postbuckling analysis in the context of the Finite Element Method (FEM). It is emphasized that this mode of analysis primarily serves the purpose of deducing important theoretical results in Part I, which facilitate the verification of specific numerical results in Part II. Most of the structural analyses reported in Part II are performed by means of the FEM, but without regard for Koiter’s initial postbuckling analysis. Section 3 is devoted to symmetric bifurcation. In Section 4, new mathematical conditions for the transition from imperfection sensitivity to imperfection insensitivity are presented. Section 5 refers to the general case of nonlinear prebuckling paths. In the framework of sensitivity analyses also topics such as hilltop bifurcation and transition from bifurcation buckling to no loss of stability are addressed. Section 6 covers the special case of linear prebuckling paths. Section 7 deals with the completeness of solutions from Koiter’s initial postbuckling analysis, which are characterized by the vanishing of the first one of those terms in the aforementioned series expansion for the load parameter, that normally do not vanish for symmetric bifurcation. The Conclusions of Part I (Section 8) are followed by four Appendices. Appendix A is devoted to the computation of the coefficient tensors for Koiter’s initial postbuckling analysis in the context of the FEM. The Appendices B and C contain mathematical details related to Sections 2, and 3 and 7, respectively. Appendix D contains a description of mathematical properties of the so-called consistently linearized eigenvalue problem. The investigation of these properties is motivated by the need to ensure the completeness of those specific solutions for the initial postbuckling paths, which were mentioned in the context of the brief description of the contents of Section 7. Moreover, these properties permit verification of theoretical results for limiting cases “by inspection” of corresponding eigenvalue curves.

Part II of the paper consists of three Sections: 1 Introduction, 2 Numerical Investigation, and 3 Conclusions.

Among the topics that are not treated in this paper are (a) multiple bifurcation, (b) material nonlinearity, and (c) imperfections.

Re (a): The increase in mathematical complexity would outweigh the added value of information resulting from consideration of multiple bifurcation.

Re (b): The increase in programming work would outweigh the added value resulting from an extension of the present work to material nonlinearity, the more as such an extension would still not include plasticity.

Re (c): Consideration of imperfections must be preceded by comprehension of the perfect situation, which is the main goal of the present work.

This work is firmly embedded in the FEM. As mentioned previously, mathematical details that are related to the paper are given in Appendix A. Preliminary numerical studies on the influence of mesh refinement on the numerical results presented in Part II of this paper [12] were performed routinely. They are not documented in the paper.

2 Koiter's initial postbuckling analysis in the context of the FEM

The starting point of the theoretical investigation is Koiter's initial postbuckling analysis (Koiter [8]). Fig. 1 refers to such an analysis. Point C denotes the bifurcation point. Point D is located on the secondary path. This point is characterized by the load level $\lambda = \lambda_D$ and the corresponding displacement $\tilde{\mathbf{u}}(\lambda_D) + \mathbf{v}_D$. Primary and secondary paths

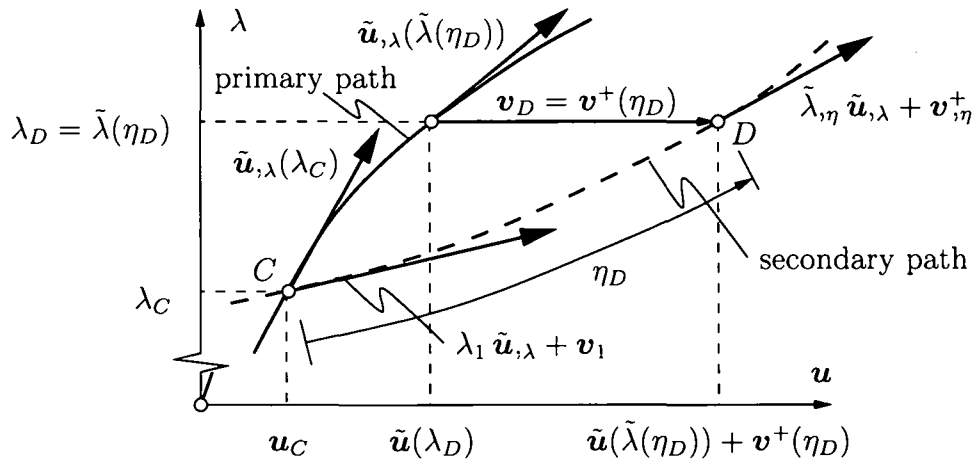


Fig. 1. Initial postbuckling analysis at the bifurcation point C

are represented by piecewise smooth curves $\mathbf{u} = \tilde{\mathbf{u}}(\lambda)$ and $\mathbf{u} = \mathbf{u}^+(\eta) = \tilde{\mathbf{u}}(\tilde{\lambda}(\eta)) + \mathbf{v}^+(\eta)$, respectively, where η is a path parameter. For static, proportional loading,

$$\mathbf{G}(\mathbf{u}, \lambda) := \mathbf{F}^I(\mathbf{u}) - \mathbf{P}(\lambda) = \mathbf{0} \quad (1)$$

is a necessary and sufficient condition for equilibrium of mechanical systems discretized by the FEM (Zienkiewicz and Taylor [14]). $\mathbf{F}^I(\mathbf{u})$ is the vector of the internal node forces whereas $\mathbf{P}(\lambda) = \mathbf{P}_0 + \lambda\bar{\mathbf{P}}$ is the vector of the external node forces. \mathbf{P}_0 and $\bar{\mathbf{P}}$ are given vectors of reference nodal loads.

One solution of (1) is the *primary path* $\mathbf{u} = \tilde{\mathbf{u}}(\lambda)$. Assuming that $\tilde{\mathbf{u}}(\lambda)$ is known, a (non-linear) coordinate transformation

$$(\mathbf{v}, \eta) \rightarrow (\mathbf{u}, \lambda) = (\tilde{\mathbf{u}}(\tilde{\lambda}(\eta)) + \mathbf{v}, \tilde{\lambda}(\eta)) \quad (2)$$

is performed such that $(\mathbf{v} = \mathbf{0}, \eta = 0) \mapsto (\mathbf{u}_C, \lambda_C)$. Substituting (2) into the expression for $\mathbf{G}(\mathbf{u}, \lambda)$ contained in (1), yields the definition of the out-of-balance force in terms of \mathbf{v} and η as

$$\mathbf{G}^+(\mathbf{v}, \eta) := \mathbf{G}(\tilde{\mathbf{u}}(\tilde{\lambda}(\eta)) + \mathbf{v}, \tilde{\lambda}(\eta)). \quad (3)$$

The *secondary path* represents a non-trivial solution $\mathbf{v} = \mathbf{v}^+(\eta)$ of $\mathbf{G}^+(\mathbf{v}, \eta) = \mathbf{0}$. Adopting Koiter's concept of an initial postbuckling analysis (Koiter [8]), $\mathbf{G}^+(\mathbf{v}, \eta)$ can be expressed as a Taylor series. Choosing the bifurcation point C as the reference point characterized by $\mathbf{v}_0 = \mathbf{0}$ and $\eta_0 = 0$, one obtains

$$\begin{aligned} \mathbf{G}^+(\mathbf{v}, \eta) = & \mathbf{G}^+(\mathbf{0}, 0) + \mathbf{G}_{,\mathbf{v}}^+ \cdot \mathbf{v} + \mathbf{G}_{,\eta}^+ \eta + \frac{1}{2} \mathbf{G}_{,\mathbf{v}\mathbf{v}}^+ : \mathbf{v} \otimes \mathbf{v} + \mathbf{G}_{,\mathbf{v}\eta}^+ \cdot \mathbf{v} \eta + \frac{1}{2} \mathbf{G}_{,\eta\eta}^+ \eta^2 \\ & + \frac{1}{6} \mathbf{G}_{,\mathbf{v}\mathbf{v}\mathbf{v}}^+ : \mathbf{v} \otimes \mathbf{v} \otimes \mathbf{v} + \frac{1}{2} \mathbf{G}_{,\mathbf{v}\mathbf{v}\eta}^+ : \mathbf{v} \otimes \mathbf{v} \eta + \frac{1}{2} \mathbf{G}_{,\mathbf{v}\eta\eta}^+ \cdot \mathbf{v} \eta^2 + \frac{1}{6} \mathbf{G}_{,\eta\eta\eta}^+ \eta^3 \\ & + \mathcal{O}(\mathbf{v} \otimes \mathbf{v} \otimes \mathbf{v} \otimes \mathbf{v}, \mathbf{v} \otimes \mathbf{v} \otimes \mathbf{v} \eta, \mathbf{v} \otimes \mathbf{v} \eta^2, \mathbf{v} \eta^3, \eta^4). \end{aligned} \quad (4)$$

The computation of the first-order tensors (vectors) $\mathbf{G}_{,\eta}^+$, $\mathbf{G}_{,\eta\eta}^+$, $\mathbf{G}_{,\eta\eta\eta}^+$, ..., second-order tensors (matrices) $\mathbf{G}_{,\mathbf{v}}^+$, $\mathbf{G}_{,\mathbf{v}\eta}^+$, $\mathbf{G}_{,\mathbf{v}\eta\eta}^+$, ..., third-order tensors $\mathbf{G}_{,\mathbf{v}\mathbf{v}}^+$, $\mathbf{G}_{,\mathbf{v}\mathbf{v}\eta}^+$, ..., fourth-order tensors $\mathbf{G}_{,\mathbf{v}\mathbf{v}\mathbf{v}}^+$, ..., etc., is explained in Appendix A. Each single term in (4) represents a vector-valued function of \mathbf{v} and η .

Assuming a sufficiently smooth solution for both $\mathbf{v}^+(\eta)$ and $\tilde{\lambda}(\eta)$, these functions can be formulated as series expansions (Koiter [8], Reiteringer [11]):

$$\mathbf{v}^+(\eta) = \mathbf{v}_1 \eta + \mathbf{v}_2 \eta^2 + \mathbf{v}_3 \eta^3 + \dots, \quad (5)$$

$$\tilde{\lambda}(\eta) = \lambda_C + \lambda_1 \eta + \lambda_2 \eta^2 + \lambda_3 \eta^3 + \dots. \quad (6)$$

where $\mathbf{v}_1, \mathbf{v}_2, \mathbf{v}_3, \dots$ are the *residual vectors* and $\lambda_1, \lambda_2, \lambda_3, \dots$ are *load coefficients* associated with the secondary (postbuckling) path. The residual vectors determine the deformation pattern of this path. The load coefficients govern the type of bifurcation, i.e. *symmetric/unsymmetric* and *imperfection sensitive/insensitive*, noting that unsymmetric bifurcation is always imperfection sensitive.

Substituting (6) and (5) into (4) and re-ordering the resulting relation according to the order of η , yields

$$\mathbf{G}^+(\mathbf{v}^+(\eta), \eta) = \eta^1 \cdot (\tilde{\mathbf{K}}_T \cdot \mathbf{v}_1) + \eta^2 \cdot \left(\tilde{\mathbf{K}}_T \cdot \mathbf{v}_2 + \lambda_1 \tilde{\mathbf{K}}_{T,\lambda} \cdot \mathbf{v}_1 + \frac{1}{2} \mathbf{K}_{T,\mathbf{u}} : \mathbf{v}_1 \otimes \mathbf{v}_1 \right)$$

$$\begin{aligned}
& + \eta^3 \cdot \left(\tilde{\mathbf{K}}_T \cdot \mathbf{v}_3 + \lambda_2 \tilde{\mathbf{K}}_{T,\lambda} \cdot \mathbf{v}_1 + \lambda_1 \tilde{\mathbf{K}}_{T,\lambda} \cdot \mathbf{v}_2 + \frac{1}{2} \lambda_1^2 \underline{\tilde{\mathbf{K}}}_{T,\lambda\lambda} \cdot \mathbf{v}_1 \right. \\
& \quad \left. + \mathbf{K}_{T,\mathbf{u}} : \mathbf{v}_1 \otimes \mathbf{v}_2 + \frac{1}{2} \lambda_1 \mathbf{K}_{T,\mathbf{u}\lambda} : \mathbf{v}_1 \otimes \mathbf{v}_1 + \frac{1}{6} \mathbf{K}_{T,\mathbf{u}\mathbf{u}} : \mathbf{v}_1 \otimes \mathbf{v}_1 \otimes \mathbf{v}_1 \right) \\
& + \eta^4 \cdot (\text{see App. B}) + \eta^5 \cdot (\text{see App. B}) + \eta^6 \cdot (\text{see App. B}) + \mathcal{O}(\eta^7) = \mathbf{0}. \quad (7)
\end{aligned}$$

For this work the coefficient vectors of η^1 , η^2 , \dots , and η^6 are needed. Because of the relatively great length of the expressions for the coefficients η^4 , η^5 , and η^6 , they have been transferred to Appendix B. Underlined matrices in (7) and in other expressions in this Section vanish in case of linear primary (prebuckling) paths. Such matrices also occur in Sections 4, 5, and 7, and in the Appendices. However, in these Sections and in Appendix D they are not underlined because the special case of linear prebuckling paths is not explicitly considered therein.

For (7) to be satisfied, each expression in parentheses must vanish separately. The resulting relations allow to compute \mathbf{v}_1 , λ_1 and \mathbf{v}_2 , λ_2 and $\mathbf{v}_3, \dots, \lambda_5$ and \mathbf{v}_6 successively (Reitinger [11]). The following brief demonstration is restricted to computation of \mathbf{v}_1 , λ_1 and \mathbf{v}_2 , and λ_2 . It starts with setting the coefficient vector of η^1 equal to zero, which gives

$$\tilde{\mathbf{K}}_T \cdot \mathbf{v}_1 = \mathbf{0}, \quad (8)$$

where \mathbf{v}_1 is the eigenvector. Setting the coefficient vector of η^2 equal to zero and premultiplying it by \mathbf{v}_1^T , enables computation of λ_1 as

$$\lambda_1 = -\frac{1}{2} \frac{\mathbf{v}_1^T \mathbf{K}_{T,\mathbf{u}} : \mathbf{v}_1 \otimes \mathbf{v}_1}{\mathbf{v}_1^T \tilde{\mathbf{K}}_{T,\lambda} \cdot \mathbf{v}_1}. \quad (9)$$

Eq. (9) can be rewritten formally as

$$a_0 \lambda_1 + b_0 = 0, \quad (10)$$

where

$$a_0 = -\frac{\mathbf{v}_1^T \tilde{\mathbf{K}}_{T,\lambda} \cdot \mathbf{v}_1}{\mathbf{v}_1^T \tilde{\mathbf{K}}_{T,\lambda} \cdot \mathbf{v}_1} = -1 \quad (11)$$

and

$$b_0 = -\frac{1}{2} \frac{\mathbf{v}_1^T \mathbf{K}_{T,\mathbf{u}} : \mathbf{v}_1 \otimes \mathbf{v}_1}{\mathbf{v}_1^T \tilde{\mathbf{K}}_{T,\lambda} \cdot \mathbf{v}_1}. \quad (12)$$

The motivation for this formulation is consistency with relations which will be presented in the following.

Setting the expression for the coefficient vector of η^2 equal to zero, yields

$$\tilde{\mathbf{K}}_T \cdot \mathbf{v}_2 = -\tilde{\mathbf{K}}_{T,\lambda} \cdot \mathbf{v}_1 \lambda_1 - \frac{1}{2} \mathbf{K}_{T,\mathbf{u}} : \mathbf{v}_1 \otimes \mathbf{v}_1 \quad (13)$$

with λ_1 according to (9). From (13) \mathbf{v}_2 can be computed, noting that $\tilde{\mathbf{K}}_T$ has a rank one deficiency at the stability limit, with \mathbf{v}_1 as the eigenvector (see (8)). Eq. (9) ensures that

the right-hand side of (13) is orthogonal to the eigenvector \mathbf{v}_1 . Setting the coefficient vector of η^3 equal to zero and premultiplying it by \mathbf{v}_1^T , enables computation of λ_2 as

$$\lambda_2 = -\frac{1}{\mathbf{v}_1^T \tilde{\mathbf{K}}_{T,\lambda} \cdot \mathbf{v}_1} \left[\frac{1}{2} \lambda_1^2 \mathbf{v}_1^T \tilde{\mathbf{K}}_{T,\lambda\lambda} \cdot \mathbf{v}_1 + \lambda_1 \left(\mathbf{v}_1^T \tilde{\mathbf{K}}_{T,\lambda} \cdot \mathbf{v}_2 + \frac{1}{2} \mathbf{v}_1^T \mathbf{K}_{T,u\lambda} : \mathbf{v}_1 \otimes \mathbf{v}_1 \right) + \mathbf{v}_1^T \mathbf{K}_{T,u} : \mathbf{v}_1 \otimes \mathbf{v}_2 + \frac{1}{6} \mathbf{v}_1^T \mathbf{K}_{T,uu} : \mathbf{v}_1 \otimes \mathbf{v}_1 \otimes \mathbf{v}_1 \right]. \quad (14)$$

Eq. (14) can be rewritten formally as

$$a_1 \lambda_1^2 + b_1 \lambda_1 + c_1 = 0, \quad (15)$$

where

$$a_1 = -\frac{1}{2} \frac{\mathbf{v}_1^T \tilde{\mathbf{K}}_{T,\lambda\lambda} \cdot \mathbf{v}_1}{\mathbf{v}_1^T \tilde{\mathbf{K}}_{T,\lambda} \cdot \mathbf{v}_1} \quad (16)$$

represents a so-called *nonlinearity coefficient* which vanishes trivially, i.e. because of $\tilde{\mathbf{K}}_{T,\lambda\lambda} = \mathbf{0}$, in case of linear prebuckling paths,

$$b_1 = -\frac{1}{\mathbf{v}_1^T \tilde{\mathbf{K}}_{T,\lambda} \cdot \mathbf{v}_1} \left(\mathbf{v}_1^T \tilde{\mathbf{K}}_{T,\lambda} \cdot \mathbf{v}_2 + \frac{1}{2} \mathbf{v}_1^T \mathbf{K}_{T,u\lambda} : \mathbf{v}_1 \otimes \mathbf{v}_1 \right), \quad (17)$$

and

$$c_1 = d_1 - \lambda_2 \quad (18)$$

with

$$d_1 = -\frac{1}{\mathbf{v}_1^T \tilde{\mathbf{K}}_{T,\lambda} \cdot \mathbf{v}_1} \left(\mathbf{v}_1^T \mathbf{K}_{T,u} : \mathbf{v}_1 \otimes \mathbf{v}_2 + \frac{1}{6} \mathbf{v}_1^T \mathbf{K}_{T,uu} : \mathbf{v}_1 \otimes \mathbf{v}_1 \otimes \mathbf{v}_1 \right). \quad (19)$$

By analogy to (15), the following formal relations are obtained by setting the expressions for the coefficient vectors of η^4 , η^5 , and η^6 in (B.1) (see the Eqs. (B.4)–(B.6)) equal to zero and premultiplying the resulting relations by $-\mathbf{v}_1^T / \mathbf{v}_1^T \tilde{\mathbf{K}}_{T,\lambda} \mathbf{v}_1$:

$$a_1^* \lambda_1^3 + b_1^* \lambda_1^2 + c_1^* \lambda_1 + d_1^* = 0 \quad \text{with} \quad d_1^* = e_1^* - \lambda_3, \quad (20)$$

$$\hat{a}_1 \lambda_1^4 + \hat{b}_1 \lambda_1^3 + \hat{c}_1 \lambda_1^2 + \hat{d}_1 \lambda_1 + \hat{e}_1 = 0 \quad \text{with} \quad \hat{e}_1 = \hat{f}_1 - \lambda_4, \quad (21)$$

$$\tilde{a}_1 \lambda_1^5 + \tilde{b}_1 \lambda_1^4 + \tilde{c}_1 \lambda_1^3 + \tilde{d}_1 \lambda_1^2 + \tilde{e}_1 \lambda_1 + \tilde{f}_1 = 0 \quad \text{with} \quad \tilde{f}_1 = \tilde{g}_1 - \lambda_5. \quad (22)$$

The coefficients a_1^* , \hat{a}_1 , and \tilde{a}_1 are given as

$$a_1^* = -\frac{1}{6} \frac{\mathbf{v}_1^T \tilde{\mathbf{K}}_{T,\lambda\lambda\lambda} \mathbf{v}_1}{\mathbf{v}_1^T \tilde{\mathbf{K}}_{T,\lambda} \mathbf{v}_1}, \quad \hat{a}_1 = -\frac{1}{24} \frac{\mathbf{v}_1^T \tilde{\mathbf{K}}_{T,\lambda\lambda\lambda\lambda} \mathbf{v}_1}{\mathbf{v}_1^T \tilde{\mathbf{K}}_{T,\lambda} \mathbf{v}_1}, \quad \tilde{a}_1 = -\frac{1}{120} \frac{\mathbf{v}_1^T \tilde{\mathbf{K}}_{T,\lambda\lambda\lambda\lambda\lambda} \mathbf{v}_1}{\mathbf{v}_1^T \tilde{\mathbf{K}}_{T,\lambda} \mathbf{v}_1}. \quad (23)$$

Just as a_1 , these coefficients vanish trivially in case of linear prebuckling paths. Hence, they also represent *nonlinearity coefficients*. The coefficients b_1^* , \hat{b}_1 , and \tilde{b}_1 are given as

$$b_1^* = -\frac{1}{\mathbf{v}_1^T \tilde{\mathbf{K}}_{T,\lambda} \mathbf{v}_1} \left(\frac{1}{2} \mathbf{v}_1^T \tilde{\mathbf{K}}_{T,\lambda\lambda} \mathbf{v}_2 + \frac{1}{4} \mathbf{v}_1^T \mathbf{K}_{T,u\lambda\lambda} \mathbf{v}_1 \mathbf{v}_1 \right), \quad (24)$$

$$\hat{b}_1 = -\frac{1}{\mathbf{v}_1^T \tilde{\mathbf{K}}_{T,\lambda} \mathbf{v}_1} \left(\frac{1}{6} \mathbf{v}_1^T \tilde{\mathbf{K}}_{T,\lambda\lambda\lambda} \mathbf{v}_2 + \frac{1}{12} \mathbf{v}_1^T \mathbf{K}_{T,u\lambda\lambda\lambda} \mathbf{v}_1 \mathbf{v}_1 \right), \quad (25)$$

$$\tilde{b}_1 = -\frac{1}{\mathbf{v}_1^T \tilde{\mathbf{K}}_{T,\lambda} \mathbf{v}_1} \left(\frac{1}{24} \mathbf{v}_1^T \tilde{\mathbf{K}}_{T,\lambda\lambda\lambda\lambda} \mathbf{v}_2 + \frac{1}{48} \mathbf{v}_1^T \mathbf{K}_{T,u\lambda\lambda\lambda\lambda} \mathbf{v}_1 \mathbf{v}_1 \right). \quad (26)$$

The expressions for the coefficients c_1^* , \hat{f}_1 , \tilde{e}_1 , which will be needed later, are given in Appendix C.

3 Symmetric bifurcation

Symmetric bifurcation is characterized by

$$\lambda_1 = \lambda_3 = \dots = 0. \quad (27)$$

If this condition is not satisfied by the original structure and for the given loading, it must be enforced in the course of the conversion process (Bochenek [1]). This may require modifications of the original design which, for different reasons, are unfeasible. Irrespective of the feasibility of such modifications, this step is beyond the scope of the present work.

For symmetric bifurcation, some of the coefficients of (10), (15), and (20)–(22) *must* vanish. In this context, the term “vanishing” means that the respective coefficient is zero for arbitrary values of a design parameter κ . Additionally, some of the remaining coefficients *may* vanish. This may either be the case for arbitrary or for specific values of κ . The ones that must vanish are underlined in the following array:

$$a_0 \quad \underline{b_0}, \quad (28)$$

$$a_1 \quad \underline{b_1} \quad \underline{c_1}, \quad (29)$$

$$a_1^* \quad \underline{b_1^*} \quad c_1^* \quad \underline{d_1^*}, \quad (30)$$

$$\hat{a}_1 \quad \underline{\hat{b}_1} \quad \hat{c}_1 \quad \underline{\hat{d}_1} \quad \hat{e}_1, \quad (31)$$

$$\tilde{a}_1 \quad \underline{\tilde{b}_1} \quad \tilde{c}_1 \quad \underline{\tilde{d}_1} \quad \tilde{e}_1 \quad \underline{\tilde{f}_1}. \quad (32)$$

Substitution of (18) into

$$c_1 = 0 \quad (33)$$

(see (29)) yields

$$\lambda_2 = d_1, \quad (34)$$

with d_1 according to (19). Substitution of (C.3) with $\lambda_3 = 0$ into (21.2) and insertion of the result into

$$\hat{e}_1 = 0 \quad (35)$$

(see (31)) gives

$$\lambda_4 = a_1 \lambda_2^2 + b_2 \lambda_2 + d_3 \quad (36)$$

with a_1 , b_2 , and d_3 according to (16), (C.2), and (C.4), and with λ_2 according to (34).

The vanishing of b_0 , c_1 , d_1^* , \hat{e}_1 , and \tilde{f}_1 (see (28)–(32)) are necessary conditions for $\lambda_1 = 0$. To explain why also b_1 , b_1^* , \hat{b}_1 and \hat{d}_1 , and \tilde{b}_1 and \tilde{d}_1 vanish for symmetric bifurcation (see (29)–(32)), at first, (15) is rewritten as

$$\left(\lambda_1 + \frac{b_1}{a_1} \right) \lambda_1 + \frac{c_1}{a_1} = 0 \quad (a_1 \neq 0). \quad (37)$$

Symmetric bifurcation requires

$$\frac{c_1}{a_1} = 0 \quad \text{with} \quad c_1 = c_1(\kappa) = 0. \quad (38)$$

Substitution of (38.1) into (37) yields the two roots

$$(\lambda_1)_1 = 0 \quad \text{and} \quad (\lambda_1)_2 = -\frac{b_1}{a_1}. \quad (39)$$

The relations

$$b_1 = b_1(\kappa) = 0 \quad \text{and} \quad c_1 = c_1(\kappa) = 0 \quad (40)$$

satisfy the condition for a double root of (15), given as

$$b_1^2 - 4a_1c_1 = 0. \quad (41)$$

Hence, $\lambda_1 = 0$ is a double root of (15). The logic of this result provides the rationale for (40.1). This result is not affected by $a_1 = 0$ which may occur either for a specific value or for arbitrary values of κ .

Substitution of

$$b_1^* = 0, \quad d_1^* = 0, \quad \hat{b}_1 = 0, \quad \hat{d}_1 = 0, \quad \tilde{b}_1 = 0, \quad \tilde{d}_1 = 0, \quad \tilde{f}_1 = 0 \quad (42)$$

(see (30)–(32)) into (20)–(22) yields the following relations:

$$\left(\lambda_1^2 + \frac{c_1^*}{a_1^*} \right) \lambda_1 = 0 \quad (a_1^* \neq 0) \quad \rightarrow \quad (\lambda_1)_1 = 0, \quad (\lambda_1)_{2,3} = \pm \sqrt{-\frac{c_1^*}{a_1^*}}, \quad (43)$$

$$\left(\lambda_1^2 + \frac{\hat{c}_1}{\hat{a}_1} \right) \lambda_1^2 = 0 \quad (\hat{a}_1 \neq 0) \quad \rightarrow \quad (\lambda_1)_{1,2} = 0, \quad (\lambda_1)_{3,4} = \pm \sqrt{-\frac{\hat{c}_1}{\hat{a}_1}}, \quad (44)$$

$$\left(\lambda_1^4 + \frac{\tilde{c}_1}{\tilde{a}_1} \lambda_1^2 + \frac{\tilde{e}_1}{\tilde{a}_1} \right) \lambda_1 = 0 \quad (\tilde{a}_1 \neq 0) \quad \rightarrow \quad (\lambda_1)_1 = 0,$$

$$(\lambda_1)_{2,3,4,5} = \pm \sqrt{-\frac{\tilde{c}_1}{2\tilde{a}_1} \pm \sqrt{\left(\frac{\tilde{c}_1}{2\tilde{a}_1} \right)^2 - \frac{\tilde{e}_1}{\tilde{a}_1}}}. \quad (45)$$

Hence, for $c_1^* \neq 0$ and $\tilde{e}_1 \neq 0$, $\lambda_1 = 0$ is a single root of (20) and (22), respectively, and for $\hat{c}_1 \neq 0$ a double root of (21).

In contrast to the underlined coefficients in (28)–(32), which *must* vanish for arbitrary values of κ , c_1^* is a coefficient that *may* vanish for arbitrary values of κ . Substitution of

$$c_1^* = c_1^*(\kappa) = 0 \quad (46)$$

into (43.1) yields

$$\lambda_1^3 = 0 \quad \rightarrow \quad (\lambda)_{1,2,3} = 0. \quad (47)$$

Hence, $\lambda_1 = 0$ is a triple root of (20). Substitution of (C.1) into (46) results in

$$2a_1\lambda_2 + b_2 = 0 \quad (48)$$

with b_2 according to (C.2). Solving (36) for λ_2 , gives

$$\lambda_2 = -\frac{b_2}{2a_1} \pm \sqrt{\left(\frac{b_2}{2a_1}\right)^2 - \frac{d_3 - \lambda_4}{a_1}} \quad (a_1 \neq 0). \quad (49)$$

Because of (48), the discriminant in (49) vanishes:

$$b_2^2 - 4a_1(d_3 - \lambda_4) = 0. \quad (50)$$

Elimination of b_2 in (50) by means of (48) yields

$$\lambda_4 = -a_1\lambda_2^2 + d_3. \quad (51)$$

In addition to c_1^* , also a_1^* may vanish for arbitrary values of κ . For

$$a_1^* = a_1^*(\kappa) = 0 \quad \text{and} \quad c_1^* = c_1^*(\kappa) = 0, \quad (52)$$

(43) does not hold. The Eqs. (52) are associated with

$$\tilde{e}_1 = \tilde{e}_1(\kappa) = 0. \quad (53)$$

Substitution of (53) into (45.1) yields

$$\left(\lambda_1^2 + \frac{\tilde{c}_1}{\tilde{a}_1}\right)\lambda_1^3 = 0 \quad (\tilde{a}_1 \neq 0) \quad \rightarrow \quad (\lambda_1)_{1,2,3} = 0, \quad (\lambda_1)_{4,5} = \pm\sqrt{-\frac{\tilde{c}_1}{\tilde{a}_1}}. \quad (54)$$

Hence, $\lambda_1 = 0$ is a triple root of (22). Substitution of (C.5) with $\lambda_3 = 0$ into (53) results in

$$2a_1\lambda_4 + b_4 = 0. \quad (55)$$

Substitution of (52.1) into (C.6) and of the so-obtained result for b_4 into (55) gives

$$\lambda_4 = -\frac{1}{2a_1}(b_2^*\lambda_2 + c_2^*) \quad (a_1 \neq 0). \quad (56)$$

In addition to (52), a_1 may vanish for arbitrary values of κ , i.e.

$$a_1 = a_1(\kappa) = 0. \quad (57)$$

In this case, also (37) does not hold.

If (46) holds true, a_1 and λ_2 vanish for the same value of κ , for which, following from (48), $b_2 = 0$. This is not the case, if (46) is not valid. Rewriting (36) as

$$\left(\frac{1}{\lambda_2}\right)^2 + \frac{b_2}{d_3 - \lambda_4} \left(\frac{1}{\lambda_2}\right) + \frac{a_1}{d_3 - \lambda_4} = 0 \quad (d_3 - \lambda_4 \neq 0) \quad (58)$$

and specializing (58) for

$$\frac{a_1}{d_3 - \lambda_4} = 0, \quad (59)$$

gives

$$\left(\frac{1}{\lambda_2} + \frac{b_2}{d_3 - \lambda_4}\right) \frac{1}{\lambda_2} = 0. \quad (60)$$

The two solutions of (60) are

$$\left(\frac{1}{\lambda_2}\right)_1 = 0 \quad \text{and} \quad \left(\frac{1}{\lambda_2}\right)_2 = -\frac{b_2}{d_3 - \lambda_4}. \quad (61)$$

As follows from (61.2) for $b_2 \neq 0$ and $d_3 - \lambda_4 \neq 0$, $(\lambda_2)_2 \neq 0$.

Remarkably, symmetric bifurcation from nonlinear prebuckling paths is associated either with

$$\mathbf{v}_j^{*T} \tilde{\mathbf{K}}_{T,\lambda\lambda} \mathbf{v}_1 = 0, \quad j \neq 1, \quad (62)$$

where \mathbf{v}_j^* is the j -th eigenvector of the so-called ‘‘consistently linearized eigenproblem’’ (see Appendix D), or with

$$\mathbf{v}_1^T \tilde{\mathbf{K}}_{T,\lambda\lambda\lambda} \mathbf{v}_1 = 0 \quad \xrightarrow{(23.1)} \quad a_1^* = 0 \quad (\text{see (46.1)}). \quad (63)$$

Eq. (62) occurs together either with $c_1^*(\kappa) \neq 0$ or with $c_1^*(\kappa) = 0 \rightarrow$ Eqs. (48) and (51), whereas Eq. (63) only occurs together with $c_1^*(\kappa) = 0$. The Eqs. (62) and (63) result in two different modes of disintegration of an expression that holds for unsymmetric bifurcation from nonlinear prebuckling paths (see (145)–(147)).

4 Triples of values λ_4, a_1, a_1^* for $\lambda_2 = 0$

This Section refers to the general case of nonlinear prebuckling paths. Hence, $\tilde{\mathbf{K}}_{T,\lambda\lambda} \neq \mathbf{0}$, $\tilde{\mathbf{K}}_{T,\lambda\lambda\lambda} \neq \mathbf{0}, \dots$

Following from (34),

$$d_1 = 0 \quad \rightarrow \quad \lambda_2 = 0. \quad (64)$$

Substitution of (64.2) into (36) gives

$$\lambda_4 = d_3. \quad (65)$$

The triples of values λ_4, a_1, a_1^* for $\lambda_2 = 0$, which will be presented in the following, determine whether a transition from imperfection sensitivity to imperfection insensitivity occurs and, if it does, how it occurs.

For

$$\mathbf{v}_j^{*T} \tilde{\mathbf{K}}_{T,\lambda\lambda} \mathbf{v}_1 = 0, \quad j \neq 1, \quad a_1 \neq 0 \quad \text{and} \quad a_1^* \neq 0, \quad (66)$$

or

$$\tilde{\mathbf{K}}_{T,\lambda\lambda} \mathbf{v}_1 = \mathbf{0} \xrightarrow{(16)} a_1 = 0 \quad \text{and} \quad a_1^* \neq 0, \quad (67)$$

$$\lambda_{2k} = 0, \quad k = 1, 2, \dots, \quad (68)$$

(see Part II of this work [12]). Substitution of (27) and (68) into (6) yields

$$\tilde{\lambda}(\eta) = \lambda_C = \text{const.} \quad (69)$$

Such a transition was investigated by Tarnai [13] and by the authors of Part II of this work [12] for the case of a bar-and-joint assembly composed of rigid members and elastic springs.

For

$$\mathbf{v}_1^T \tilde{\mathbf{K}}_{T,\lambda\lambda} \mathbf{v}_1 = 0 \xrightarrow{(16)} a_1 = 0 \quad \text{and} \quad \mathbf{v}_1^T \tilde{\mathbf{K}}_{T,\lambda\lambda\lambda} \mathbf{v}_1 = 0 \xrightarrow{(23.1)} a_1^* = 0, \quad (70)$$

$$\lambda_2 = 0 \quad \text{and} \quad \lambda_4 < 0 \quad (\text{see Part II of this work [12]}). \quad (71)$$

For

$$\tilde{\mathbf{K}}_{T,\lambda\lambda} \mathbf{v}_1 = \mathbf{0} \xrightarrow{(16)} a_1 = 0 \quad \text{and} \quad \mathbf{v}_1^T \tilde{\mathbf{K}}_{T,\lambda\lambda\lambda} \mathbf{v}_1 = 0 \xrightarrow{(23.1)} a_1^* = 0, \quad (72)$$

$$\lambda_2 = 0 \quad \text{and} \quad \lambda_4 = 0 \quad (\text{see Part II of this work [12]}). \quad (73)$$

The Eqs. (73) are associated with

$$\lambda_6 < 0 \quad (74)$$

and, thus, with imperfection sensitivity (see Part II of this work [12]).

Hence, for $\lambda_2 = 0$, the following triples of values λ_4, a_1, a_1^* are obtained:

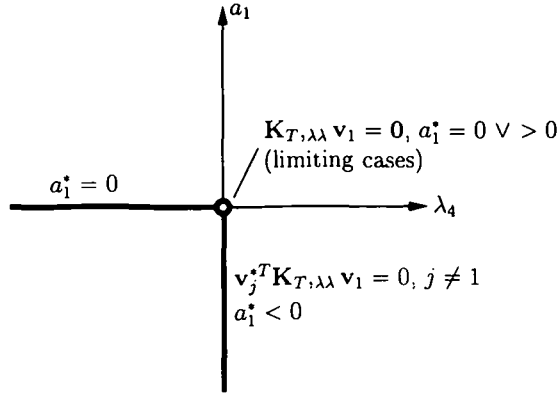


Fig. 2. Half-axes $\lambda_4 \leq 0$ and $a_1 \leq 0$ as geometric loci of all points associated with $\lambda_2 = 0$

$$\lambda_4 = 0, \quad a_1 < 0, \quad a_1^* < 0, \quad (75)$$

$$\lambda_4 = 0, \quad a_1 = 0 \quad (\text{with } \tilde{\mathbf{K}}_{T, \lambda \lambda} \mathbf{v}_1 = \mathbf{0}), \quad a_1^* > 0, \quad (76)$$

$$\lambda_4 < 0, \quad a_1 = 0 \quad (\text{with } \tilde{\mathbf{K}}_{T, \lambda \lambda} \mathbf{v}_1 \neq \mathbf{0}), \quad a_1^* = 0, \quad (77)$$

$$\lambda_4 = 0, \quad a_1 = 0 \quad (\text{with } \tilde{\mathbf{K}}_{T, \lambda \lambda} \mathbf{v}_1 = \mathbf{0}), \quad a_1^* = 0. \quad (78)$$

The thick parts of the two lines in Fig. 2 show the geometric loci of all points in the λ_4 - a_1 plane of the λ_2 - λ_4 - a_1 space, which are solutions of (36) with $\lambda_2 = 0$. It is seen that these geometric loci are restricted to the two half-axes $\lambda_4 \leq 0$ and $a_1 \leq 0$. This seems to be the consequence of the restriction to symmetric bifurcation, excluding, e.g. the possibility of $\lambda_1 = 0, \lambda_2 = 0, \lambda_3 \neq 0, \dots$. Another consequence of this restriction is the fact that only five out of the eight octants into which the three-dimensional space can be divided by the λ_2 - λ_4 - a_1 coordinate system are geometric loci of triples of values $(\lambda_2, \lambda_4, a_1)$ that are solutions of (36) (see Fig. 3). The octants I, II, and IV are characterized by

$$\mathbf{v}_1^T \tilde{\mathbf{K}}_{T, \lambda} \mathbf{v}_1 = -1 \quad (\text{see (D.11)}) \quad \text{and} \quad \mathbf{v}_1^T \tilde{\mathbf{K}}_{T, \lambda \lambda} \mathbf{v}_1 \geq 0, \quad (79)$$

octant V by

$$\mathbf{v}_1^T \tilde{\mathbf{K}}_{T, \lambda} \mathbf{v}_1 = -1 \quad (\text{see (D.11)}) \quad \text{and} \quad \mathbf{v}_1^T \tilde{\mathbf{K}}_{T, \lambda \lambda} \mathbf{v}_1 \leq 0, \quad (80)$$

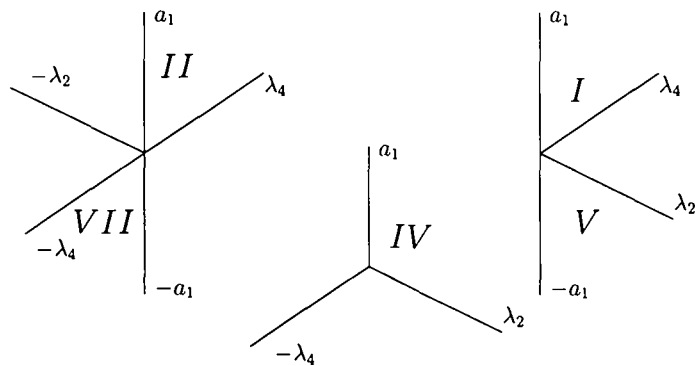


Fig. 3. Five octants as geometric loci of triples of values $(\lambda_2, \lambda_4, a_1)$ for $\lambda_C > 0$

and octant VII by

$$\mathbf{v}_1^T \tilde{\mathbf{K}}_{T,\lambda} \mathbf{v}_1 = -1 \quad (\text{see (D.11)}) \quad \text{and} \quad \mathbf{v}_1^T \tilde{\mathbf{K}}_{T,\lambda\lambda} \mathbf{v}_1 \leq 0 \quad (81)$$

or by

$$\mathbf{v}_1^T \tilde{\mathbf{K}}_{T,\lambda} \mathbf{v}_1 = 1 \quad (\text{see (D.11)}) \quad \text{and} \quad \mathbf{v}_1^T \tilde{\mathbf{K}}_{T,\lambda\lambda} \mathbf{v}_1 \geq 0, \quad (82)$$

all of which correlate with $\lambda = \lambda_C > 0$ (see Fig. 1). A positive value of λ_C can always be achieved by means of a suitable definition of a positive reference load.

5 General case: nonlinear prebuckling paths

5.1 Sensitivity analysis

Fig. 4 shows qualitative plots of eight curves $\lambda_2 = \lambda_2(\kappa)$, $\lambda_4 = \lambda_4(\kappa)$, $a_1 = a_1(\kappa)$. For each point on these curves Eq. (8) holds. Each curve contains at least one point T , characterized by

$$\lambda_2 = 0. \quad (83)$$

The plane curve $\overline{S=T} \quad \overline{F}$ in Fig. 4(e) is the limiting case of space curves of the form shown in Fig. 4(d). The vertical line $\overline{S=T} \quad \overline{F=T}$ in Fig. 4(f), the horizontal line $\overline{S=T} \quad \overline{F=T}$ in Fig. 4(h), and point $S=F=T$ in Fig. 4(g) represent degenerations of space curves. The arrows on the curves in Fig. 4 correspond to the increase of the value of the design parameter κ . The starting point of such a curve is denoted as S and the final point as F . The starting points in Figs. 4(a)–4(d) and the final points in Figs. 4(a)–4(e) are arbitrarily chosen points. The final points in Figs. 4(f)–4(h) refer to “final situations” (transition from bifurcation buckling to no buckling). The corresponding values of κ are κ_S and $\kappa_F > \kappa_S$. In line with the purpose of this paper, reflected by its title, S is restricted to

$$\lambda_2 \leq 0. \quad (84)$$

If the sign of inequality holds in (84) (see Figs. 4(a)–4(d)),

$$\kappa_S < \kappa_T, \quad (85)$$

where κ_T is the value of κ corresponding to point T . The sign of equality in (84) holds for $S=T$ (see Figs. 4(e)–4(h)) with

$$\kappa_S = \kappa_T. \quad (86)$$

In Fig. 4(e), $\lambda_2(\kappa) \geq 0$, $\lambda_4(\kappa) = 0$, $a_1(\kappa) \geq 0$, in Fig. 4(f), $\lambda_2(\kappa) = 0$, $\lambda_4(\kappa) = 0$, $a_1(\kappa) < 0$, in Fig. 4(g), $\lambda_2(\kappa) = 0$, $\lambda_4(\kappa) = 0$, $a_1(\kappa) = 0$, and in Fig. 4(h), $\lambda_2(\kappa) = 0$, $\lambda_4(\kappa) < 0$, $a_1(\kappa) = 0$. As shown in Fig. 4(b), $\lambda_2(\kappa = \kappa_F)$ may be negative. Point H is a bifurcation point coinciding with a snap-through point. In Figs. 4(f)–4(h), $F=T$ represents the point of transition from bifurcation buckling to no buckling, denoted as N . It is characterized by the

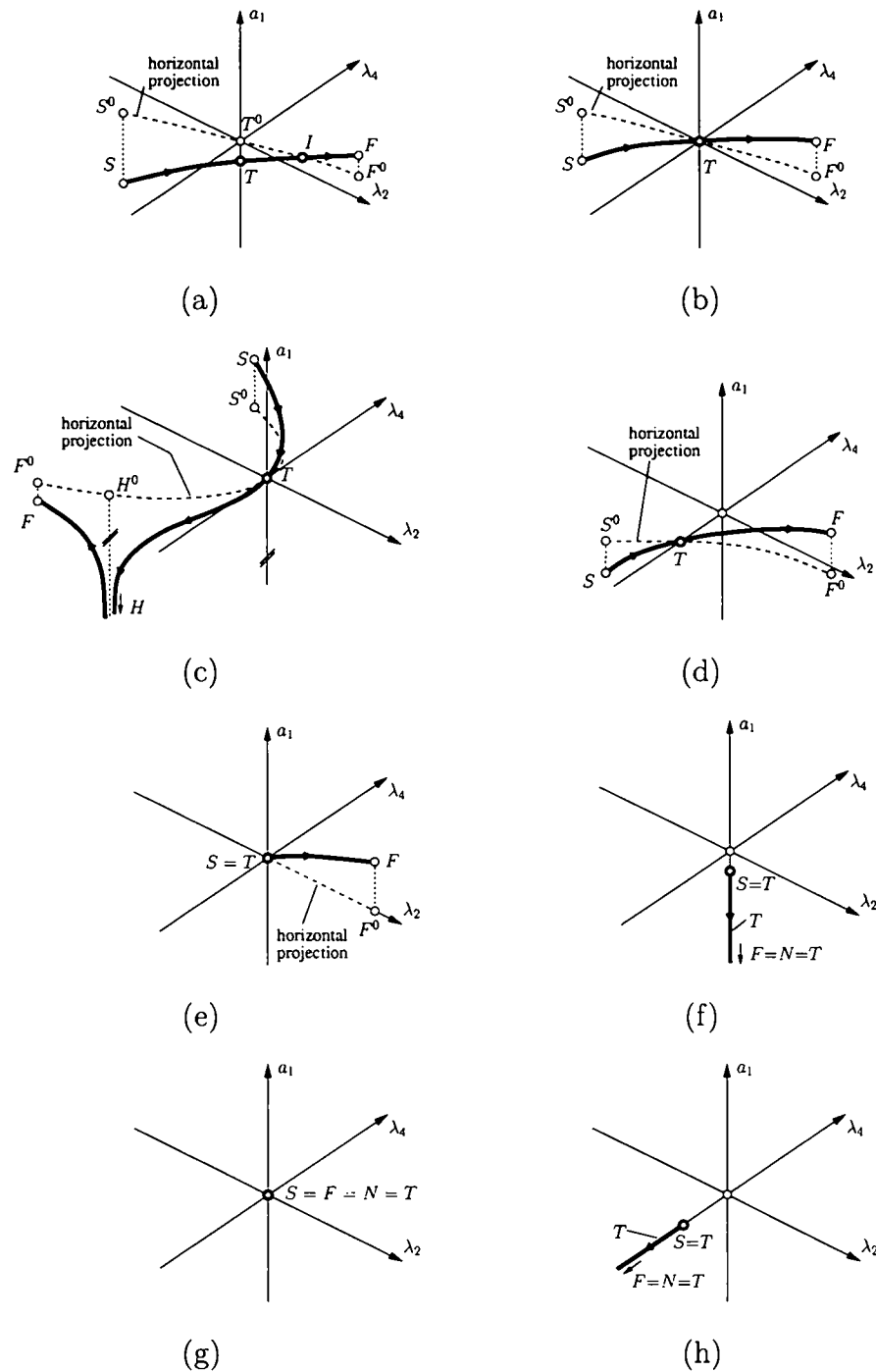


Fig. 4. Qualitative plots of curves $\lambda_2 = \lambda_2(\kappa)$, $\lambda_4 = \lambda_4(\kappa)$, $a_1 = a_1(\kappa)$, with (at least) one point $T(\lambda_2 = 0, \lambda_4, a_1)$

[κ refers to the stiffness of a vertical elastic spring attached to the vertex of a pin-jointed bar (Fig. 4(a)) and of a *von Mises* truss (Fig. 4(b)) and to the center of a cylindrical panel with two different thicknesses (Figs. 4(d) and 4(e)), respectively, at which a vertical load is applied; to the thickness of the panel (Fig. 4(c)); and to the initial rise of the pin-jointed bar (Fig. 4(f)), of the truss (Fig. 4(g)), and of the panel without and with the spring (Fig. 4(g) and Fig. 4(h), respectively); details of the three structures are given in Figs. 1, 4, and 9 in Part II of this work [12]]

degeneration of the secondary paths to one point each on the respective load-displacement diagram, coinciding with a saddle point on this curve. The dashed curves in Fig. 4 are the projections of the respective curves onto the λ_2 - λ_4 plane. S^0 and F^0 are the projections of S and F onto this plane.

According to Fig. 4, at point T , with the exception of Figs. 4(a) and 4(f) for which (48) does not hold, $a_1 = 0$. A distinctive feature at point $T(\lambda_2 = 0, \lambda_4, a_1 = 0)$ are the two different modes of vanishing of a_1 . In contrast to the situation at point T in Figs. 4(d) and 4(h), which is characterized by $\lambda_4 \neq 0$, at point T in Figs. 4(b), 4(c), 4(e), and 4(g), with $\lambda_4 = 0$,

$$\tilde{\mathbf{K}}_{T,\lambda\lambda} \mathbf{v}_1 = \mathbf{0} \xrightarrow{(16)} a_1 = 0, \quad (87)$$

which is a stronger condition than the vanishing of the quadratic form $\mathbf{v}_1^T \tilde{\mathbf{K}}_{T,\lambda\lambda} \mathbf{v}_1$.

Another distinctive feature of the curves $\lambda_2 = \lambda_2(\kappa)$, $\lambda_4 = \lambda_4(\kappa)$, $a_1 = a_1(\kappa)$ at point T ($\lambda_2 = 0$, λ_4 , $a_1 = 0$) follows from the first two partial derivatives of (48) with respect to κ , which are obtained as

$$2(a_{1,\kappa} \lambda_2 + a_1 \lambda_{2,\kappa}) + b_{2,\kappa} = 0 \quad \text{and} \quad 2(a_{1,\kappa\kappa} \lambda_2 + 2a_{1,\kappa} \lambda_{2,\kappa} + a_1 \lambda_{2,\kappa\kappa}) + b_{2,\kappa\kappa} = 0. \quad (88)$$

Specialization of the Eqs. (88) for $\lambda_2 = 0$ and $a_1 = 0$ gives

$$b_{2,\kappa} = 0 \quad \text{and} \quad 2a_{1,\kappa} \lambda_{2,\kappa} + b_{2,\kappa\kappa} = 0. \quad (89)$$

At point $T(\lambda_2 = 0, \lambda_4, a_1 = 0)$ also $\lambda_{2,\kappa}$ may vanish, which is the case at this point in Figs. 4(c) and 4(g), and at points T in Fig. 4(h). In contrast to point T in Fig. 4(c), at point T in Fig. 4(g) and at points T in Fig. 4(h),

$$a_{1,\kappa} = 0. \quad (90)$$

Differentiation of (16) with respect to κ yields

$$a_{1,\kappa} = -\frac{1}{2} \left[\frac{(2 \mathbf{v}_1^T \tilde{\mathbf{K}}_{T,\lambda\lambda} \mathbf{v}_{1,\kappa} + \mathbf{v}_1^T \mathbf{K}_{T,\lambda\lambda\kappa} \mathbf{v}_1) \mathbf{v}_1^T \tilde{\mathbf{K}}_{T,\lambda} \mathbf{v}_1}{(\mathbf{v}_1^T \tilde{\mathbf{K}}_{T,\lambda} \mathbf{v}_1)^2} - \frac{(2 \mathbf{v}_1^T \tilde{\mathbf{K}}_{T,\lambda} \mathbf{v}_{1,\kappa} + \mathbf{v}_1^T \mathbf{K}_{T,\lambda\kappa} \mathbf{v}_1) \mathbf{v}_1^T \tilde{\mathbf{K}}_{T,\lambda\lambda} \mathbf{v}_1}{(\mathbf{v}_1^T \tilde{\mathbf{K}}_{T,\lambda} \mathbf{v}_1)^2} \right]. \quad (91)$$

Specialization of (91) for $a_1 = 0$, considering (16), and for $a_{1,\kappa} = 0$ results in

$$2 \mathbf{v}_1^T \tilde{\mathbf{K}}_{T,\lambda\lambda} \mathbf{v}_{1,\kappa} + \mathbf{v}_1^T \mathbf{K}_{T,\lambda\lambda\kappa} \mathbf{v}_1 = 0, \quad (92)$$

where

$$\mathbf{K}_{T,\lambda\lambda\kappa} = \tilde{\mathbf{K}}_{T,\lambda\lambda\lambda} \lambda_{,\kappa} + \mathbf{K}_{T,\lambda\lambda\mathbf{u}} \mathbf{u}_{,\kappa} \quad \text{with} \quad \lambda_{,\kappa} \equiv \lambda_{C,\kappa} \quad \text{and} \quad \mathbf{u}_{,\kappa} \equiv \mathbf{u}_{C,\kappa}. \quad (93)$$

Substitution of (93) into (92) gives

$$2 \mathbf{v}_1^T \tilde{\mathbf{K}}_{T,\lambda\lambda} \mathbf{v}_{1,\kappa} + \mathbf{v}_1^T \tilde{\mathbf{K}}_{T,\lambda\lambda\lambda} \mathbf{v}_1 \lambda_{C,\kappa} + \mathbf{v}_1^T \mathbf{K}_{T,\lambda\lambda\mathbf{u}} \mathbf{u}_{,\kappa} \mathbf{v}_1 = 0. \quad (94)$$

At point T in Fig. 4(g) (*von Mises* truss), because of (87.1), (94) disintegrates into two parts. At points T in Fig. 4(h), because of (63.1), (94) disintegrates into two other parts. At point T in Fig. 4(g) (cylindrical panel), because of (63.1) and (87.1), (94) disintegrates into three parts.

Table 1 contains the values of $\lambda_{2,\kappa}$, λ_4 , and a_1 for points $T(\lambda_2 = 0, \lambda_4, a_1)$ in Figs. 4(a)–4(h). The topic of completeness of these solutions will be addressed in Section 7.

Table 1

Values of $\lambda_{2,\kappa}$, λ_4 , and a_1 for points $T(\lambda_2 = 0, \lambda_4, a_1)$ in Figs. 4(a)–4(h)

Fig. 4()	a	b	c	d	e	f	g	h
$\lambda_{2,\kappa}$	$\neq 0$	$\neq 0$	0	$\neq 0$	$\lambda_2(\kappa) \geq 0$	$\lambda_2(\kappa) = 0$	$\lambda_2(\kappa) = 0$	$\lambda_2(\kappa) = 0$
λ_4	0	0	0	< 0	$\lambda_4(\kappa) = 0$	$\lambda_4(\kappa) = 0$	$\lambda_4(\kappa) = 0$	$\lambda_4(\kappa) < 0$
a_1	< 0	0	0	0	$a_1(\kappa) \geq 0$	$a_1(\kappa) < 0$	$a_1(\kappa) = 0$	$a_1(\kappa) = 0$

In the following, the individual plots of curves $\lambda_2 = \lambda_2(\kappa)$, $\lambda_4 = \lambda_4(\kappa)$, $a_1 = a_1(\kappa)$ in Fig. 4 will be discussed.

5.2 Discussion of Figs. 4(a)–4(h)

Each point of the eight curves in Fig. 4 is associated with Eq. (8). An arbitrary point of the curves in Figs. 4(a) and 4(b) is additionally associated with Eq. (62) and an arbitrary point of the curves in Figs. 4(c), 4(d), and 4(e) with Eq. (63).

Each point T of the eight curves in Fig. 4 is associated with the Eqs. (64). Point T in Fig. 4(a) and points T in Fig. 4(f) are additionally associated with (66). Point T in Figs. 4(b), 4(c), 4(e), and 4(g) is additionally associated with (67.1) and (72.1), respectively. Moreover, point T in Fig. 4(b) is also associated with (67.2), whereas point T in Figs. 4(c) and 4(e) is also associated with (72.2); point T in Fig. 4(g) may also be associated with this relation. Point T in Fig. 4(d) and points T in Fig. 4(h) are additionally associated with (70).

- Fig. 4(a). At point T ,

$$\lambda_2 = 0, \quad \lambda_4 = 0, \quad \lambda_6 = 0, \dots, \quad a_1 < 0, \quad a_1^* < 0. \quad (95)$$

At this point, the transition from imperfection sensitivity into imperfection insensitivity occurs. At point I ,

$$\lambda_2 > 0, \quad \lambda_4 > 0, \quad \lambda_6 > 0, \dots, \quad \tilde{\mathbf{K}}_{T,\lambda\lambda} \mathbf{v}_1 = \mathbf{0} \xrightarrow{(16)} a_1 = 0, \quad a_1^* > 0. \quad (96)$$

- Fig. 4(b). At point T ,

$$\lambda_2 = 0, \quad \lambda_4 = 0, \quad \lambda_6 = 0, \dots, \quad \tilde{\mathbf{K}}_{T,\lambda\lambda} \mathbf{v}_1 = \mathbf{0} \xrightarrow{(16)} a_1 = 0, \quad a_1^* > 0. \quad (97)$$

At this point, the transition from imperfection sensitivity into imperfection insensitivity occurs.

• *Fig. 4(c)*. In contrast to Figs. 4(a) and 4(b), Fig. 4(c) does not indicate a conversion from an imperfection-sensitive into an imperfection-insensitive structure at point T . However, a transition from $\lambda_4 > 0$ to $\lambda_4 < 0$ occurs at this point of the space curve. As mentioned previously, point H is a bifurcation point coinciding with a snap-through point. This situation is referred to as hilltop bifurcation (Fujii [3]). As will be shown in the following, point H represents an improper cusp of the space curve in Fig. 4(b), characterized by $a_1 = -\infty$. Hilltop bifurcation is restricted to octant VII in Fig. 3. Thus,

$$\lambda_2 < 0, \quad \lambda_4 < 0. \quad (98)$$

Obviously, hilltop bifurcation is associated with imperfection sensitivity.

In order to prove that $a_1 = -\infty$ for point H , $\tilde{\mathbf{K}}_{T,\lambda}$ and $\tilde{\mathbf{K}}_{T,\lambda\lambda}$ are expressed in terms of a path parameter ξ and inserted in (16):

$$a_1 = -\frac{1}{2} \frac{v_1^T \frac{\tilde{\mathbf{K}}_{T,\xi\xi} \lambda_{,\xi} - \tilde{\mathbf{K}}_{T,\xi} \lambda_{,\xi\xi}}{(\lambda_{,\xi})^3} v_1}{v_1^T \frac{\tilde{\mathbf{K}}_{T,\xi}}{\lambda_{,\xi}} v_1} = -\frac{1}{2\lambda_{,\xi}} \left(\frac{v_1^T \tilde{\mathbf{K}}_{T,\xi\xi} v_1}{v_1^T \tilde{\mathbf{K}}_{T,\xi} v_1} - \frac{\lambda_{,\xi\xi}}{\lambda_{,\xi}} \right). \quad (99)$$

(In contrast to the path parameter η (see (2)), ξ refers to the primary path.)

At point H ,

$$d\lambda = 0 \quad \rightarrow \quad \lambda_{,\xi} = 0. \quad (100)$$

Insertion of (100.2) into (99) and consideration of

$$\lambda_{,\xi\xi} < 0 \quad (101)$$

and of the fact that the first term in parentheses in (99) remains finite, results in

$$a_1 = -\infty, \quad q. e. d. \quad (102)$$

Furthermore, at point H ,

$$a_{1,\kappa} = 0, \quad a_{1,\kappa\kappa} = \infty, \quad (103)$$

indicating the aforementioned improper cusp of the space curve $\lambda_2 = \lambda_2(\kappa)$, $\lambda_4 = \lambda_4(\kappa)$, $a_1 = a_1(\kappa)$ in Fig. 4(c).

As mentioned previously, the parameter of the space curve illustrated in Fig. 4(c) refers to the thickness of a cylindrical panel (see Part II of this work [12]). According to expectation, the uniform increase of the thickness of this structure results in an increase of the buckling pressure. However, it does not result in the desired conversion of the initial postbuckling behavior from imperfection sensitive into imperfection insensitive.

• *Fig. 4(d)*. Point S is assumed to be a point located on the space curve shown in Fig. 4(c). Hence, the space curve in Fig. 4(d) can be thought of as being the second part of a sequence of two curves, the first of which is a portion of the space curve shown in Fig. 4(c). Because of the transition from $\lambda_2 < 0$ to $\lambda_2 > 0$ at point T , a conversion from an imperfection-sensitive into an imperfection-insensitive structure occurs. In contrast to the situation at point T in Figs. 4(a)–4(c), characterized by $\lambda_4 = 0$, however,

$$\lambda_4 < 0. \quad (104)$$

• *Fig. 4(e)*. This Figure refers to the special case $S=T$ of the general situation illustrated in Fig. 4(d). Hence, point $S=T$ agrees with point T in Fig. 4(c). Fig. 4(e) is characterized by

$$\lambda_4(\kappa) = 0. \quad (105)$$

• *Fig. 4(f)*. Point $S=T$ is assumed to agree with point T in Fig. 4(a). Hence, the thick vertical line in Fig. 4(f) can be thought of as being the second part of a sequence of two curves, the first of which is a portion of the space curve shown in Fig. 4(a). Point $F=N=T$ refers to the previously mentioned limiting case of transition from bifurcation buckling to no buckling. It is characterized by

$$\lambda_{,\xi} = 0, \quad \lambda_{,\xi\xi} = 0, \quad v_1 = 0, \quad (106)$$

indicating saddle points on the primary paths and the degeneration of the secondary paths to these points, respectively (see point C in Fig. 5(a)). Hence, the second term in parentheses in (99) is an indeterminate expression. Application of de L'Hospital's rule to this expression gives

$$\frac{\lambda_{,\xi\xi}}{\lambda_{,\xi}} = \frac{0}{0} = \frac{\lambda_{,\xi\xi\xi}}{\lambda_{,\xi\xi}} = \infty. \quad (107)$$

Since the first term in parentheses in (99) remains finite,

$$a_1 = -\infty. \quad (108)$$

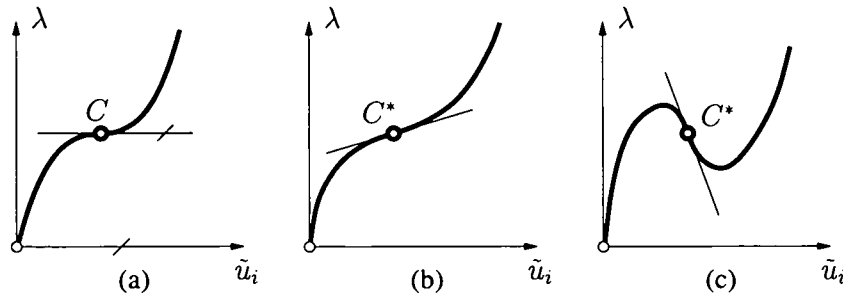


Fig. 5. Degeneration of secondary paths to a point on load-displacement curves [saddle point (Fig. 5(a)) and point of inflection (Figs. 5(b) and 5(c)), respectively]

The eigenvector of the singular matrix $\tilde{\mathbf{K}}_T$ follows from specialization of the infinitesimally incremental equilibrium equation

$$\tilde{\mathbf{K}}_T d\tilde{\mathbf{u}} = d\lambda \bar{\mathbf{P}} \quad (109)$$

for $d\lambda = 0$. Thus, $d\tilde{\mathbf{u}}$ is the eigenvector of $\tilde{\mathbf{K}}_T$.

• *Fig. 4(g)*. Point $S=T$ is assumed to agree with point T in Fig. 4(b) and Fig. 4(c), respectively. Hence, the origin of the system of reference in Fig. 4(g) can be thought of as being the second part of a sequence of curves, the first of which is a portion of the space curve shown in Fig. 4(b) and Fig. 4(c), respectively. At point T , (67.1) holds true. Expressing $\tilde{\mathbf{K}}_{T,\lambda\lambda}$ in terms of the path parameter ξ , gives

$$\frac{\frac{\tilde{\mathbf{K}}_{T,\xi\xi} \lambda_{,\xi} - \tilde{\mathbf{K}}_{T,\xi} \lambda_{,\xi\xi}}{(\lambda_{,\xi})^3}}{\frac{\mathbf{v}_1^T \tilde{\mathbf{K}}_{T,\xi} \mathbf{v}_1}{\lambda_{,\xi}}}. \quad (110)$$

Substitution of (110) into (67.1) yields

$$\left(\tilde{\mathbf{K}}_{T,\xi\xi} - \frac{\lambda_{,\xi\xi}}{\lambda_{,\xi}} \tilde{\mathbf{K}}_{T,\xi} \right) \mathbf{v}_1 = \mathbf{0}. \quad (111)$$

Point $F=N=T$ refers to the limiting case of transition from bifurcation buckling to no buckling, characterized by (106) and Fig. 5(a). Application of de L'Hospital's rule to the indeterminate expression $(\lambda_{,\xi\xi}/\lambda_{,\xi}) \mathbf{v}_1$ gives

$$\frac{\lambda_{,\xi\xi} \mathbf{v}_1}{\lambda_{,\xi}} = \frac{0}{0} \cdot \mathbf{0} = \frac{\lambda_{,\xi\xi\xi} \mathbf{v}_1 + \lambda_{,\xi\xi} \mathbf{v}_{1,\xi}}{\lambda_{,\xi\xi}} = \mathbf{v}_{1,\xi}. \quad (112)$$

Hence, for this limiting case,

$$\tilde{\mathbf{K}}_{T,\xi} \mathbf{v}_{1,\xi} = \mathbf{0}, \quad (113)$$

which indicates that $\tilde{\mathbf{K}}_{T,\xi}$ is a singular matrix with $\mathbf{v}_{1,\xi}$ as the eigenvector. As occurs for the limiting case associated with point $F=N=T$ in Fig. 4(f),

$$\tilde{\mathbf{K}}_T d\tilde{\mathbf{u}} = \mathbf{0}. \quad (114)$$

• *Fig. 4(h)*. Point $S=T$ is assumed to agree with point T in Fig. 4(d). Hence, the thick horizontal line in Fig. 4(h) can be thought of as being the second part of a sequence of curves, the first of which is a portion of the space curve shown in Fig. 4(d). At point T , (70.1) holds true. Consequently, the expression in parentheses in (99) must vanish. Thus,

$$\frac{\lambda_{,\xi\xi}}{\lambda_{,\xi}} = \frac{\mathbf{v}_1^T \tilde{\mathbf{K}}_{T,\xi\xi} \mathbf{v}_1}{\mathbf{v}_1^T \tilde{\mathbf{K}}_{T,\xi} \mathbf{v}_1}. \quad (115)$$

Point $F=N=T$ refers to the limiting case of transition from bifurcation buckling to no buckling, characterized by (106) and Fig. 5(a). Application of de L'Hospital's rule to the indeterminate expressions in (115) yields

$$\frac{\lambda_{,\xi\xi\xi}}{\lambda_{,\xi\xi}} = \frac{\mathbf{v}_{1,\xi}^T \tilde{\mathbf{K}}_{T,\xi\xi} \mathbf{v}_{1,\xi}}{\mathbf{v}_{1,\xi}^T \tilde{\mathbf{K}}_{T,\xi} \mathbf{v}_{1,\xi}}. \quad (116)$$

Because of $\lambda_{,\xi\xi} = 0$ and $\lambda_{,\xi\xi\xi} \neq 0$,

$$\mathbf{v}_{1,\xi}^T \tilde{\mathbf{K}}_{T,\xi} \mathbf{v}_{1,\xi} = 0. \quad (117)$$

Just as point C in Fig. 5(a), also point C^* in Figs. 5(b) and 5(c) refers to the transition to no loss of stability. (As far as Fig. 5(c) is concerned, this transition is irrelevant because it is preceded by snap-through.) However, in contrast to the situation at point C in Fig. 5(a), where $\tilde{\mathbf{K}}_T$ is just still singular, at point C^* in Figs. 5(b) and 5(c), $\tilde{\mathbf{K}}_T$ has just become regular.

To investigate the situation at this point, Eq. (109) is rewritten as

$$\tilde{\mathbf{K}}_T \tilde{\mathbf{u}}_{,\lambda} = \tilde{\mathbf{P}}. \quad (118)$$

Differentiation of (118) with respect to λ gives

$$\tilde{\mathbf{K}}_T \tilde{\mathbf{u}}_{,\lambda\lambda} + \tilde{\mathbf{K}}_{T,\lambda} \tilde{\mathbf{u}}_{,\lambda} \tilde{\mathbf{u}}_{,\lambda} = \mathbf{0}. \quad (119)$$

At point C^* , (119) disintegrates into

$$\tilde{\mathbf{K}}_T \tilde{\mathbf{u}}_{,\lambda\lambda} = \mathbf{0} \quad \text{and} \quad \tilde{\mathbf{K}}_{T,\lambda} \tilde{\mathbf{u}}_{,\lambda} \tilde{\mathbf{u}}_{,\lambda} = \mathbf{0}. \quad (120)$$

Since $\tilde{\mathbf{K}}_T$ is regular,

$$\tilde{\mathbf{u}}_{,\lambda\lambda} = \mathbf{0}. \quad (121)$$

Expressing $\tilde{\mathbf{u}}_{,\lambda\lambda}$ in terms of the path parameter ξ , yields

$$\tilde{\mathbf{u}}_{,\lambda\lambda} = \frac{\tilde{\mathbf{u}}_{,\xi\xi} \lambda_{,\xi} - \tilde{\mathbf{u}}_{,\xi} \lambda_{,\xi\xi}}{(\lambda_{,\xi})^3}. \quad (122)$$

Substitution of (122) into (121) and consideration of $\lambda_{,\xi} \neq 0$ results in

$$\tilde{\mathbf{u}}_{,\xi\xi} \lambda_{,\xi} - \tilde{\mathbf{u}}_{,\xi} \lambda_{,\xi\xi} = \mathbf{0}. \quad (123)$$

Since (121) represents a global property in the sense that all active degrees of freedom are concerned, (123) must disintegrate into

$$\tilde{\mathbf{u}}_{,\xi\xi} = \mathbf{0} \quad \text{and} \quad \lambda_{,\xi\xi} = 0. \quad (124)$$

Eq. (121) must not be confused with the vanishing of the second derivative of specific degrees of freedom with respect to λ , such as

$$\tilde{u}_{i,\lambda\lambda} = 0 \xrightarrow{(123)} \tilde{u}_{i,\xi\xi} \lambda_{,\xi} - \tilde{u}_{i,\xi} \lambda_{,\xi\xi} = 0, \quad (125)$$

where

$$\lambda_{,\xi} \neq 0, \quad \tilde{u}_{i,\xi} \neq 0, \quad \lambda_{,\xi\xi} \neq 0, \quad \tilde{u}_{i,\xi\xi} \neq 0. \quad (126)$$

Numerical examples concerning the modes of transition from bifurcation buckling to no buckling illustrated in Fig. 5 will be presented in Part II of this work [12].

6 Special case: linear prebuckling paths

In the first paragraph of Subchapter 5.2, referring to the general case of symmetric bifurcation from nonlinear prebuckling paths, the assertion was made that an arbitrary point of the first two curves in Fig. 4 is associated with

$$\mathbf{v}_j^{*T} \tilde{\mathbf{K}}_{T,\lambda\lambda} \mathbf{v}_1 = 0, \quad j \neq 1, \quad (127)$$

and of the next three curves with

$$\mathbf{v}_1^T \tilde{\mathbf{K}}_{T,\lambda\lambda\lambda} \mathbf{v}_1 = 0 \xrightarrow{(23.1)} a_1^* = 0. \quad (128)$$

These conditions are the reason for restrictions on the curves $\lambda_2 = \lambda_2(\kappa)$, $\lambda_4 = \lambda_4(\kappa)$, $a_1 = a_1(\kappa)$ in Fig. 4.

For the special case of bifurcation from linear prebuckling paths,

$$\tilde{\mathbf{K}}_{T,\lambda\lambda} = \mathbf{0} \xrightarrow{(16)} a_1 = 0, \quad \tilde{\mathbf{K}}_{T,\lambda\lambda\lambda} = \mathbf{0} \xrightarrow{(23.1)} a_1^* = 0. \quad (129)$$

Hence, the relations (127) and (128) are satisfied trivially. Because of the absence of non-trivial relations replacing (127) and (128) for the special case considered, there are no restrictions on the plane curves $\lambda_2 = \lambda_2(\kappa)$, $\lambda_4 = \lambda_4(\kappa)$, analogous to the ones for the general case.

Eq. (34) does not contain a term that vanishes for the special case of linear prebuckling paths. Hence, irrespective of whether the prebuckling paths are nonlinear or linear,

$$\lambda_2 = d_1. \quad (130)$$

Because of (129.1), the first term on the right-hand side of (36) vanishes trivially for the special case of linear prebuckling paths. Hence, (36) is reduced to

$$\lambda_4 = b_2 \lambda_2 + d_3. \quad (131)$$

The expressions for d_1 (see (19)), b_2 (see (C.2)), and d_3 (see (C.4)) do not contain terms that vanish for the special case of linear prebuckling paths.

Following from (130),

$$d_1 = 0 \quad \rightarrow \quad \lambda_2 = 0. \quad (132)$$

Hence, the condition for $\lambda_2 = 0$ is the same as for the general case (see (64)). However, the additional conditions associated with (64) for the general case, which were mentioned in the second paragraph of Subsection 5.2, are satisfied trivially for the special case of linear prebuckling paths.

Substitution of (132.2) into (131) gives

$$\lambda_4 = d_3, \quad (133)$$

which agrees with (65). Following from (131),

$$b_2 \lambda_2 + d_3 = 0 \quad \rightarrow \quad \lambda_4 = 0. \quad (134)$$

Following from (130) and (133), for

$$d_1 = 0 \quad \text{and} \quad d_3 = 0, \quad (135)$$

$$\lambda_2 = 0 \quad \text{and} \quad \lambda_4 = 0. \quad (136)$$

Figs. 6(a) and 6(b) show plots of two curves $\lambda_2 = \lambda_2(\kappa)$, $\lambda_4 = \lambda_4(\kappa)$, which contain one point T and one point Q each, for which

$$\lambda_2 = 0 \quad \text{and} \quad \lambda_4 = 0, \quad (137)$$

respectively. In Fig. 6(c), these two points coincide.

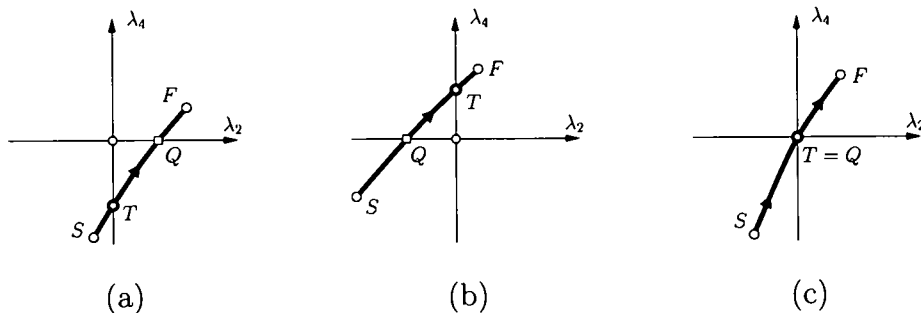


Fig. 6. Plots of curves $\lambda_2 = \lambda_2(\kappa)$, $\lambda_4 = \lambda_4(\kappa)$, with one point $T(\lambda_2 = 0, \lambda_4)$ and one point $Q(\lambda_2, \lambda_4 = 0)$ each

[κ refers to the ratio of the length of the rods of a pin-jointed bar. All rods are connected by hinges. Rotational and extensional springs are attached to the hinges (the three illustrations refer to different values of the spring constant of the extensional spring); details of the structure are given in Fig. 17 of Part II of this work [12]]

7 Completeness of solutions from Koiter's initial postbuckling analysis, containing $\lambda_2 = 0$

For bifurcation from nonlinear prebuckling paths,

$$\mathbf{v}_{1,\lambda}^* = c_{11} \mathbf{v}_1, \quad (138)$$

where (see (D.14))

$$c_{11} = a_1. \quad (139)$$

In general, $a_1 \neq 0$. Eq. (138) follows from specialization of (D.6) for

$$c_{1j} = 0, \quad j \neq 1, \quad (140)$$

resulting from substitution of $\lambda_1^* = \lambda$ into (D.10). [$\lambda_1^* - \lambda$ is the first eigenvalue and \mathbf{v}_1^* is the corresponding eigenvector of the so-called consistently linearized eigenproblem (see Appendix D). At the stability limit, $\lambda_1^* = \lambda = \lambda_C$ and $\mathbf{v}_1^* = \mathbf{v}_1$.]

Distinctive features between unsymmetric and symmetric bifurcation from nonlinear prebuckling paths follow from

$$\mathbf{v}_{1,\lambda\lambda}^* = \sum_{j=1}^n c_{1j,\lambda} \mathbf{v}_j^* + c_{11} \mathbf{v}_{1,\lambda}^*, \quad (141)$$

where

$$c_{11,\lambda} = -\frac{1}{2} \frac{2\mathbf{v}_1^{*T} \tilde{\mathbf{K}}_{T,\lambda\lambda} \mathbf{v}_{1,\lambda}^* + \mathbf{v}_1^{*T} \tilde{\mathbf{K}}_{T,\lambda\lambda\lambda} \mathbf{v}_1}{\mathbf{v}_1^{*T} \tilde{\mathbf{K}}_{T,\lambda} \mathbf{v}_1}, \quad (142)$$

resulting from derivation of (D.13) with respect to λ , consideration of (D.11), and specialization of the result for $\mathbf{v}_1^* = \mathbf{v}_1$, and

$$c_{1j,\lambda} = \frac{1}{\lambda_1^* - \lambda_j^*} \frac{\mathbf{v}_j^{*T} \tilde{\mathbf{K}}_{T,\lambda\lambda} \mathbf{v}_1}{\mathbf{v}_j^{*T} \tilde{\mathbf{K}}_{T,\lambda} \mathbf{v}_j^*}, \quad j \neq 1, \quad (143)$$

following from derivation of (D.10) with respect to λ and specialization of the result for $\lambda_1^* = \lambda$ and $\mathbf{v}_1^* = \mathbf{v}_1$. [$\lambda_j^* - \lambda$ is the j -th eigenvalue and \mathbf{v}_j^* is the corresponding eigenvector of the consistently linearized eigenproblem (see Appendix D).]

Substitution of (138) into (142) yields

$$c_{11,\lambda} = -\frac{1}{2} \frac{2(\mathbf{v}_1^{*T} \tilde{\mathbf{K}}_{T,\lambda\lambda} \mathbf{v}_1) c_{11} + \mathbf{v}_1^{*T} \tilde{\mathbf{K}}_{T,\lambda\lambda\lambda} \mathbf{v}_1}{\mathbf{v}_1^{*T} \tilde{\mathbf{K}}_{T,\lambda} \mathbf{v}_1} = 2a_1^2 + 3a_1^*, \quad (144)$$

where use of (16), (23.1), and (139) was made. Substitution of (138) with (139), and of (144) into (141) gives

$$\mathbf{v}_{1,\lambda\lambda}^* = 3(a_1^2 + a_1^*) \mathbf{v}_1 + \sum_{j=2}^n c_{1j,\lambda} \mathbf{v}_j^*. \quad (145)$$

Following from (62) and (63), respectively, for symmetric bifurcation from nonlinear prebuckling paths, (145) disintegrates either into

$$\mathbf{v}_{1,\lambda\lambda}^* = 3(a_1^2 + a_1^*)\mathbf{v}_1 \quad \wedge \quad c_{1j,\lambda} = 0, \quad j \neq 1, \quad (146)$$

or into

$$\mathbf{v}_{1,\lambda\lambda}^* = 3a_1^2\mathbf{v}_1 + \sum_{j=2}^n c_{1j,\lambda}\mathbf{v}_j^* \quad \wedge \quad a_1^* = 0. \quad (147)$$

In contrast to the second expression for $\mathbf{v}_{1,\lambda\lambda}^*$, the first expression only involves \mathbf{v}_1 .

For the special case of $\lambda_2 = 0$ within the framework of symmetric bifurcation from nonlinear prebuckling paths (points T in Figs. 4(a)–4(h)), $d_1 = 0$ (see (64)). For point T in

$$\text{Fig. 4(a): } \mathbf{v}_{1,\lambda}^* = a_1\mathbf{v}_1, \quad \mathbf{v}_{1,\lambda\lambda}^* = 3(a_1^2 + a_1^*)\mathbf{v}_1, \quad (148)$$

$$\text{Fig. 4(b): } \tilde{\mathbf{K}}_{T,\lambda\lambda}\mathbf{v}_1 = \mathbf{0} \xrightarrow{(16)} a_1 = 0, \quad (149)$$

$$\xrightarrow{(138),(139)} \mathbf{v}_{1,\lambda}^* = \mathbf{0}, \quad \xrightarrow{(146.1)} \mathbf{v}_{1,\lambda\lambda}^* = 3a_1^*\mathbf{v}_1, \quad (150)$$

$$\text{Fig. 4(c): } \tilde{\mathbf{K}}_{T,\lambda\lambda}\mathbf{v}_1 = \mathbf{0} \xrightarrow{(16)} a_1 = 0, \quad (151)$$

$$\xrightarrow{(138),(139)} \mathbf{v}_{1,\lambda}^* = \mathbf{0}, \quad \xrightarrow{(147.1)} \mathbf{v}_{1,\lambda\lambda}^* = \mathbf{0}, \quad (152)$$

$$\text{Fig. 4(d): } \mathbf{v}_1^T \tilde{\mathbf{K}}_{T,\lambda\lambda}\mathbf{v}_1 = 0 \xrightarrow{(16)} a_1 = 0, \quad (153)$$

$$\xrightarrow{(138),(139)} \mathbf{v}_{1,\lambda}^* = \mathbf{0}, \quad \xrightarrow{(147.1)} \mathbf{v}_{1,\lambda\lambda}^* = \sum_{j=2}^n c_{1j,\lambda}\mathbf{v}_j^*, \quad (154)$$

Fig. 4(e): same as in Fig. 4(c),

Fig. 4(f): same as in Fig. 4(a),

Fig. 4(g): same as in Fig. 4(b) or Fig. 4(c),

Fig. 4(h): same as in Fig. 4(d),

Hence, for the special case of $\lambda_2 = 0$ within the framework of symmetric bifurcation, $d_1 = 0$ and $\mathbf{v}_{1,\lambda}^*$ is either parallel to \mathbf{v}_1 (see (148.1)) or zero (see (150.1), (152.1), and (154.1)). If, for this special case, $\mathbf{v}_{1,\lambda}^*$ is parallel to \mathbf{v}_1 , then also $\mathbf{v}_{1,\lambda\lambda}^*$ is parallel to \mathbf{v}_1 (see (148.2)). If $\mathbf{v}_{1,\lambda}^*$ is zero, then $\mathbf{v}_{1,\lambda\lambda}^*$ is either parallel to \mathbf{v}_1 (see (150.2)) or orthogonal to \mathbf{v}_1 with respect to $\tilde{\mathbf{K}}_{T,\lambda}$ (see (154.2) and (D.7.2)), or zero (see (152.2)). Because of

$$c_{1j,\lambda} = c_{1j,\lambda}(\kappa) = 0, \quad j \neq 1 \quad \vee \quad a_1^* = a_1^*(\kappa) = 0, \quad (155)$$

it follows from (146) that the Eqs. (148) and (150) represent a complete subset of solutions for $\mathbf{v}_{1,\lambda}^*$ and $\mathbf{v}_{1,\lambda\lambda}^*$ associated with $\lambda_2 = 0$. For the same reason and because of the fact that in case of (155.2) a_1 and λ_2 necessarily vanish for the same value of κ (see Section 4), it follows from (147) that also the Eqs. (152) and (154) represent a complete subset of solutions for $\mathbf{v}_{1,\lambda}^*$ and $\mathbf{v}_{1,\lambda\lambda}^*$ associated with $\lambda_2 = 0$. Because of (151.1),

$$c_{1j,\lambda}(\lambda_2 = 0) = 0, \quad j \neq 1. \quad (156)$$

Hence, for the respective value of κ the general disjunction expressed by (155) exceptionally becomes a conjunction. The sum of the two aforementioned subsets of solutions for $\mathbf{v}_{1,\lambda}^*$ and $\mathbf{v}_{1,\lambda\lambda}^*$ associated with $\lambda_2 = 0$ represents the complete set of such solutions.

For symmetric bifurcation from linear prebuckling paths, the relations (127) and (128) are satisfied trivially. Hence, the preceding considerations are irrelevant. There is no condition for $\lambda_2 = 0$ in addition to $d_1 = 0$ (see (132)).

8 Conclusions

- Conversion from imperfection-sensitive into imperfection-insensitive structures requires symmetric bifurcation. If this condition is not satisfied by the original structure and for the given loading, it must be enforced in the course of the conversion process. This may require modifications of the original design which, for different reasons, are unfeasible.
- Symmetric bifurcation from nonlinear prebuckling paths is associated either with

$$\mathbf{v}_j^{*T} \tilde{\mathbf{K}}_{T,\lambda\lambda} \mathbf{v}_1 = 0, \quad j \neq 1 \quad (\text{see (62)})$$

or with

$$\mathbf{v}_1^T \tilde{\mathbf{K}}_{T,\lambda\lambda\lambda} \mathbf{v}_1 = 0 \quad (\text{see (63)}).$$

- Eq. (62) occurs together either with $c_1^*(\kappa) \neq 0$ or with $c_1^*(\kappa) = 0$, the latter resulting in

$$2a_1\lambda_2 + b_2 = 0 \quad (\text{see (48)}) \quad \text{and} \quad \lambda_4 = -a_1\lambda_2^2 + d_3 \quad (\text{see (51)}).$$

Eq. (63) only occurs together with $c_1^*(\kappa) = 0 \rightarrow$ Eqs. (48) and (51). The Eqs. (62) and (63) result in two different modes of disintegration of an expression that holds for unsymmetric bifurcation from nonlinear prebuckling paths (see (145)–(147)).

- The geometric loci of all points in the λ_4 - a_1 plane of the λ_2 - λ_4 - a_1 space, which are solutions of

$$\lambda_4 = a_1\lambda_2^2 + b_2\lambda_2 + d_3 \quad (\text{see (36)})$$

with $\lambda_2 = 0$, are restricted to the two half-axes $\lambda_4 \leq 0$ and $a_1 \leq 0$ (see Fig. 2). This restriction seems to be a consequence of the condition for symmetric bifurcation,

$$\lambda_1 = \lambda_3 = \dots = 0 \quad (\text{see (27)}),$$

which is stronger than the conditions $\lambda_1 = 0$ and $\lambda_3 = 0$ on which the above expression for λ_4 is based.

- The relations (66) and (67), respectively, refer to modes of conversion from imperfection-sensitive into imperfection-insensitive structures, which are characterized by

$$\lambda_2 = \lambda_4 = \lambda_6 = \dots = 0 \quad (\text{see (68)}).$$

- The relations (70) refer to a mode of conversion from imperfection-sensitive into imperfection-insensitive structures, which is characterized by

$$\lambda_2 = 0, \quad \lambda_4 < 0 \quad (\text{see (71)}).$$

- $\lambda_2 = 0$ is a necessary but not a sufficient condition for the transition from imperfection sensitivity to imperfection insensitivity. For

$$\lambda_2 = 0, \quad \lambda_4 = 0, \quad \lambda_6 < 0,$$

such a transition does not occur (see point T in Fig. 4(c)). This situation is characterized by

$$\tilde{\mathbf{K}}_{T,\lambda\lambda} \mathbf{v}_1 = \mathbf{0} \quad \text{and} \quad \mathbf{v}_1^T \tilde{\mathbf{K}}_{T,\lambda\lambda\lambda} \mathbf{v}_1 = 0 \quad (\text{see (78.2) and (78.3)}).$$

- Hilltop bifurcation is characterized by

$$\lambda_2 < 0, \quad \lambda_4 < 0, \quad a_1 = -\infty \quad (\text{see (98) and (102), respectively}).$$

- The transition from bifurcation buckling to no loss of stability is characterized by

$$\lambda_{,\xi} = 0, \quad \lambda_{,\xi\xi} = 0, \quad \mathbf{v}_1 = \mathbf{0} \quad (\text{see (106)}),$$

indicating the existence of saddle points on the primary paths and the degeneration of the secondary paths to these points, respectively (see point C in Fig. 5(a)).

Alternatively,

$$\tilde{\mathbf{u}}_{,\xi\xi} = \mathbf{0}, \quad \lambda_{,\xi\xi} = 0, \quad (\text{see (126)}),$$

indicating the existence of points of inflection on the primary paths and the degeneration of the secondary paths to these points, respectively (see point C^* in Figs. 5(b) and 5(c)).

- For the special case of linear prebuckling paths,

$$\tilde{\mathbf{K}}_{T,\lambda\lambda} = \mathbf{0}, \quad \tilde{\mathbf{K}}_{T,\lambda\lambda\lambda} = \mathbf{0}, \quad \dots \quad (\text{see (129)}).$$

Hence, (62) and (63) are satisfied trivially.

- For this special case, in contrast to the general case of symmetric bifurcation from non-linear prebuckling paths, $\lambda_2 = 0$ may also occur jointly with $\lambda_4 > 0$ (see Fig. 6(b)).
- To each point on a space curve $\lambda_2 = \lambda_2(\kappa)$, $\lambda_4 = \lambda_4(\kappa)$, $a_1 = a_1(\kappa)$ (see Fig. 4) a curve $\lambda_1^*(\lambda)$ can be related, which is part of the solution of the consistently linearized eigenproblem (see Appendix D). It was shown that the curves $\lambda_1^*(\lambda)$ related to point $T(\lambda_2 = 0, \lambda_4, a_1)$ in Fig. 4 (with the exception of Figs. 4(a) and 4(f)) have specific geometric properties at the bifurcation point $\lambda_1^* = \lambda$.

- The investigation of these properties was motivated by the need to ensure the completeness of the solutions for the initial postbuckling paths with $\lambda_2 = 0$ for the general case of symmetric bifurcation from nonlinear prebuckling paths (see (148)–(154)).
- Reducing the initial rise of an imperfection-sensitive structure eventually results in the transition from bifurcation buckling to no loss of stability. However, such a reduction is associated with a decrease of the stability limit. Increasing the stiffness of a structure by means of a uniform increase of its thickness does not result in the conversion from imperfection sensitivity into insensitivity. Increasing the stiffness of an elastic spring, suitably attached to the structure, however, usually enables its conversion from an imperfection-sensitive into an imperfection-insensitive structure. Based on these conclusions from Part II of this work [12], it seems that additional supports of a structure may be effective means to achieve the desired conversion.
- A challenge for future scientific work is to investigate the effectiveness of different modes of additional support of the original structure, which are feasible from the design standpoint, to accomplish such a conversion.

Acknowledgments

The authors are indebted to B. Krenn for many helpful remarks and particularly for informing them about the existence of a case of conversion from an imperfection-sensitive into an imperfection-insensitive structure (see Fig. 4(a)), which they have missed originally. The second author thankfully acknowledges partial financial support by the Austrian Science Fund under the contract P14808.

Appendices

A Coefficient tensors for Koiter's postbuckling analysis in the context of the FEM

Because of successive application of the chain rule, the expressions for some of the coefficient tensors in (4) become relatively lengthy. Introduction of special tensor-valued functions and of a rule for differentiation, which combines partial and directional derivatives, allows to write these expressions in comparatively compact form.

In the standard FEM, $\mathbf{G}_{,\mathbf{u}}$ is referred to as the tangent stiffness matrix $\mathbf{K}_T(\mathbf{u})$. For proportional loading, $\mathbf{G}_{,\mathbf{u}}$ does not explicitly depend on λ . Nevertheless, a matrix curve

$$\tilde{\mathbf{K}}_T(\lambda) := \mathbf{K}_T(\tilde{\mathbf{u}}(\lambda)) = \mathbf{G}_{,\mathbf{u}}(\tilde{\mathbf{u}}(\lambda)), \quad \lambda \in \mathcal{J} \subset \mathbb{R}, \quad (\text{A.1})$$

may be defined along the equilibrium path $\mathbf{u} = \tilde{\mathbf{u}}(\lambda)$. This matrix function is identical with the tangent stiffness matrix $\mathbf{K}_T(\lambda)$ in papers by Helnwein [5], Helnwein and Mang [6], and Helnwein et al. [7]. In the present paper, $\tilde{\mathbf{K}}_T(\lambda)$ indicates equilibrium states on the primary path whereas $\mathbf{K}_T(\mathbf{u})$ refers to configurations which, in general, represent out-of-balance states. The main objective of introducing the above definition of $\tilde{\mathbf{K}}_T(\lambda)$ is to increase the compactness of the expressions for the coefficient tensors in (4).

The tangent, curvature, and higher-order derivatives of the matrix curve (A.1) along the equilibrium path are computed as follows:

$$\tilde{\mathbf{K}}_{T,\lambda}(\lambda) = \mathbf{G}_{,\mathbf{uu}} \cdot \tilde{\mathbf{u}}_{,\lambda}, \quad (\text{A.2})$$

$$\tilde{\mathbf{K}}_{T,\lambda\lambda}(\lambda) = \mathbf{G}_{,\mathbf{uuu}} : \tilde{\mathbf{u}}_{,\lambda} \otimes \tilde{\mathbf{u}}_{,\lambda} + \mathbf{G}_{,\mathbf{uu}} \cdot \tilde{\mathbf{u}}_{,\lambda\lambda}, \quad (\text{A.3})$$

$$\tilde{\mathbf{K}}_{T,\lambda\lambda\lambda}(\lambda) = \mathbf{G}_{,\mathbf{uuuu}} : \tilde{\mathbf{u}}_{,\lambda} \otimes \tilde{\mathbf{u}}_{,\lambda} \otimes \tilde{\mathbf{u}}_{,\lambda} + 3 \mathbf{G}_{,\mathbf{uuu}} : \tilde{\mathbf{u}}_{,\lambda} \otimes \tilde{\mathbf{u}}_{,\lambda\lambda} + \mathbf{G}_{,\mathbf{uu}} \cdot \tilde{\mathbf{u}}_{,\lambda\lambda\lambda}, \quad (\text{A.4})$$

$$\vdots \quad \quad \quad \vdots \quad \quad \quad \cdot$$

The chosen notation emphasizes that these relations only hold for points located on the primary path $\tilde{\mathbf{u}}(\lambda)$.

To increase the compactness of the notation, a special rule for differentiation of derivatives of a tensor-valued function $\mathbf{A}(\mathbf{u}, \lambda)$ with respect to the load parameter λ is introduced:

$$[\mathbf{A}(\mathbf{u}, \lambda)]_{,\lambda} := \frac{\partial}{\partial \lambda} \mathbf{A}(\mathbf{u}, \lambda) + \frac{d}{d\alpha} \mathbf{A}(\mathbf{u} + \alpha \tilde{\mathbf{u}}_{,\lambda}(\lambda), \lambda) \Big|_{\alpha=0}. \quad (\text{A.5})$$

Applying (A.5) to the tangent stiffness matrix $\mathbf{K}_T(\mathbf{u})$, yields

$$\begin{aligned} \mathbf{K}_{T,\lambda}(\mathbf{u}, \lambda) &= [\mathbf{K}_T(\mathbf{u})]_{,\lambda} = [\mathbf{G}_{,\mathbf{u}}(\mathbf{u})]_{,\lambda} \\ &= \frac{\partial}{\partial \lambda} \mathbf{G}_{,\mathbf{u}}(\mathbf{u}) + \frac{d}{d\alpha} \Big|_{\alpha=0} \mathbf{G}_{,\mathbf{u}}(\mathbf{u} + \alpha \tilde{\mathbf{u}}_{,\lambda}(\lambda)) = \mathbf{G}_{,\mathbf{uu}}(\mathbf{u}) \cdot \tilde{\mathbf{u}}_{,\lambda}(\lambda). \end{aligned} \quad (\text{A.6})$$

Specialization of (A.6) for points on the primary path gives $\mathbf{K}_{T,\lambda}(\tilde{\mathbf{u}}(\lambda), \lambda) = \tilde{\mathbf{K}}_{T,\lambda}(\lambda)$. The partial derivative $\partial \mathbf{K}_T(\mathbf{u}) / \partial \lambda = \partial \mathbf{G}_{,\mathbf{u}}(\mathbf{u}) / \partial \lambda$ vanishes because, as mentioned previously, $\mathbf{G}_{,\mathbf{u}}$ does not explicitly depend on λ . Nevertheless, differentiation according to (A.5)

generates functions which are defined in the whole domain of (\mathbf{u}, λ) . In contrast to these functions, the ones according to the Eqs. (A.2)–(A.4) are only defined along the primary path $\tilde{\mathbf{u}}(\lambda)$.

As an example, $\mathbf{K}_{T,\mathbf{u}\lambda\lambda}(\mathbf{u}, \lambda) = [\mathbf{K}_{T,\mathbf{u}\lambda}(\mathbf{u})]_{,\lambda}$ will be computed in the following:

$$\begin{aligned} \mathbf{K}_{T,\mathbf{u}\lambda\lambda}(\mathbf{u}, \lambda) &= [\mathbf{K}_{T,\mathbf{u}\lambda}(\mathbf{u})]_{,\lambda} = [\mathbf{G}_{,\mathbf{u}\mathbf{u}\mathbf{u}}(\mathbf{u}) \cdot \tilde{\mathbf{u}}_{,\lambda}(\lambda)]_{,\lambda} \\ &= \frac{\partial}{\partial \lambda} (\mathbf{G}_{,\mathbf{u}\mathbf{u}\mathbf{u}} \cdot \tilde{\mathbf{u}}_{,\lambda}) + \frac{d}{d\alpha} \Big|_{\alpha=0} [\mathbf{G}_{,\mathbf{u}\mathbf{u}\mathbf{u}}(\mathbf{u} + \alpha \tilde{\mathbf{u}}_{,\lambda}(\lambda)) \cdot \tilde{\mathbf{u}}_{,\lambda}] \\ &= \mathbf{G}_{,\mathbf{u}\mathbf{u}\mathbf{u}} \cdot \tilde{\mathbf{u}}_{,\lambda\lambda} + \mathbf{G}_{,\mathbf{u}\mathbf{u}\mathbf{u}\mathbf{u}} : \tilde{\mathbf{u}}_{,\lambda} \otimes \tilde{\mathbf{u}}_{,\lambda}. \end{aligned} \quad (\text{A.7})$$

Comparison of this result with the one obtained from differentiation of (A.3) with respect to \mathbf{u} yields the symmetry relation $\mathbf{K}_{T,\mathbf{u}\lambda\lambda} = \mathbf{K}_{T,\lambda\lambda\mathbf{u}}$. Analogous symmetry relations hold for all other mixed derivatives.

Further simplifications follow from the function $\tilde{\mathbf{G}}(\lambda) : \mathcal{J} \rightarrow \mathbb{R}^n$ as:

$$\tilde{\mathbf{G}}(\lambda) := \mathbf{G}(\tilde{\mathbf{u}}(\lambda), \lambda) \equiv \mathbf{0}, \quad (\text{A.8})$$

$$\tilde{\mathbf{G}}_{,\lambda} = \mathbf{G}_{,\mathbf{u}} \cdot \tilde{\mathbf{u}}_{,\lambda} + \mathbf{G}_{,\lambda} = \tilde{\mathbf{K}}_T \cdot \tilde{\mathbf{u}}_{,\lambda} - \tilde{\mathbf{P}} = \mathbf{0}, \quad (\text{A.9})$$

$$\tilde{\mathbf{G}}_{,\lambda\lambda} = \mathbf{G}_{,\mathbf{u}\mathbf{u}} : \tilde{\mathbf{u}}_{,\lambda} \otimes \tilde{\mathbf{u}}_{,\lambda} + \mathbf{G}_{,\mathbf{u}} \cdot \tilde{\mathbf{u}}_{,\lambda\lambda} = \mathbf{0}, \quad (\text{A.10})$$

$$\tilde{\mathbf{G}}_{,\lambda\lambda\lambda} = \mathbf{G}_{,\mathbf{u}\mathbf{u}\mathbf{u}} : \tilde{\mathbf{u}}_{,\lambda} \otimes \tilde{\mathbf{u}}_{,\lambda} \otimes \tilde{\mathbf{u}}_{,\lambda} + 3 \mathbf{G}_{,\mathbf{u}\mathbf{u}} : \tilde{\mathbf{u}}_{,\lambda} \otimes \tilde{\mathbf{u}}_{,\lambda\lambda} + \mathbf{G}_{,\mathbf{u}} \cdot \tilde{\mathbf{u}}_{,\lambda\lambda\lambda} = \mathbf{0}, \quad (\text{A.11})$$

$$\vdots \quad \quad \quad \vdots \quad \quad \quad \cdot$$

Eq. (A.8) expresses a trivial identity which directly results from the definition of the primary path $\tilde{\mathbf{u}}(\lambda)$. The Eqs. (A.9), (A.10), (A.11), ... allow successive computation of the vectors $\tilde{\mathbf{u}}_{,\lambda}$, $\tilde{\mathbf{u}}_{,\lambda\lambda}$, $\tilde{\mathbf{u}}_{,\lambda\lambda\lambda}$, ... Because of $\det \mathbf{G}_{,\mathbf{u}}|_{\mathbf{u}_C} = \det \tilde{\mathbf{K}}_T|_{\lambda_C} = 0$, the evaluation of these vectors at a bifurcation point C requires use of their limits, as $\lambda \rightarrow \lambda_C$. Moreover, the above relations cause the vanishing of the vectors $\mathbf{G}_{,\eta}^+|_C$, $\mathbf{G}_{,\eta\eta}^+|_C$, $\mathbf{G}_{,\eta\eta\eta}^+|_C$, ...

Computation of the first-order coefficient tensors (vectors) $\mathbf{G}_{,\eta}^+$, $\mathbf{G}_{,\eta\eta}^+$, $\mathbf{G}_{,\eta\eta\eta}^+$, ..., second-order tensors (matrices) $\mathbf{G}_{,\mathbf{v}}^+$, $\mathbf{G}_{,\mathbf{v}\eta}^+$, $\mathbf{G}_{,\mathbf{v}\eta\eta}^+$, ..., third-order tensors $\mathbf{G}_{,\mathbf{v}\mathbf{v}}^+$, $\mathbf{G}_{,\mathbf{v}\mathbf{v}\eta}^+$, ..., fourth-order tensors $\mathbf{G}_{,\mathbf{v}\mathbf{v}\mathbf{v}}^+$, ..., etc., appearing in (4), follows a simple pattern. All of them depend on \mathbf{v} and η and must be expressed in terms of $\mathbf{G}(\mathbf{u}, \lambda)$. Let $\mathbf{A}^+(\mathbf{v}, \eta) := \mathbf{A}(\tilde{\mathbf{u}}(\tilde{\lambda}(\eta)) + \mathbf{v}, \tilde{\lambda}(\eta))$ be one of these tensor-valued functions. The differential of this function can be written as

$$d\mathbf{A}^+(\mathbf{v}, \eta) = \mathbf{A}_{,\mathbf{v}}^+(\mathbf{v}, \eta) \cdot d\mathbf{v} + \mathbf{A}_{,\eta}^+(\mathbf{v}, \eta) d\eta \quad (\text{A.12})$$

$$\begin{aligned} &= d\mathbf{A}(\tilde{\mathbf{u}}(\tilde{\lambda}(\eta)) + \mathbf{v}, \tilde{\lambda}(\eta)) \\ &= \mathbf{A}_{,\mathbf{u}} \cdot d\mathbf{v} + [\mathbf{A}_{,\mathbf{u}} \cdot \tilde{\mathbf{u}}_{,\lambda} + \mathbf{A}_{,\lambda}] \tilde{\lambda}_{,\eta}(\eta) d\eta. \end{aligned} \quad (\text{A.13})$$

Comparison of the Eqs. (A.12) and (A.13) yields

$$\mathbf{A}_{,\mathbf{v}}^+(\mathbf{v}, \eta) = \mathbf{A}_{,\mathbf{u}}|_{(\mathbf{u},\lambda)=(\tilde{\mathbf{u}}(\tilde{\lambda}(\eta))+\mathbf{v},\tilde{\lambda}(\eta))} \quad (\text{A.14})$$

$$\mathbf{A}_{,\eta}^+(\mathbf{v}, \eta) = \left[(\mathbf{A}_{,\mathbf{u}} \cdot \tilde{\mathbf{u}}_{,\lambda} + \mathbf{A}_{,\lambda}) \tilde{\lambda}_{,\eta} \right] \Big|_{(\mathbf{u},\lambda)=(\tilde{\mathbf{u}}(\tilde{\lambda}(\eta))+\mathbf{v},\tilde{\lambda}(\eta))}. \quad (\text{A.15})$$

Eventually, the coefficient tensors in (4) are obtained by evaluating the expressions for these relations at the bifurcation point C : $(\mathbf{v}, \eta) = (\mathbf{0}, 0)$ (or $(\mathbf{u}, \lambda) = (\tilde{\mathbf{u}}(\lambda_C), \lambda_C)$).

Table A.1 contains the coefficient tensors as occurring in (4), evaluated at C . Note that $\mathbf{G}_{,u\lambda} = \tilde{\mathbf{K}}_{T,\lambda} = \mathbf{G}_{,\lambda u} = -\tilde{\mathbf{P}}_{,u} = \mathbf{0}$.

Table A.1

Coefficient tensors for Koiter's post-buckling analysis in the context of the FEM, evaluated at the bifurcation point C

$$\begin{aligned}
\mathbf{G}_{,v}^+|_C &= (\mathbf{G}_{,u})|_C = \tilde{\mathbf{K}}_T(\lambda_C) \\
\mathbf{G}_{,\eta}^+|_C &= (\mathbf{G}_{,u} \cdot \tilde{u}_{,\lambda} + \mathbf{G}_{,\lambda})|_C \tilde{\lambda}_{,\eta} \stackrel{(A.9)}{=} \lambda_1 \tilde{\mathbf{G}}_{,\lambda} = \mathbf{0} \\
\mathbf{G}_{,vv}^+|_C &= (\mathbf{G}_{,uu})|_C = \mathbf{K}_{T,u}(u_C) \\
\mathbf{G}_{,v\eta}^+|_C &= (\mathbf{G}_{,uu} \cdot \tilde{u}_{,\lambda} \tilde{\lambda}_{,\eta})|_C \stackrel{(A.6)}{=} \lambda_1 \mathbf{K}_{T,\lambda}(u_C, \lambda_C) \stackrel{(A.2)}{=} \lambda_1 \tilde{\mathbf{K}}_{T,\lambda}(\lambda_C) \\
\mathbf{G}_{,\eta\eta}^+|_C &= (\mathbf{G}_{,uu} : \tilde{u}_{,\lambda} \otimes \tilde{u}_{,\lambda} + \mathbf{G}_{,u} \cdot \tilde{u}_{,\lambda\lambda})|_C (\tilde{\lambda}_{,\eta})^2 + (\mathbf{G}_{,u} \cdot \tilde{u}_{,\lambda} + \mathbf{G}_{,\lambda})|_C \tilde{\lambda}_{,\eta\eta} \\
&= (\lambda_1)^2 \tilde{\mathbf{G}}_{,\lambda\lambda} + 2\lambda_2 \tilde{\mathbf{G}}_{,\lambda} \stackrel{(A.9),(A.10)}{=} \mathbf{0} \\
\mathbf{G}_{,vvv}^+|_C &= (\mathbf{G}_{,uuu})|_C = \mathbf{K}_{T,uu}(u_C) \\
\mathbf{G}_{,vv\eta}^+|_C &= (\mathbf{G}_{,uuu} \cdot \tilde{u}_{,\lambda} \tilde{\lambda}_{,\eta})|_C = \lambda_1 \mathbf{K}_{T,uu}(u_C) \cdot \tilde{u}_{,\lambda}(\lambda_C) = \lambda_1 \mathbf{K}_{T,u\lambda}(u_C, \lambda_C) \\
\mathbf{G}_{,v\eta\eta}^+|_C &= (\tilde{\lambda}_{,\eta}^2 \tilde{\mathbf{K}}_{T,\lambda\lambda} + \tilde{\lambda}_{,\eta\eta} \tilde{\mathbf{K}}_{T,\lambda})|_C = (\lambda_1)^2 \tilde{\mathbf{K}}_{T,\lambda\lambda}(\lambda_C) + 2\lambda_2 \tilde{\mathbf{K}}_{T,\lambda}(\lambda_C) \\
\mathbf{G}_{,\eta\eta\eta}^+|_C &= \mathbf{0} \\
\mathbf{G}_{,vvvv}^+|_C &= (\mathbf{G}_{,uuuu})|_C = \mathbf{K}_{T,uuu}(u_C) \\
\mathbf{G}_{,vvv\eta}^+|_C &= (\mathbf{G}_{,uuuu} \cdot \tilde{u}_{,\lambda} \tilde{\lambda}_{,\eta})|_C = \lambda_1 \mathbf{K}_{T,uu\lambda}(u_C, \lambda_C) \\
\mathbf{G}_{,vv\eta\eta}^+|_C &= \left[(\mathbf{G}_{,uuuu} : \tilde{u}_{,\lambda} \otimes \tilde{u}_{,\lambda} + \mathbf{G}_{,uuu} \cdot \tilde{u}_{,\lambda\lambda}) (\tilde{\lambda}_{,\eta})^2 + (\mathbf{G}_{,uuu} \cdot \tilde{u}_{,\lambda} \tilde{\lambda}_{,\eta\eta}) \right]|_C \\
&= (\lambda_1)^2 \mathbf{K}_{T,u\lambda\lambda}(u_C, \lambda_C) + 2\lambda_2 \mathbf{K}_{T,u\lambda}(u_C, \lambda_C) \\
\mathbf{G}_{,v\eta\eta\eta}^+|_C &= (\tilde{\lambda}_{,\eta})^3 \tilde{\mathbf{K}}_{T,\lambda\lambda\lambda}(\lambda_C) + 3\tilde{\lambda}_{,\eta} \tilde{\lambda}_{,\eta\eta} \tilde{\mathbf{K}}_{T,\lambda\lambda}(\lambda_C) + \tilde{\lambda}_{,\eta\eta\eta} \tilde{\mathbf{K}}_{T,\lambda}(\lambda_C) \\
\mathbf{G}_{,\eta\eta\eta\eta}^+|_C &= \mathbf{0}
\end{aligned}$$

B Coefficient vectors of $\eta^1, \eta^2, \eta^3, \eta^4, \eta^5$, and η^6

Eq. (7) can formally be expressed as

$$\mathbf{G}^+(\mathbf{v}^+(\eta), \eta) = \eta^1 \cdot \mathbf{a} + \eta^2 \cdot \mathbf{b} + \eta^3 \cdot \mathbf{c} + \eta^4 \cdot \mathbf{d} + \eta^5 \cdot \mathbf{e} + \eta^6 \cdot \mathbf{f} + \mathcal{O}(\eta^7) = \mathbf{0}, \quad (\text{B.1})$$

where the coefficients $\mathbf{a}, \mathbf{b}, \dots, \mathbf{f}$ represent vector-valued expressions. The expressions for \mathbf{a}, \mathbf{b} , and \mathbf{c} are contained in (7). In order to write the comparatively lengthy expressions for \mathbf{d}, \mathbf{e} , and \mathbf{f} , not contained in (7), more concisely, the abbreviations

$$\mathbf{A} : \mathbf{u} \otimes \mathbf{v} \rightarrow \mathbf{A} \mathbf{u} \mathbf{v}, \quad \mathbf{B} : \mathbf{u} \otimes \mathbf{v} \otimes \mathbf{w} \rightarrow \mathbf{B} \mathbf{u} \mathbf{v} \mathbf{w}, \quad \dots, \quad \mathbf{u}, \mathbf{v}, \mathbf{w} \in \mathbb{R}^n, \quad (\text{B.2})$$

will be used in what follows. It is noteworthy that all of these expressions result in vectors in \mathbb{R}^n . To obtain the expressions for \mathbf{d}, \mathbf{e} , and \mathbf{f} , the symmetry relations

$$\mathbf{K}_{T,\mathbf{u}} : \mathbf{v} \otimes \mathbf{w} = \mathbf{G}_{,\mathbf{u}\mathbf{u}} : \mathbf{v} \otimes \mathbf{w} = \mathbf{G}_{,\mathbf{u}\mathbf{u}} : \mathbf{w} \otimes \mathbf{v} = \mathbf{K}_{T,\mathbf{u}} : \mathbf{w} \otimes \mathbf{v} \quad (\text{B.3})$$

for arbitrary vectors $\mathbf{v}, \mathbf{w} \in \mathbb{R}^n$, must be used.

Making use of Table A.1 and of Eqs. (4) and (5), the coefficients \mathbf{d}, \mathbf{e} , and \mathbf{f} are obtained as

$$\begin{aligned} \mathbf{d} = & \lambda_1^3 \frac{1}{6} \tilde{\mathbf{K}}_{T,\lambda\lambda\lambda} \mathbf{v}_1 + \lambda_1^2 \left(\frac{1}{2} \tilde{\mathbf{K}}_{T,\lambda\lambda} \mathbf{v}_2 + \frac{1}{4} \mathbf{K}_{T,\mathbf{u}\lambda\lambda} \mathbf{v}_1 \mathbf{v}_1 \right) \\ & + \lambda_1 \left(\lambda_2 \tilde{\mathbf{K}}_{T,\lambda\lambda} \mathbf{v}_1 + \tilde{\mathbf{K}}_{T,\lambda} \mathbf{v}_3 + \mathbf{K}_{T,\mathbf{u}\lambda} \mathbf{v}_1 \mathbf{v}_2 + \frac{1}{6} \mathbf{K}_{T,\mathbf{u}\mathbf{u}\lambda} \mathbf{v}_1 \mathbf{v}_1 \mathbf{v}_1 \right) \\ & + \lambda_2 \left(\tilde{\mathbf{K}}_{T,\lambda} \mathbf{v}_2 + \frac{1}{2} \mathbf{K}_{T,\mathbf{u}\lambda} \mathbf{v}_1 \mathbf{v}_1 \right) + \lambda_3 \tilde{\mathbf{K}}_{T,\lambda} \mathbf{v}_1 + \tilde{\mathbf{K}}_T \mathbf{v}_4 + \mathbf{K}_{T,\mathbf{u}} \mathbf{v}_1 \mathbf{v}_3 \\ & + \frac{1}{2} \mathbf{K}_{T,\mathbf{u}} \mathbf{v}_2 \mathbf{v}_2 + \frac{1}{2} \mathbf{K}_{T,\mathbf{u}\mathbf{u}} \mathbf{v}_1 \mathbf{v}_1 \mathbf{v}_2 + \frac{1}{24} \mathbf{K}_{T,\mathbf{u}\mathbf{u}\mathbf{u}} \mathbf{v}_1 \mathbf{v}_1 \mathbf{v}_1 \mathbf{v}_1, \end{aligned} \quad (\text{B.4})$$

$$\begin{aligned} \mathbf{e} = & \lambda_1^4 \frac{1}{24} \tilde{\mathbf{K}}_{T,\lambda\lambda\lambda\lambda} \mathbf{v}_1 + \lambda_1^3 \left(\frac{1}{6} \tilde{\mathbf{K}}_{T,\lambda\lambda\lambda} \mathbf{v}_2 + \frac{1}{12} \mathbf{K}_{T,\mathbf{u}\lambda\lambda\lambda} \mathbf{v}_1 \mathbf{v}_1 \right) \\ & + \lambda_1^2 \left(\lambda_2 \frac{1}{2} \tilde{\mathbf{K}}_{T,\lambda\lambda\lambda} \mathbf{v}_1 + \frac{1}{2} \tilde{\mathbf{K}}_{T,\lambda\lambda} \mathbf{v}_3 + \frac{1}{2} \mathbf{K}_{T,\mathbf{u}\lambda\lambda} \mathbf{v}_1 \mathbf{v}_2 + \frac{1}{12} \mathbf{K}_{T,\mathbf{u}\mathbf{u}\lambda\lambda} \mathbf{v}_1 \mathbf{v}_1 \mathbf{v}_1 \right) \\ & + \lambda_1 \left[\lambda_3 \tilde{\mathbf{K}}_{T,\lambda\lambda} \mathbf{v}_1 + \lambda_2 \left(\tilde{\mathbf{K}}_{T,\lambda\lambda} \mathbf{v}_2 + \frac{1}{2} \mathbf{K}_{T,\mathbf{u}\lambda\lambda} \mathbf{v}_1 \mathbf{v}_1 \right) + \tilde{\mathbf{K}}_{T,\lambda} \mathbf{v}_4 + \mathbf{K}_{T,\mathbf{u}\lambda} \mathbf{v}_1 \mathbf{v}_3 \right. \\ & \quad \left. + \frac{1}{2} \mathbf{K}_{T,\mathbf{u}\lambda} \mathbf{v}_2 \mathbf{v}_2 + \frac{1}{2} \mathbf{K}_{T,\mathbf{u}\mathbf{u}\lambda} \mathbf{v}_1 \mathbf{v}_1 \mathbf{v}_2 + \frac{1}{24} \mathbf{K}_{T,\mathbf{u}\mathbf{u}\mathbf{u}\lambda} \mathbf{v}_1 \mathbf{v}_1 \mathbf{v}_1 \mathbf{v}_1 \right] \\ & + \lambda_2^2 \frac{1}{2} \tilde{\mathbf{K}}_{T,\lambda\lambda} \mathbf{v}_1 + \lambda_2 \left(\tilde{\mathbf{K}}_{T,\lambda} \mathbf{v}_3 + \mathbf{K}_{T,\mathbf{u}\lambda} \mathbf{v}_1 \mathbf{v}_2 + \frac{1}{6} \mathbf{K}_{T,\mathbf{u}\mathbf{u}\lambda} \mathbf{v}_1 \mathbf{v}_1 \mathbf{v}_1 \right) \\ & + \lambda_3 \left(\tilde{\mathbf{K}}_{T,\lambda} \mathbf{v}_2 + \frac{1}{2} \mathbf{K}_{T,\mathbf{u}\lambda} \mathbf{v}_1 \mathbf{v}_1 \right) + \lambda_4 \tilde{\mathbf{K}}_{T,\lambda} \mathbf{v}_1 \\ & + \tilde{\mathbf{K}}_T \mathbf{v}_5 + \mathbf{K}_{T,\mathbf{u}} \mathbf{v}_1 \mathbf{v}_4 + \mathbf{K}_{T,\mathbf{u}} \mathbf{v}_2 \mathbf{v}_3 + \frac{1}{2} \mathbf{K}_{T,\mathbf{u}\mathbf{u}} \mathbf{v}_1 \mathbf{v}_1 \mathbf{v}_3 + \frac{1}{2} \mathbf{K}_{T,\mathbf{u}\mathbf{u}} \mathbf{v}_1 \mathbf{v}_2 \mathbf{v}_2 \\ & + \frac{1}{6} \mathbf{K}_{T,\mathbf{u}\mathbf{u}\mathbf{u}} \mathbf{v}_1 \mathbf{v}_1 \mathbf{v}_1 \mathbf{v}_2 + \frac{1}{120} \mathbf{K}_{T,\mathbf{u}\mathbf{u}\mathbf{u}\mathbf{u}} \mathbf{v}_1 \mathbf{v}_1 \mathbf{v}_1 \mathbf{v}_1 \mathbf{v}_1, \end{aligned} \quad (\text{B.5})$$

and

$$\begin{aligned}
\mathbf{f} = & \lambda_1^5 \frac{1}{120} \tilde{\mathbf{K}}_{T,\lambda\lambda\lambda\lambda\lambda} \mathbf{v}_1 + \lambda_1^4 \left(\frac{1}{24} \tilde{\mathbf{K}}_{T,\lambda\lambda\lambda\lambda} \mathbf{v}_2 + \frac{1}{48} \mathbf{K}_{T,u\lambda\lambda\lambda\lambda} \mathbf{v}_1 \mathbf{v}_1 \right) \\
& + \lambda_1^3 \left(\lambda_2 \frac{1}{6} \tilde{\mathbf{K}}_{T,\lambda\lambda\lambda\lambda} \mathbf{v}_1 + \frac{1}{6} \tilde{\mathbf{K}}_{T,\lambda\lambda\lambda} \mathbf{v}_3 + \frac{1}{6} \mathbf{K}_{T,u\lambda\lambda\lambda} \mathbf{v}_1 \mathbf{v}_2 + \frac{1}{36} \mathbf{K}_{T,uu\lambda\lambda\lambda} \mathbf{v}_1 \mathbf{v}_1 \mathbf{v}_1 \right) \\
& + \lambda_1^2 \left[\lambda_3 \frac{1}{2} \tilde{\mathbf{K}}_{T,\lambda\lambda\lambda} \mathbf{v}_1 + \lambda_2 \left(\frac{1}{2} \tilde{\mathbf{K}}_{T,\lambda\lambda\lambda} \mathbf{v}_2 + \frac{1}{4} \mathbf{K}_{T,u\lambda\lambda\lambda} \mathbf{v}_1 \mathbf{v}_1 \right) + \frac{1}{2} \tilde{\mathbf{K}}_{T,\lambda\lambda} \mathbf{v}_4 \right. \\
& \quad \left. + \frac{1}{2} \mathbf{K}_{T,u\lambda\lambda} \mathbf{v}_1 \mathbf{v}_3 + \frac{1}{4} \mathbf{K}_{T,u\lambda\lambda} \mathbf{v}_2 \mathbf{v}_2 + \frac{1}{4} \mathbf{K}_{T,uu\lambda\lambda} \mathbf{v}_1 \mathbf{v}_1 \mathbf{v}_2 + \frac{1}{48} \mathbf{K}_{T,uuu\lambda\lambda} \mathbf{v}_1 \mathbf{v}_1 \mathbf{v}_1 \mathbf{v}_1 \right] \\
& + \lambda_1 \left[\lambda_4 \tilde{\mathbf{K}}_{T,\lambda\lambda} \mathbf{v}_1 + \lambda_3 \left(\tilde{\mathbf{K}}_{T,\lambda\lambda} \mathbf{v}_2 + \frac{1}{2} \mathbf{K}_{T,u\lambda\lambda} \mathbf{v}_1 \mathbf{v}_1 \right) \right. \\
& \quad + \lambda_2^2 \frac{1}{2} \tilde{\mathbf{K}}_{T,\lambda\lambda\lambda} \mathbf{v}_1 + \lambda_2 \left(\tilde{\mathbf{K}}_{T,\lambda\lambda} \mathbf{v}_3 + \mathbf{K}_{T,u\lambda\lambda} \mathbf{v}_1 \mathbf{v}_2 + \frac{1}{6} \mathbf{K}_{T,uu\lambda\lambda} \mathbf{v}_1 \mathbf{v}_1 \mathbf{v}_1 \right) \\
& \quad + \tilde{\mathbf{K}}_{T,\lambda} \mathbf{v}_5 + \mathbf{K}_{T,u\lambda} \mathbf{v}_1 \mathbf{v}_4 + \mathbf{K}_{T,u\lambda} \mathbf{v}_2 \mathbf{v}_3 + \frac{1}{2} \mathbf{K}_{T,uu\lambda} \mathbf{v}_1 \mathbf{v}_1 \mathbf{v}_3 + \frac{1}{2} \mathbf{K}_{T,uu\lambda} \mathbf{v}_1 \mathbf{v}_2 \mathbf{v}_2 \\
& \quad \left. + \frac{1}{6} \mathbf{K}_{T,uuu\lambda} \mathbf{v}_1 \mathbf{v}_1 \mathbf{v}_1 \mathbf{v}_2 + \frac{1}{120} \mathbf{K}_{T,uuuu\lambda} \mathbf{v}_1 \mathbf{v}_1 \mathbf{v}_1 \mathbf{v}_1 \mathbf{v}_1 \right] \\
& + \lambda_2^2 \left(\frac{1}{2} \tilde{\mathbf{K}}_{T,\lambda\lambda} \mathbf{v}_2 + \frac{1}{4} \mathbf{K}_{T,u\lambda\lambda} \mathbf{v}_1 \mathbf{v}_1 \right) + \lambda_2 \left(\tilde{\mathbf{K}}_{T,\lambda} \mathbf{v}_4 + \mathbf{K}_{T,u\lambda} \mathbf{v}_1 \mathbf{v}_3 \right. \\
& \quad \left. + \frac{1}{2} \mathbf{K}_{T,u\lambda} \mathbf{v}_2 \mathbf{v}_2 + \frac{1}{2} \mathbf{K}_{T,uu\lambda} \mathbf{v}_1 \mathbf{v}_1 \mathbf{v}_2 + \frac{1}{24} \mathbf{K}_{T,uuu\lambda} \mathbf{v}_1 \mathbf{v}_1 \mathbf{v}_1 \mathbf{v}_1 \right) \\
& + \lambda_3 \left(\lambda_2 \tilde{\mathbf{K}}_{T,\lambda\lambda} \mathbf{v}_1 + \tilde{\mathbf{K}}_{T,\lambda} \mathbf{v}_3 + \mathbf{K}_{T,u\lambda} \mathbf{v}_1 \mathbf{v}_2 + \frac{1}{6} \mathbf{K}_{T,uu\lambda} \mathbf{v}_1 \mathbf{v}_1 \mathbf{v}_1 \right) \\
& + \lambda_4 \left(\tilde{\mathbf{K}}_{T,\lambda} \mathbf{v}_2 + \frac{1}{2} \mathbf{K}_{T,u\lambda} \mathbf{v}_1 \mathbf{v}_1 \right) + \lambda_5 \tilde{\mathbf{K}}_{T,\lambda} \mathbf{v}_1 \\
& + \tilde{\mathbf{K}}_T \mathbf{v}_6 + \mathbf{K}_{T,u} \mathbf{v}_1 \mathbf{v}_5 + \mathbf{K}_{T,u} \mathbf{v}_2 \mathbf{v}_4 + \frac{1}{2} \mathbf{K}_{T,u} \mathbf{v}_3 \mathbf{v}_3 + \frac{1}{2} \mathbf{K}_{T,uu} \mathbf{v}_1 \mathbf{v}_1 \mathbf{v}_4 \\
& + \mathbf{K}_{T,uu} \mathbf{v}_1 \mathbf{v}_2 \mathbf{v}_3 + \frac{1}{6} \mathbf{K}_{T,uu} \mathbf{v}_2 \mathbf{v}_2 \mathbf{v}_2 + \frac{1}{6} \mathbf{K}_{T,uuu} \mathbf{v}_1 \mathbf{v}_1 \mathbf{v}_1 \mathbf{v}_3 + \frac{1}{4} \mathbf{K}_{T,uuu} \mathbf{v}_1 \mathbf{v}_1 \mathbf{v}_2 \mathbf{v}_2 \\
& + \frac{1}{24} \mathbf{K}_{T,uuuu} \mathbf{v}_1 \mathbf{v}_1 \mathbf{v}_1 \mathbf{v}_1 \mathbf{v}_2 + \frac{1}{720} \mathbf{K}_{T,uuuuu} \mathbf{v}_1 \mathbf{v}_1 \mathbf{v}_1 \mathbf{v}_1 \mathbf{v}_1 \mathbf{v}_1. \tag{B.6}
\end{aligned}$$

C Coefficients c_1^* , \hat{f}_1 , \tilde{e}_1 and b_2 , d_3 , b_4

For the general case of nonlinear prebuckling paths, the coefficients c_1^* , \hat{f}_1 , and \tilde{e}_1 , occurring in the Eqs. (20), (21), and (22), respectively, are needed. Abbreviations according to (B.2) are used. Premultiplying the coefficient of λ_1 in (B.4) by $-\mathbf{v}_1^T/\mathbf{v}_1^T \tilde{\mathbf{K}}_{T,\lambda} \mathbf{v}_1$, yields

$$c_1^* = 2 a_1 \lambda_2 + b_2 \quad (\text{C.1})$$

with a_1 according to (16) and

$$b_2 = -\frac{1}{\mathbf{v}_1^T \tilde{\mathbf{K}}_{T,\lambda} \mathbf{v}_1} \left(\mathbf{v}_1^T \tilde{\mathbf{K}}_{T,\lambda} \mathbf{v}_3 + \mathbf{v}_1^T \mathbf{K}_{T,u\lambda} \mathbf{v}_1 \mathbf{v}_2 + \frac{1}{6} \mathbf{v}_1^T \mathbf{K}_{T,uu\lambda} \mathbf{v}_1 \mathbf{v}_1 \mathbf{v}_1 \right). \quad (\text{C.2})$$

Premultiplying those terms in (B.5) by $-\mathbf{v}_1^T/\mathbf{v}_1^T \tilde{\mathbf{K}}_{T,\lambda} \mathbf{v}_1$, which do not contain λ_1 , and considering (8), gives $\hat{f}_1 - \lambda_4$, where

$$\hat{f}_1 = b_1 \lambda_3 + a_1 \lambda_2^2 + b_2 \lambda_2 + d_3 \quad (\text{C.3})$$

with a_1 , b_1 , and b_2 according to the Eqs. (16), (17), and (C.2), respectively, and

$$d_3 = -\frac{1}{\mathbf{v}_1^T \tilde{\mathbf{K}}_{T,\lambda} \mathbf{v}_1} \left(\mathbf{v}_1^T \mathbf{K}_{T,u} \mathbf{v}_1 \mathbf{v}_4 + \mathbf{v}_1^T \mathbf{K}_{T,u} \mathbf{v}_2 \mathbf{v}_3 + \frac{1}{120} \mathbf{v}_1^T \mathbf{K}_{T,uuuu} \mathbf{v}_1 \mathbf{v}_1 \mathbf{v}_1 \mathbf{v}_1 \right. \\ \left. + \frac{1}{2} \mathbf{v}_1^T \mathbf{K}_{T,uu} \mathbf{v}_1 \mathbf{v}_1 \mathbf{v}_3 + \frac{1}{2} \mathbf{v}_1^T \mathbf{K}_{T,uu} \mathbf{v}_1 \mathbf{v}_2 \mathbf{v}_2 + \frac{1}{6} \mathbf{v}_1^T \mathbf{K}_{T,uuu} \mathbf{v}_1 \mathbf{v}_1 \mathbf{v}_1 \mathbf{v}_2 \right). \quad (\text{C.4})$$

Premultiplying the coefficient of λ_1 in (B.6) by $-\mathbf{v}_1^T/\mathbf{v}_1^T \tilde{\mathbf{K}}_{T,\lambda} \mathbf{v}_1$, yields

$$\tilde{e}_1 = 2 a_1 \lambda_4 + 2 b_1^* \lambda_3 + b_4 \quad (\text{C.5})$$

with a_1 and b_1^* according to (16) and (24), respectively, and

$$b_4 = 3 a_1^* \lambda_2^2 + b_2^* \lambda_2 + c_2^* \quad (\text{C.6})$$

with a_1^* according to (23.1),

$$b_2^* = -\frac{1}{\mathbf{v}_1^T \tilde{\mathbf{K}}_{T,\lambda} \mathbf{v}_1} \left(\mathbf{v}_1^T \tilde{\mathbf{K}}_{T,\lambda\lambda} \mathbf{v}_3 + \mathbf{v}_1^T \mathbf{K}_{T,u\lambda\lambda} \mathbf{v}_1 \mathbf{v}_2 + \frac{1}{6} \mathbf{v}_1^T \mathbf{K}_{T,uu\lambda\lambda} \mathbf{v}_1 \mathbf{v}_1 \mathbf{v}_1 \right), \quad (\text{C.7})$$

and

$$c_2^* = -\frac{1}{\mathbf{v}_1^T \tilde{\mathbf{K}}_{T,\lambda} \mathbf{v}_1} \left(\mathbf{v}_1^T \tilde{\mathbf{K}}_{T,\lambda} \mathbf{v}_5 + \mathbf{v}_1^T \mathbf{K}_{T,u\lambda} \mathbf{v}_1 \mathbf{v}_4 + \mathbf{v}_1^T \mathbf{K}_{T,u\lambda} \mathbf{v}_2 \mathbf{v}_3 \right. \\ \left. + \frac{1}{2} \mathbf{v}_1^T \mathbf{K}_{T,uu\lambda} \mathbf{v}_1 \mathbf{v}_1 \mathbf{v}_3 + \frac{1}{2} \mathbf{v}_1^T \mathbf{K}_{T,uu\lambda} \mathbf{v}_1 \mathbf{v}_2 \mathbf{v}_2 \right. \\ \left. + \frac{1}{6} \mathbf{v}_1^T \mathbf{K}_{T,uuu\lambda} \mathbf{v}_1 \mathbf{v}_1 \mathbf{v}_1 \mathbf{v}_2 + \frac{1}{120} \mathbf{v}_1^T \mathbf{K}_{T,uuuu\lambda} \mathbf{v}_1 \mathbf{v}_1 \mathbf{v}_1 \mathbf{v}_1 \mathbf{v}_1 \right). \quad (\text{C.8})$$

D Mathematical properties of the consistently linearized eigenproblem

To each point on a space curve $\lambda_2 = \lambda_2(\kappa)$, $\lambda_4 = \lambda_4(\kappa)$, $a_1 = a_1(\kappa)$ (see Fig. 4) a curve $\lambda_1^*(\lambda)$ can be related, which is part of the solution of the so-called consistently linearized eigenproblem. The mathematical formulation of this eigenproblem reads (Helnwein [5])

$$\left[\tilde{\mathbf{K}}_T + (\lambda^* - \lambda) \tilde{\mathbf{K}}_{T,\lambda} \right] \mathbf{v}^* = \mathbf{0}, \quad (\text{D.1})$$

where $\lambda^* - \lambda$ is the eigenvalue and \mathbf{v}^* is the eigenvector. For $\mathbf{v}^* = \mathbf{v}_1^* = \mathbf{v}_1$, because of (8),

$$\lambda^* = \lambda_1^* = \lambda, \quad (\text{D.2})$$

representing the load level at the stability limit.

It will be shown that, in general, the curves $\lambda_1^*(\lambda)$ related to point T ($\lambda_2 = 0$, λ_4 , a_1) in Fig. 4 have specific geometric properties at the bifurcation point $\lambda_1^* = \lambda$. The investigation of these properties is motivated by the need to ensure the completeness of the solutions for the initial postbuckling paths with $\lambda_2 = 0$ for the general case of symmetric bifurcation from nonlinear primary paths (see Section 7). Moreover, these properties permit verification of theoretical results for limiting cases "by inspection" of the corresponding curves $\lambda_1^*(\lambda)$. In view of the complexity of some of the relevant mathematical expressions, no practical alternative is available.

Derivation of (D.1) with respect to λ gives

$$\left[\lambda_{1,\lambda}^* \tilde{\mathbf{K}}_{T,\lambda} + (\lambda^* - \lambda) \tilde{\mathbf{K}}_{T,\lambda\lambda} \right] \mathbf{v}^* + \left[\tilde{\mathbf{K}}_T + (\lambda^* - \lambda) \tilde{\mathbf{K}}_{T,\lambda} \right] \mathbf{v}_{,\lambda}^* = \mathbf{0}. \quad (\text{D.3})$$

Writing (D.3) for the first eigenpair, which is a function of λ , yields

$$\left[\lambda_{1,\lambda}^* \tilde{\mathbf{K}}_{T,\lambda} + (\lambda_1^* - \lambda) \tilde{\mathbf{K}}_{T,\lambda\lambda} \right] \mathbf{v}_1^* + \left[\tilde{\mathbf{K}}_T + (\lambda_1^* - \lambda) \tilde{\mathbf{K}}_{T,\lambda} \right] \mathbf{v}_{1,\lambda}^* = \mathbf{0}. \quad (\text{D.4})$$

Premultiplication of (D.4) by \mathbf{v}_1^{*T} and use of (D.1) gives

$$\lambda_{1,\lambda}^* = -(\lambda_1^* - \lambda) \frac{\mathbf{v}_1^{*T} \tilde{\mathbf{K}}_{T,\lambda\lambda} \mathbf{v}_1^*}{\mathbf{v}_1^{*T} \tilde{\mathbf{K}}_{T,\lambda} \mathbf{v}_1^*}. \quad (\text{D.5})$$

Expressing $\mathbf{v}_{1,\lambda}^*$ in terms of the eigenvectors \mathbf{v}_j^* , $j = 1, 2, \dots, n$, results in

$$\mathbf{v}_{1,\lambda}^* = \sum_{j=1}^n c_{1j} \mathbf{v}_j^*. \quad (\text{D.6})$$

Inserting (D.6) into (D.4), premultiplying the obtained relation by \mathbf{v}_j^{*T} , $j \neq 1$, and making use of the orthogonality conditions

$$\mathbf{v}_j^{*T} \tilde{\mathbf{K}}_T \mathbf{v}_1^* = 0, \quad \mathbf{v}_j^{*T} \tilde{\mathbf{K}}_{T,\lambda} \mathbf{v}_1^* = 0, \quad (\text{D.7})$$

following from (D.1), gives

$$(\lambda_1^* - \lambda) \mathbf{v}_j^{*T} \tilde{\mathbf{K}}_{T,\lambda\lambda} \mathbf{v}_1^* + \mathbf{v}_j^{*T} \left[\tilde{\mathbf{K}}_T + (\lambda_1^* - \lambda) \tilde{\mathbf{K}}_{T,\lambda} \right] c_{1j} \mathbf{v}_j^* = 0. \quad (\text{D.8})$$

Writing (D.1) for the j -th eigenpair, which is a function of λ , and premultiplying the obtained relation by \mathbf{v}_j^{*T} , yields

$$\mathbf{v}_j^{*T} \left[\tilde{\mathbf{K}}_T + (\lambda_j^* - \lambda) \tilde{\mathbf{K}}_{T,\lambda} \right] \mathbf{v}_j^* = 0. \quad (\text{D.9})$$

Insertion of (D.9) into (D.8) results in

$$c_{1j} = -\frac{\lambda_1^* - \lambda}{\lambda_1^* - \lambda_j^*} \cdot \frac{\mathbf{v}_j^{*T} \tilde{\mathbf{K}}_{T,\lambda\lambda} \mathbf{v}_1^*}{\mathbf{v}_j^{*T} \tilde{\mathbf{K}}_{T,\lambda} \mathbf{v}_j^*}. \quad (\text{D.10})$$

In order to determine c_{11} , \mathbf{v}_1^* is normalized such that

$$\mathbf{v}_1^{*T} \tilde{\mathbf{K}}_{T,\lambda} \mathbf{v}_1^* = -1 \vee 1, \quad (\text{D.11})$$

implying $\lambda_1^*(\lambda = 0) > 0$, which can always be achieved by means of a suitable definition of a positive reference load. Derivation of (D.11) with respect to λ gives

$$2\mathbf{v}_1^{*T} \tilde{\mathbf{K}}_{T,\lambda} \mathbf{v}_{1,\lambda}^* + \mathbf{v}_1^{*T} \tilde{\mathbf{K}}_{T,\lambda\lambda} \mathbf{v}_1^* = 0. \quad (\text{D.12})$$

Substitution of (D.6) into (D.12) and consideration of (D.7.2) results in

$$c_{11} = -\frac{1}{2} \frac{\mathbf{v}_1^{*T} \tilde{\mathbf{K}}_{T,\lambda\lambda} \mathbf{v}_1^*}{\mathbf{v}_1^{*T} \tilde{\mathbf{K}}_{T,\lambda} \mathbf{v}_1^*}. \quad (\text{D.13})$$

Specializing (D.13) for the stability limit by setting $\mathbf{v}_1^* = \mathbf{v}_1$ and comparing the relation for c_{11} with (16), it is seen that

$$c_{11} = a_1. \quad (\text{D.14})$$

Apart from exceptional cases, which will be treated later, specialization of (D.5) and (D.10) for the stability limit $\lambda_1^* = \lambda$ yields

$$\lambda_{1,\lambda}^* = 0 \quad (\text{D.15})$$

and

$$c_{1j} = 0, \quad j \neq 1, \quad (\text{D.16})$$

respectively. Substituting (D.16) into (D.6), gives

$$\mathbf{v}_{1,\lambda}^* = c_{11} \mathbf{v}_1^* \quad \text{with} \quad \mathbf{v}_1^* = \mathbf{v}_1. \quad (\text{D.17})$$

In order to show that the nonlinearity coefficient a_1 is proportional to the curvature of the eigenvalue curve at the bifurcation point, (D.3) is differentiated with respect to λ :

$$\begin{aligned} & \left[\lambda_{,\lambda\lambda}^* \tilde{\mathbf{K}}_{T,\lambda} + (2\lambda_{,\lambda}^* - 1) \tilde{\mathbf{K}}_{T,\lambda\lambda} + (\lambda^* - \lambda) \tilde{\mathbf{K}}_{T,\lambda\lambda\lambda} \right] \mathbf{v}^* \\ & + 2 \left[\lambda_{,\lambda}^* \tilde{\mathbf{K}}_{T,\lambda} + (\lambda^* - \lambda) \tilde{\mathbf{K}}_{T,\lambda\lambda} \right] \mathbf{v}_{,\lambda}^* + \left[\tilde{\mathbf{K}}_T + (\lambda^* - \lambda) \tilde{\mathbf{K}}_{T,\lambda} \right] \mathbf{v}_{,\lambda\lambda}^* = \mathbf{0}. \end{aligned} \quad (\text{D.18})$$

Writing (D.18) for the first eigenpair and specializing the obtained relation for the bifurcation point by inserting the Eqs. (D.2) and (D.15) and setting $\mathbf{v}_1^* = \mathbf{v}_1$, gives

$$\left(\lambda_{1,\lambda\lambda}^* \tilde{\mathbf{K}}_{T,\lambda} - \tilde{\mathbf{K}}_{T,\lambda\lambda} \right) \mathbf{v}_1 + \tilde{\mathbf{K}}_T \mathbf{v}_{1,\lambda\lambda}^* = \mathbf{0}. \quad (\text{D.19})$$

Premultiplication of (D.19) by \mathbf{v}_1^T and consideration of (8) yields

$$\lambda_{1,\lambda\lambda}^* = \frac{\mathbf{v}_1^T \tilde{\mathbf{K}}_{T,\lambda\lambda} \mathbf{v}_1}{\mathbf{v}_1^T \tilde{\mathbf{K}}_{T,\lambda} \mathbf{v}_1}. \quad (\text{D.20})$$

Comparison of (D.20) with (16) shows that

$$a_1 = -\frac{1}{2} \lambda_{1,\lambda\lambda}^* \Big|_{\lambda_1^* = \lambda}, \quad (\text{D.21})$$

which proves the correctness of the preceding assertion.

Specializing (D.21) for $a_1 = 0$ and (D.17) for $c_{11} = a_1 = 0$, gives

$$\lambda_{1,\lambda\lambda}^* = 0 \quad (\text{D.22})$$

and

$$\mathbf{v}_{1,\lambda}^* = \mathbf{0}, \quad (\text{D.23})$$

respectively. Hence, point I in Fig. 4(a), point T in Figs. 4(b)–4(e) and 4(g), and points T in Fig. 4(h) correlate with special points on the corresponding curves $\lambda_1^*(\lambda)$ and $\mathbf{v}_1^*(\lambda)$ at the bifurcation point $\lambda_1^* = \lambda$.

- *Point I in Fig. 4(a).* Substitution of (148.2) into (D.19) and consideration of (8) gives

$$\left(\lambda_{1,\lambda\lambda}^* \tilde{\mathbf{K}}_{T,\lambda} - \tilde{\mathbf{K}}_{T,\lambda\lambda} \right) \mathbf{v}_1 = \mathbf{0}. \quad (\text{D.24})$$

At point I ,

$$\tilde{\mathbf{K}}_{T,\lambda\lambda} \mathbf{v}_1 = \mathbf{0} \xrightarrow{(16)} a_1 = 0. \quad (\text{D.25})$$

Following from (D.24) and (D.25),

$$\lambda_{1,\lambda\lambda}^* = 0. \quad (\text{D.26})$$

In Part II of this work [12] it is shown numerically that the curve $\lambda_1^*(\lambda)$ related to point I in Fig. 4(a) has a saddle point at the bifurcation point $\lambda_1^* = \lambda$.

- *Point T in Fig. 4(b).* At this point, (D.24) and (D.25) (which is equal to (149)) hold. Consequently, $\lambda_{1,\lambda\lambda}^* = 0$. In Part II of this work [12] it is shown numerically that the curve $\lambda_1^*(\lambda)$ related to point T in Fig. 4(b) has a saddle point at the bifurcation point $\lambda_1^* = \lambda$.

• *Point T in Fig. 4(c)*. At this point, (D.24) and (D.25) (which is equal to (151)) hold. Consequently, $\lambda_{1,\lambda\lambda}^* = 0$. However, in contrast to the situation at point *T* in Fig. 4(b), the curve $\lambda_1^*(\lambda)$ related to point *T* in Fig. 4(c) has a planar point at the bifurcation point $\lambda_1^* = \lambda$, $\lambda_{1,\lambda}^* = 0$. Hence, in addition to $\lambda_{1,\lambda\lambda}^* = 0$, also $\lambda_{1,\lambda\lambda\lambda}^* = 0$. This assertion is based on the following observation: the curvature of the curve $\lambda_1^*(\lambda)$ related to an arbitrary point on the space curve in Fig. 4(c), has a maximum value at the bifurcation point $\lambda_1^* = \lambda$, $\lambda_{1,\lambda}^* = 0$. Hence,

$$\left\{ \frac{\lambda_{1,\lambda\lambda}^*}{[1 + (\lambda_{1,\lambda}^*)^2]^{\frac{3}{2}}} \right\}_{,\lambda} \Big|_{\lambda_1^*,\lambda=0} = 0, \quad \left\{ \frac{\lambda_{1,\lambda\lambda}^*}{[1 + (\lambda_{1,\lambda}^*)^2]^{\frac{3}{2}}} \right\}_{,\lambda\lambda} \Big|_{\lambda_1^*,\lambda=0} < 0. \quad (\text{D.27})$$

From (D.27.1),

$$\frac{\lambda_{1,\lambda\lambda\lambda}^* [1 + (\lambda_{1,\lambda}^*)^2]^{\frac{3}{2}} - 3 (\lambda_{1,\lambda\lambda}^*)^2 \lambda_{1,\lambda}^* [1 + (\lambda_{1,\lambda}^*)^2]^{\frac{1}{2}}}{[1 + (\lambda_{1,\lambda}^*)^2]^3} \Big|_{\lambda_1^*,\lambda=0} = \lambda_{1,\lambda\lambda\lambda}^* = 0. \quad (\text{D.28})$$

Derivation of (D.18) with respect to λ results in

$$\begin{aligned} & \left[\lambda_{1,\lambda\lambda\lambda}^* \tilde{\mathbf{K}}_{T,\lambda} + 3 \lambda_{1,\lambda\lambda}^* \tilde{\mathbf{K}}_{T,\lambda\lambda} + (3 \lambda_{1,\lambda}^* - 2) \tilde{\mathbf{K}}_{T,\lambda\lambda\lambda} + (\lambda^* - \lambda) \tilde{\mathbf{K}}_{T,\lambda\lambda\lambda\lambda} \right] \mathbf{v}^* + \\ & 3 \left[\lambda_{1,\lambda\lambda}^* \tilde{\mathbf{K}}_{T,\lambda} + (2 \lambda_{1,\lambda}^* - 1) \tilde{\mathbf{K}}_{T,\lambda\lambda} + (\lambda^* - \lambda) \tilde{\mathbf{K}}_{T,\lambda\lambda\lambda} \right] \mathbf{v}_{1,\lambda}^* + \\ & 3 \left[\lambda_{1,\lambda}^* \tilde{\mathbf{K}}_{T,\lambda} + (\lambda^* - \lambda) \tilde{\mathbf{K}}_{T,\lambda\lambda} \right] \mathbf{v}_{1,\lambda\lambda}^* + \left[\tilde{\mathbf{K}}_T + (\lambda^* - \lambda) \tilde{\mathbf{K}}_{T,\lambda} \right] \mathbf{v}_{1,\lambda\lambda\lambda}^* = 0. \end{aligned} \quad (\text{D.29})$$

Writing (D.29) for the first eigenpair and specializing the result for the bifurcation point, i.e. for $\lambda_1^* = \lambda$, $\lambda_{1,\lambda}^* = 0$, $\lambda_{1,\lambda\lambda\lambda}^* = 0$, and $\mathbf{v}_1^* = \mathbf{v}_1$, gives

$$(3 \lambda_{1,\lambda\lambda}^* \tilde{\mathbf{K}}_{T,\lambda\lambda} - 2 \tilde{\mathbf{K}}_{T,\lambda\lambda\lambda}) \mathbf{v}_1 + 3 (\lambda_{1,\lambda\lambda}^* \tilde{\mathbf{K}}_{T,\lambda} - \tilde{\mathbf{K}}_{T,\lambda\lambda}) \mathbf{v}_{1,\lambda}^* + \tilde{\mathbf{K}}_T \mathbf{v}_{1,\lambda\lambda\lambda}^* = 0. \quad (\text{D.30})$$

At point *T* in Fig. 4(c), (D.19) disintegrates into

$$\lambda_{1,\lambda\lambda}^* = 0, \quad \tilde{\mathbf{K}}_{T,\lambda\lambda} \mathbf{v}_1 = \mathbf{0} \text{ (see (151))}, \quad \mathbf{v}_{1,\lambda\lambda}^* = \mathbf{0} \text{ (see (152.2))}. \quad (\text{D.31})$$

Hence, the only difference between the disintegration of (D.19) at point *T* in Fig. 4(c) and the one at point *T* in Fig. 4(b) is the vanishing of $\mathbf{v}_{1,\lambda\lambda}^*$ at the former. Eq. (D.31.1) holds in addition to $\lambda_1^* = \lambda$, $\lambda_{1,\lambda}^* = 0$, and $\lambda_{1,\lambda\lambda\lambda}^* = 0$. Therefore, as shown numerically in Part II of this work [12], the curve $\lambda_1^*(\lambda)$ related to point *T* in Fig. 4(c) has a planar point at the bifurcation point $\lambda_1^* = \lambda$.

Inserting (D.13) into (D.17) and specializing the result for (D.31.2), gives

$$\mathbf{v}_{1,\lambda}^* = \mathbf{0}. \quad (\text{D.32})$$

Substitution of (D.31.1) and (D.32) into (D.30) results in

$$-2 \tilde{\mathbf{K}}_{T,\lambda\lambda\lambda} \mathbf{v}_1 + \tilde{\mathbf{K}}_T \mathbf{v}_{1,\lambda\lambda\lambda}^* = \mathbf{0}. \quad (\text{D.33})$$

Premultiplication of (D.33) by \mathbf{v}_1^T and consideration of (8) results in

$$\mathbf{v}_1^T \tilde{\mathbf{K}}_{T,\lambda\lambda} \mathbf{v}_1 = 0 \xrightarrow{(23.1)} a_1^* = 0 \quad (\text{see (152.3)}). \quad (\text{D.34})$$

For reasons of completeness, the situation at point H in Fig. 4(c) will be investigated in the following. Specializing the ratio of the two quadratic forms in (D.5) for the stability limit by setting $\mathbf{v}_1^* = \mathbf{v}_1$ and making use of (D.20) and (D.21), gives

$$\frac{\mathbf{v}_1^T \tilde{\mathbf{K}}_{T,\lambda\lambda} \mathbf{v}_1}{\mathbf{v}_1^T \tilde{\mathbf{K}}_{T,\lambda} \mathbf{v}_1} = -2 a_1. \quad (\text{D.35})$$

Substituting (D.35) into (D.5), yields

$$\lambda_{1,\lambda}^* |_{\lambda_1^*=\lambda} = 2 (\lambda_1^* - \lambda) |_{\lambda_1^*=\lambda} a_1. \quad (\text{D.36})$$

Because of

$$\lambda_1^* - \lambda = 0 \quad \text{and} \quad a_1 = -\infty \quad (\text{see (102)}), \quad (\text{D.37})$$

the expression for $\lambda_{1,\lambda}^* |_{\lambda_1^*=\lambda}$ is an indeterminate expression. (In the following, $|_{\lambda_1^*=\lambda}$ will be omitted.)

Inserting (99) into (D.36), results in

$$\lambda_{1,\lambda}^* = \frac{(\lambda_1^* - \lambda) \lambda_{,\xi\xi}}{(\lambda_{,\xi})^2} \left(-\frac{\mathbf{v}_1^T \tilde{\mathbf{K}}_{T,\xi\xi} \mathbf{v}_1}{\mathbf{v}_1^T \tilde{\mathbf{K}}_{T,\xi} \mathbf{v}_1} \frac{\lambda_{,\xi}}{\lambda_{,\xi\xi}} + 1 \right). \quad (\text{D.38})$$

Application of de L'Hospital's rule to the indeterminate expression $(\lambda_1^* - \lambda)/(\lambda_{,\xi})^2$ in (D.38) and consideration of (100.2) gives

$$\lambda_{1,\lambda}^* = \frac{(\lambda_{1,\xi}^* - \lambda_{,\xi}) \lambda_{,\xi\xi}}{2 \lambda_{,\xi} \lambda_{,\xi\xi}} = \frac{1}{2} (\lambda_{1,\lambda}^* - 1), \quad (\text{D.39})$$

resulting in

$$\lambda_{1,\lambda}^* = -1, \quad (\text{D.40})$$

which agrees with the numerical result for hilltop bifurcation reported in Part II of this work [12]. Substitution of (102) into (D.21) yields

$$\lambda_{1,\lambda\lambda}^* = \infty, \quad (\text{D.41})$$

which indicates that the curve $\lambda_1^*(\lambda)$ has a singular point at $\lambda_1^* = \lambda$.

• *Point T in Fig. 4(d).* With exception of (D.31.2) and (D.31.3), the relations for point T in Fig. 4(c) also hold for point T in Fig. 4(d). At this point, (D.19) disintegrates into

$$\lambda_{1,\lambda\lambda}^* = 0 \quad \text{and} \quad -\tilde{\mathbf{K}}_{T,\lambda\lambda} \mathbf{v}_1 + \tilde{\mathbf{K}}_T \mathbf{v}_{1,\lambda\lambda}^* = \mathbf{0}. \quad (\text{D.42})$$

Premultiplication of (D.42.2) by \mathbf{v}_1^T and consideration of (8) yields

$$\mathbf{v}_1^T \tilde{\mathbf{K}}_{T,\lambda\lambda} \mathbf{v}_1 = 0 \xrightarrow{(16)} a_1 = 0. \quad (\text{D.43})$$

Premultiplication of (D.33) by \mathbf{v}_1^T and consideration of (8) results in

$$\mathbf{v}_1^T \tilde{\mathbf{K}}_{T,\lambda\lambda\lambda} \mathbf{v}_1 = 0 \xrightarrow{(23.1)} a_1^* = 0. \quad (\text{D.44})$$

The Eqs. (D.43) and (D.44) are associated with $\lambda_{1,\lambda}^* = 0$ and $\lambda_{1,\lambda\lambda}^* = 0$. Hence, as shown numerically in Part II of this work [12], also the curve $\lambda_1^*(\lambda)$ related to point T in Fig. 4(d) has a planar point at the bifurcation point $\lambda_1^* = \lambda$.

- *Point T in Fig. 4(e).* The situation at point $S=T$ in Fig. 4(e) is the same as the one at point T in Fig. 4(c). Therefore, the curve $\lambda_1^*(\lambda)$ related to point $S=T$ in Fig. 4(e) has a planar point at the bifurcation point $\lambda_1^* = \lambda$.

- *Point $F=N=T$ in Fig. 4(f).* Substitution of (106) into (99) yields an indeterminate expression for a_1 . With the help of de L'Hospital's rule, the result for this expression is obtained as

$$a_1 = -\infty. \quad (\text{D.45})$$

Because of

$$\lambda_1^* - \lambda = 0 \quad \text{and} \quad a_1 = -\infty, \quad (\text{D.46})$$

$$\lambda_{1,\lambda}^* |_{\lambda_1^*=\lambda} = 2 (\lambda_1^* - \lambda) |_{\lambda_1^*=\lambda} a_1 \quad (\text{see (D.36)}) \quad (\text{D.47})$$

is an indeterminate expression. By means of de L'Hospital's rule, the result for this expression is obtained as

$$\lambda_{1,\lambda}^* = -1, \quad (\text{D.48})$$

which agrees with (D.40). Moreover,

$$\lambda_{1,\lambda\lambda}^* = \infty \quad (\text{D.49})$$

(see (D.41)).

- *Point T in Fig. 4(g).* The situation at this point is the same as the one at point T in Fig. 4(b) (*von Mises* truss) and in Fig. 4(c) (cylindrical panel), respectively. Hence, the curves $\lambda_1^*(\lambda)$ related to point T in Fig. 4(f) have a saddle point (*von Mises* truss) and a planar point (cylindrical panel), respectively, at the bifurcation point.

Fig. D.1 (*von Mises* truss): The curve in Fig. D.1(a) that contains the bifurcation point (point C) and the dash-dotted curve in this Figure show the functions $\lambda_1^*(\lambda)$ and $\lambda_j^*(\lambda)$, both related to point T in Fig. 4(b) (*von Mises* truss), which represents a limiting case (see (97)). At point C , $\lambda_1^* = \lambda$, $\lambda_{1,\lambda}^* = 0$, and $\lambda_{1,\lambda\lambda}^* = 0$. For $\lambda > \lambda_1^*$, $\tilde{\mathbf{K}}_T$ is an indefinite matrix.

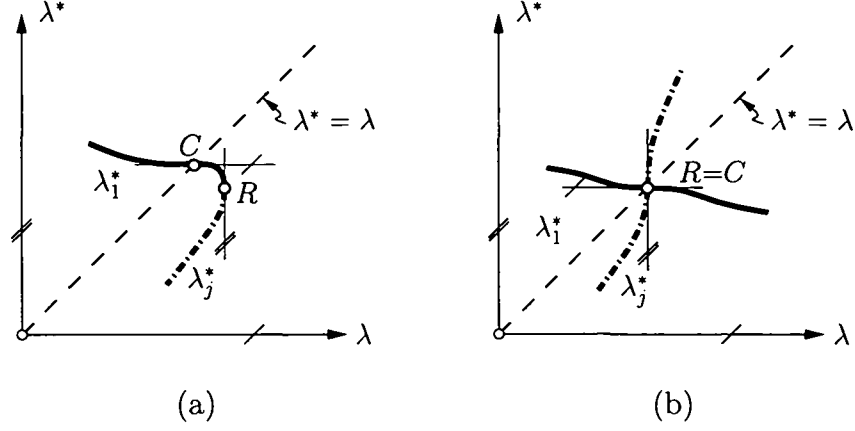


Fig. D.1. Eigenvalue curves related to (a) point T in Fig. 4(b) representing a limiting case, and (b) point $F=N=T$ (see Fig. 4(g)) representing the final situation of this limiting case

Consequently, eigenvalue functions may become complex functions. For $\lambda > \lambda_R$, where λ_R refers to point R in Fig. D.1(a), $\lambda_1^*(\lambda)$ and $\lambda_j^*(\lambda)$ are conjugate complex functions.

To understand the situation at point $R=C$ in Fig. D.1(b), which is associated with the final situation $F=N=T$ of the aforementioned limiting case, the one at point R in Fig. D.1(a) must be understood. To understand the latter, the situation for $\lambda > \lambda_R$ in Fig. D.1(a) must be investigated. For that purpose, λ^* and \mathbf{v}^* in (D.1) are replaced by

$$\lambda_1^* = Re(\lambda_1^*) + i Im(\lambda_1^*) \quad \text{and} \quad \mathbf{v}_1^* = Re(\mathbf{v}_1^*) + i Im(\mathbf{v}_1^*), \quad (\text{D.50})$$

where $Re(\)$ and $Im(\)$ denote the real and the imaginary part, respectively, of the term in parentheses. This gives

$$\left\{ \tilde{\mathbf{K}}_T + [Re(\lambda_1^*) + i Im(\lambda_1^*) - \lambda] \tilde{\mathbf{K}}_{T,\lambda} \right\} \{ Re(\mathbf{v}_1^*) + i Im(\mathbf{v}_1^*) \} = \mathbf{0}. \quad (\text{D.51})$$

The real and the imaginary part of (D.51) are obtained as

$$\left\{ \tilde{\mathbf{K}}_T + [Re(\lambda_1^*) - \lambda] \tilde{\mathbf{K}}_{T,\lambda} \right\} Re(\mathbf{v}_1^*) - Im(\lambda_1^*) \tilde{\mathbf{K}}_{T,\lambda} Im(\mathbf{v}_1^*) = \mathbf{0} \quad (\text{D.52})$$

and

$$\left\{ \tilde{\mathbf{K}}_T + [Re(\lambda_1^*) - \lambda] \tilde{\mathbf{K}}_{T,\lambda} \right\} Im(\mathbf{v}_1^*) + Im(\lambda_1^*) \tilde{\mathbf{K}}_{T,\lambda} Re(\mathbf{v}_1^*) = \mathbf{0}. \quad (\text{D.53})$$

Premultiplication of (D.52) by $Re(\mathbf{v}_1^{*T})$ and of (D.53) by $Im(\mathbf{v}_1^{*T})$ and addition of the so-obtained relations yields

$$\begin{aligned} & Re(\mathbf{v}_1^{*T}) \left\{ \tilde{\mathbf{K}}_T + [Re(\lambda_1^*) - \lambda] \tilde{\mathbf{K}}_{T,\lambda} \right\} Re(\mathbf{v}_1^*) + \\ & Im(\mathbf{v}_1^{*T}) \left\{ \tilde{\mathbf{K}}_T + [Re(\lambda_1^*) - \lambda] \tilde{\mathbf{K}}_{T,\lambda} \right\} Im(\mathbf{v}_1^*) = 0. \end{aligned} \quad (\text{D.54})$$

Premultiplication of (D.52) by $Im(\mathbf{v}_1^{*T})$ and of (D.53) by $Re(\mathbf{v}_1^{*T})$ and subtraction of the first one of the so-obtained relations from the second one results in

$$Re(\mathbf{v}_1^{*T}) \tilde{\mathbf{K}}_{T,\lambda} Re(\mathbf{v}_1^*) + Im(\mathbf{v}_1^{*T}) \tilde{\mathbf{K}}_{T,\lambda} Im(\mathbf{v}_1^*) = 0. \quad (\text{D.55})$$

Substitution of (D.55) into (D.54) gives

$$Re(\mathbf{v}_1^{*T})\tilde{\mathbf{K}}_T Re(\mathbf{v}_1^*) + Im(\mathbf{v}_1^{*T})\tilde{\mathbf{K}}_T Im(\mathbf{v}_1^*) = 0. \quad (D.56)$$

At point R , the eigenvalue $\lambda_1^* - \lambda$ is still real. Hence,

$$Im(\lambda_1^*) = 0 \xrightarrow{(D.50.1)} Re(\lambda_1^*) = \lambda_1^*. \quad (D.57)$$

The eigenvalue represents a double root of the consistently linearized eigenproblem. The dash-dotted curve in Fig. D.1(a) is the eigenvalue curve that joins the eigenvalue curve, which contains point C , at point R . Since, for $\lambda > \lambda_R$, the two eigenvalue functions $\lambda_1^* - \lambda$ and $\lambda_j^* - \lambda$ are conjugate complex functions:

$$\lambda_1^* = Re(\lambda_1^*) + i Im(\lambda_1^*), \quad \lambda_j^* = \bar{\lambda}_1^* = Re(\lambda_1^*) - i Im(\lambda_1^*). \quad (D.58)$$

Substitution of (D.57) into (D.52) and (D.53) yields

$$\left[\tilde{\mathbf{K}}_T + (\lambda_1^* - \lambda)\tilde{\mathbf{K}}_{T,\lambda} \right] Re(\mathbf{v}_1^*) = \mathbf{0} \quad \text{and} \quad \left[\tilde{\mathbf{K}}_T + (\lambda_1^* - \lambda)\tilde{\mathbf{K}}_{T,\lambda} \right] Im(\mathbf{v}_1^*) = \mathbf{0}, \quad (D.59)$$

respectively, resulting in

$$Re(\mathbf{v}_1^*) = Im(\mathbf{v}_1^*). \quad (D.60)$$

Substitution of (D.60) into (D.50.2) gives

$$\mathbf{v}_1^* = (1 + i) Re(\mathbf{v}_1^*). \quad (D.61)$$

Consequently,

$$\mathbf{v}_j^* = \bar{\mathbf{v}}_1^* = (1 - i) Re(\mathbf{v}_1^*). \quad (D.62)$$

Inserting (D.60) into (D.56) and (D.55), yields

$$Re(\mathbf{v}_1^{*T})\tilde{\mathbf{K}}_T Re(\mathbf{v}_1^*) = 0 \quad \text{and} \quad Re(\mathbf{v}_1^{*T})\tilde{\mathbf{K}}_{T,\lambda} Re(\mathbf{v}_1^*) = 0. \quad (D.63)$$

Writing (D.1) for the first eigenpair and premultiplying the so-obtained relation by \mathbf{v}_1^{*T} , yields

$$\mathbf{v}_1^{*T} \left[\tilde{\mathbf{K}}_T + (\lambda_1^* - \lambda)\tilde{\mathbf{K}}_{T,\lambda} \right] \mathbf{v}_1^* = 0. \quad (D.64)$$

Substitution of (D.61) into (D.64) gives

$$2i Re(\mathbf{v}_1^{*T}) \left[\tilde{\mathbf{K}}_T + (\lambda_1^* - \lambda)\tilde{\mathbf{K}}_{T,\lambda} \right] Re(\mathbf{v}_1^*) = 0. \quad (D.65)$$

Eq. (D.65) disintegrates into (D.63). Consequently, (D.64) disintegrates into

$$\mathbf{v}_1^{*T}\tilde{\mathbf{K}}_T\mathbf{v}_1^* = 0 \quad \text{and} \quad \mathbf{v}_1^{*T}\tilde{\mathbf{K}}_{T,\lambda}\mathbf{v}_1^* = 0. \quad (D.66)$$

Substitution of (D.61) into (D.5) results in

$$\lambda_{1,\lambda}^* = -(\lambda_1^* - \lambda) \frac{Re(\mathbf{v}_1^{*T}) \tilde{\mathbf{K}}_{T,\lambda\lambda} Re(\mathbf{v}_1^*)}{Re(\mathbf{v}_1^{*T}) \tilde{\mathbf{K}}_{T,\lambda} Re(\mathbf{v}_1^*)}. \quad (\text{D.67})$$

Because of (D.63.2) and of

$$\lambda_1^* - \lambda \neq 0 \quad \text{and} \quad Re(\mathbf{v}_1^{*T}) \tilde{\mathbf{K}}_{T,\lambda\lambda} Re(\mathbf{v}_1^*) \neq 0, \quad (\text{D.68})$$

$$\lambda_{1,\lambda}^* \Big|_{\lambda=\lambda_R} = -\infty. \quad (\text{D.69})$$

Obviously,

$$\lambda_{j,\lambda}^* \Big|_{\lambda=\lambda_R} = -\lambda_{1,\lambda}^* \Big|_{\lambda=\lambda_R} = +\infty. \quad (\text{D.70})$$

The final situation $F=N=T$ of the limiting case T is characterized by the coincidence of points C and R (see Fig. D.1(b)). Hence, the eigenvalue represents a double root of the consistently linearized eigenproblem. Its value is zero, i.e.

$$\lambda_1^* - \lambda = \lambda_j^* - \lambda = 0. \quad (\text{D.71})$$

For this limiting case, the Eqs. (106), (113), and (114) hold, i.e.

$$\lambda_{,\xi} = 0, \quad \lambda_{,\xi\xi} = 0, \quad \mathbf{v}_1 = \mathbf{0}, \quad \tilde{\mathbf{K}}_{T,\xi} \mathbf{v}_{1,\xi} = \mathbf{0}, \quad \tilde{\mathbf{K}}_T d\tilde{\mathbf{u}} = \mathbf{0}. \quad (\text{D.72})$$

By analogy to (D.72.3) and (D.72.4),

$$\mathbf{v}_j^* = \mathbf{v}_j = \mathbf{0}, \quad \tilde{\mathbf{K}}_{T,\xi} \mathbf{v}_{j,\xi}^* = \mathbf{0}. \quad (\text{D.73})$$

As regards the eigenvalue function $\lambda_1^*(\lambda) - \lambda$, the term “limiting case” means that at point C of the eigenvalue curve (see Fig. D.1(a)),

$$\lambda_1^* - \lambda = 0, \quad \lambda_{1,\lambda}^* = 0, \quad \underline{\lambda_{1,\lambda\lambda}^* = 0}, \quad (\text{D.74})$$

indicating a saddle point. In contrast to the limiting case, the underlined relation in (D.74) does not hold for the standard case. The term “final situation” (of the limiting case) means that at point $R=C$ of the eigenvalue curve (see Fig. D.1(b)),

$$\lambda_1^* - \lambda = 0, \quad \lambda_{1,\lambda}^* = 0, \quad \underline{\lambda_{1,\lambda\lambda}^* = 0}, \quad \underline{\lambda_{1,\lambda\lambda\lambda}^* = 0}, \quad \underline{\lambda_{1,\lambda\lambda\lambda\lambda}^* = 0}, \quad (\text{D.75})$$

indicating a saddle point of higher order. In contrast to this “final situation”, which is associated with the transition to no buckling (see Fig. 5(a)), the doubly underlined relations in (D.75) do not hold for the standard situation of the limiting case.

Fig. D.2 (cylindrical panel): The curve in Fig. D.2 that contains the bifurcation point (point C) and the dash-dotted curve in this Figure show the functions $\lambda_1^*(\lambda)$ and $\lambda_j^*(\lambda)$, both related to point T in Fig. 4(c) (cylindrical panel). At point C , $\lambda_1^* = \lambda$, $\lambda_{1,\lambda}^* = 0$,

$\lambda_{1,\lambda\lambda}^* = 0$, and $\lambda_{1,\lambda\lambda\lambda}^* = 0$. For $\lambda > \lambda_R$, where λ_R refers to point R in Fig. D.2, $\lambda_1^*(\lambda)$ and $\lambda_j^*(\lambda)$ are conjugate complex functions.

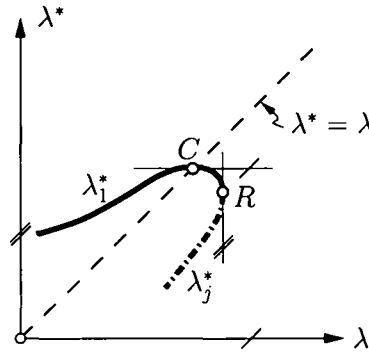
As regards the eigenvalue function $\lambda_1^*(\lambda) - \lambda$, the term "limiting case" means that at point C of the eigenvalue curve (see Fig. D.2),

$$\lambda_1^* - \lambda = 0, \quad \lambda_{1,\lambda}^* = 0, \quad \underline{\lambda_{1,\lambda\lambda}^*} = 0, \quad \lambda_{1,\lambda\lambda\lambda}^* = 0, \quad (D.76)$$

indicating a planar point. In contrast to the limiting case, the underlined relation in (D.76) does not hold for the standard case which differs from the one for the *von Mises* truss by the existence of the condition (D.76.4). The term "final situation" (of the limiting case) means that at point C ,

$$\lambda_1^* - \lambda = 0, \quad \lambda_{1,\lambda}^* = 0, \quad \underline{\lambda_{1,\lambda\lambda}^*} = 0, \quad \lambda_{1,\lambda\lambda\lambda}^* = 0, \quad \underline{\lambda_{1,\lambda\lambda\lambda\lambda}^*} = 0, \quad (D.77)$$

indicating the aforementioned saddle point of higher order. In contrast to the "final situation", which is associated with the transition to no buckling (see Fig. 5(a)), the doubly underlined relation in (D.77) does not hold for the standard situation of the limiting case.



(a)

Fig. D.2. Eigenvalue curves related to point T (see Fig. 4(c)) representing a limiting case

• *Points T in Fig. 4(h)*. The situation at points T in Fig. 4(h) is the same as the one at point T in Fig. 4(d) (cylindrical panel). Hence, the curves $\lambda_1^*(\lambda)$ related to points T in Fig. 4(h) have a planar point at the bifurcation point. Consequently, Fig. D.2 and (D.76) also apply to the points T in Fig. 4(h), whereas (D.77) also applies to the final situation $F=N=T$ of this limiting case.

References

- [1] B. Bochenek. Problems of structural optimization for post-buckling behaviour. *Structural and Multidisciplinary Optimization*, 25(5–6):423–435, 2003.
- [2] B. Bochenek and J. Kruszelecki. A new concept of optimization for postbuckling behaviour. *Engineering Optimization*, 33:503–522, 2001.
- [3] F. Fujii. Multiple hill-top branching. In L. G. Wang, C.M. and K. Ang, editors, *Proceedings of the 2nd International Conference on Structural Stability and Dynamics*. Singapore, December 16–18, 2002, World Scientific, 2002.
- [4] L. Godoy. Sensitivity of post-critical states to changes in design parameters. *International Journal for Solids and Structures*, 33(15):2177–2192, 1996.
- [5] P. Helnwein. Zur initialen Abschätzbarkeit von Stabilitätsgrenzen auf nichtlinearen Last-Verschiebungspfaden elastischer Strukturen mittels der Methode der Finiten Elemente [On ab initio estimates of stability limits on nonlinear load-displacement paths of elastic structures using the finite element method], volume 79 of *Dissertationen an der Technischen Universität Wien*. Österreichischer Kunst- und Kulturverlag, Wien, 1997. In German.
- [6] P. Helnwein and H. Mang. An asymptotic approach for the evaluation of errors resulting from estimations of stability limits in nonlinear elasticity. *Acta Mechanica*, 125:235–254, 1997.
- [7] P. Helnwein, H. Mang, and B. Pichler. Ab initio estimates of stability limits on nonlinear load-displacement paths: potential and limitations. *Computer Assisted Mechanics and Engineering Sciences*, 6(3/4):345–360, 1999.
- [8] W. Koiter. On the stability of elastic equilibrium. Translation of ‘Over de Stabieleit van het Elastisch Evenwicht’ (1945). In NASA TT F-10833. Polytechnic Institute Delft, H.J. Paris Publisher, Amsterdam, 1967.
- [9] Z. Mróz and R. Haftka. Design sensitivity analysis of non-linear structures in regular and critical states. *International Journal for Solids and Structures*, 31(15):2071–2098, 1994.
- [10] Z. Mróz and J. Piekarski. Sensitivity analysis and optimal design of non-linear structures. *International Journal for Numerical Methods in Engineering*, 42:1231–1262, 1998.
- [11] R. Reitinger. *Stabilität und Optimierung imperfektionsempfindlicher Tragwerke* [Stability and optimization of imperfection-sensitive structures]. Dr.-Ing. dissertation, Universität Stuttgart, Institut für Baustatik, 1994. Bericht Nr. 17. In German.
- [12] C. Schranz, B. Krenn, and H. Mang. Conversion of imperfection sensitive to -insensitive elastic structures II: Numerical investigation. Accepted for publication to *Computer Methods in Applied Mechanics and Engineering*.
- [13] T. Tarnai. Zero stiffness elastic structures. *International Journal of Mechanical Sciences*, 45:425–431, 2003.
- [14] O. Zienkiewicz and R. Taylor. *The Finite Element Method*, volume 2. McGraw-Hill, London, England, 4. edition, 1994.

List of Tables

1	Values of $\lambda_{2,\kappa}$, λ_4 , and a_1 for points $T(\lambda_2 = 0, \lambda_4, a_1)$ in Figs. 4(a)–4(h)	16
A.1	Coefficient tensors for Koiter’s post-buckling analysis in the context of the FEM, evaluated at the bifurcation point C	30

List of Figures

1	Initial postbuckling analysis at the bifurcation point C	3
2	Half-axes $\lambda_4 \leq 0$ and $a_1 \leq 0$ as geometric loci of all points associated with $\lambda_2 = 0$	12
3	Five octants as geometric loci of triples of values $(\lambda_2, \lambda_4, a_1)$ for $\lambda_C > 0$	12
4	Qualitative plots of curves $\lambda_2 = \lambda_2(\kappa)$, $\lambda_4 = \lambda_4(\kappa)$, $a_1 = a_1(\kappa)$, with (at least) one point $T(\lambda_2 = 0, \lambda_4, a_1)$	14
5	Degeneration of secondary paths to a point on load-displacement curves [saddle point (Fig. 5(a)) and point of inflection (Figs. 5(b) and 5(c)), respectively]	18
6	Plots of curves $\lambda_2 = \lambda_2(\kappa)$, $\lambda_4 = \lambda_4(\kappa)$, with one point $T(\lambda_2 = 0, \lambda_4)$ and one point $Q(\lambda_2, \lambda_4 = 0)$ each	22
D.1	Eigenvalue curves related to (a) point T in Fig. 4(b) representing a limiting case, and (b) point $F=N=T$ (see Fig. 4(g)) representing the final situation of this limiting case	40
D.2	Eigenvalue curves related to point T (see Fig. 4(c)) representing a limiting case	43

Conversion from Imperfection-Sensitive into Imperfection-Insensitive Elastic Structures II: Numerical Investigation ^{*}

Christian Schranz ^a, Burkhard Krenn ^a, Herbert A. Mang ^{a,*}

^a*Institute for Mechanics of Materials and Structures, Vienna University of Technology, Karlsplatz 13, A-1040 Vienna, Austria*

Abstract

A qualitative improvement of the initial postbuckling behavior of imperfection-sensitive elastic structures is their conversion into imperfection-insensitive structures. Attempts to achieve such a conversion include the increase of the thickness and of the stiffness of a spring attached to the structure, respectively, and the reduction of the rise of the undeformed structure. Four different structures serve as objects of the numerical investigation. The results of this investigation include different modes of conversion from imperfection-sensitive into imperfection-insensitive structures as well as failure to achieve such a conversion. They corroborate the theoretical results reported in Part I of this work.

Key words: symmetric bifurcation buckling, imperfection sensitivity, conversion into imperfection insensitivity, numerical investigation, finite element method

1 Introduction

In order to improve the mechanical behavior of imperfection-sensitive structures, it is not only important to investigate the influence of a stiffness increase on the prebuckling behavior and the stability limit. What is equally important is knowledge about the influence of such an increase on the postbuckling response. This was recognized e.g. by Bochenek and Kruźelecki who have dealt with optimization of the postbuckling behavior of elastic structures (Bochenek and Kruźelecki [1]). In case of loss of stability by means of symmetric bifurcation, a qualitative improvement of the postbuckling response in consequence of stiffening is the conversion from an originally imperfection-sensitive into an

* Dedicated to Prof. Thomas J.R. Hughes on the occasion of his 60th birthday

* Corresponding author.

Email addresses: Christian.Schranz@tuwien.ac.at (Christian Schranz), Burkhard.Krenn@tuwien.ac.at (Burkhard Krenn), Herbert.Mang@tuwien.ac.at (Herbert A. Mang).

imperfection-insensitive structure. Designation of a structure as either imperfection sensitive or insensitive depends on the initial postbuckling behavior (Koiter [4]) which often is (but certainly need not be) relevant for the entire postbuckling response. In any case, the search for specific modes of stiffening that result in the aforementioned conversion is of fundamental as well as of practical importance.

In Part I of this work [5], Koiter's initial postbuckling analysis [4] is applied in the context of the Finite Element Method (FEM) (Reitinger [6]) to deduce mathematical relations associated with the transition from imperfection sensitivity into insensitivity. Such a transition can obviously only be achieved for symmetric bifurcation. Of special interest are the first two non-vanishing coefficients in the polynomial expression for $\lambda(\eta)$ in Koiter's initial postbuckling analysis (see Eq. (6) in Part I of this work [5]), namely λ_2 and λ_4 . The coefficient λ_2 plays an essential role in the mathematical expression for the slope, and the coefficients λ_2 and λ_4 in the one for the curvature of (suitable projections of) the postbuckling paths at the bifurcation point. In fact, the sign of the slope of the postbuckling path at the bifurcation point is equal to the sign of λ_2 . For $\lambda_2 = 0$, which is a necessary condition for the transition from imperfection sensitivity into insensitivity, the sign of the curvature of the postbuckling path at the stability limit is equal to the sign of λ_4 . Hence, imperfection sensitivity is characterized by $\lambda_2 < 0$, and imperfection insensitivity by $\lambda_2 > 0$. If $\lambda_2 = 0$, the sign of λ_4 is relevant, and if $\lambda_2 = 0$ and $\lambda_4 = 0$, the sign of λ_6 .

For the investigation of different modes of transition from imperfection sensitivity into insensitivity, the following relationship between λ_2 and λ_4 has been derived (see Eq. (36) in Part I of this work [5]):

$$\lambda_4 = a_1 \lambda_2^2 + b_2 \lambda_2 + d_3, \quad (1)$$

where a_1 (see Eq. (16) in Part I of this work [5]) is referred to as nonlinearity coefficient because it vanishes trivially for linear prebuckling paths, and b_2 and d_3 are parameters depending on directional derivatives of the stiffness matrix $\bar{\mathbf{K}}_T$ (see Eqs. (C.2) and (C.4) in Appendix C of Part I of this work [5]). The coefficient a_1 is closely related to the curvature of the curve $\lambda_1^*(\lambda)$ (which in turn is closely related to the eigenvalue curve $\lambda_1^*(\lambda) - \lambda$ of the consistently linearized eigenproblem (Helnwein [3])), at the stability limit (see Eq. (D.21) in Part I of this work [5]). The sign of a_1 is opposite to the one of the curvature of this curve at the stability limit.

It is re-emphasized that, with the exception of the first and the last example, Koiter's initial postbuckling analysis is actually not used to compute postbuckling paths in the present numerical investigation. Primarily, it serves the purpose of deducing important theoretical results and verifying specific numerical results. Rather, the structural analyses of examples 2 and 3 are performed by means of the FEM, using the finite element program FEAP [10] with a modification (Helnwein [3]) of a shell element developed by Simo et al. [7,8]. Each numerical analysis of load-displacement paths is complemented by an accompanying linear eigenvalue analysis. Results are presented in form of load-displacement diagrams including the primary and the secondary path and of the aforementioned curve $\lambda_1^*(\lambda)$. (Although, strictly speaking, $\lambda_1^*(\lambda) - \lambda$ is the eigenvalue curve, $\lambda_1^*(\lambda)$ will, in general, be referred to as this curve.)

Fig. 4 in Part I of this work [5] shows qualitative illustrations of eight λ_2 - λ_4 - a_1 curves, with λ_2 , λ_4 , and a_1 depending on a design parameter κ . Each curve contains at least one point T , at which $\lambda_2 = 0$, which is a necessary condition for the transition from imperfection sensitivity into imperfection insensitivity. In the following, numerical examples are presented which refer to the eight curves shown in Fig. 4 in Part I [5]. The purpose of each one of these examples, which are characterized by nonlinear prebuckling paths, is conversion of the structure from imperfection sensitivity into insensitivity. Finally, one example with linear prebuckling paths will complete the numerical investigation.

2 Numerical Investigation

A pin-jointed bar (see Subchapter 2.1), a *von Mises* truss (see Subchapter 2.2) and a shallow cylindrical shell (see Subchapter 2.3) serve as examples with nonlinear prebuckling paths. Originally, each one of these three structures is imperfection sensitive. The aim of the numerical investigation is the conversion from imperfection-sensitive into imperfection-insensitive structures. Attempts to achieve this goal include different strategies such as the increase of the thickness of the structure, the increase of the stiffness of an elastic spring attached to the structure, and the reduction of the rise of the undeformed structure, termed as initial rise.

Another pin-jointed bar (see Subchapter 2.4) serves as the example with linear prebuckling paths. Here, the strategies of stiffening include the attachment of elastic springs as well as the change of the length of one of the bars.

2.1 Example 1: Pin-jointed bar with two degrees of freedom

Consider the plane pin-jointed bar in Fig. 1, composed of two rigid bars of length l and three linear-elastic springs with stiffnesses c_1 , c_2 , and c_3 , loaded by a vertical nodal force $\lambda \bar{P}$ at joint 1 of the structure; \bar{P} is the reference force and λ is a dimensionless load factor.

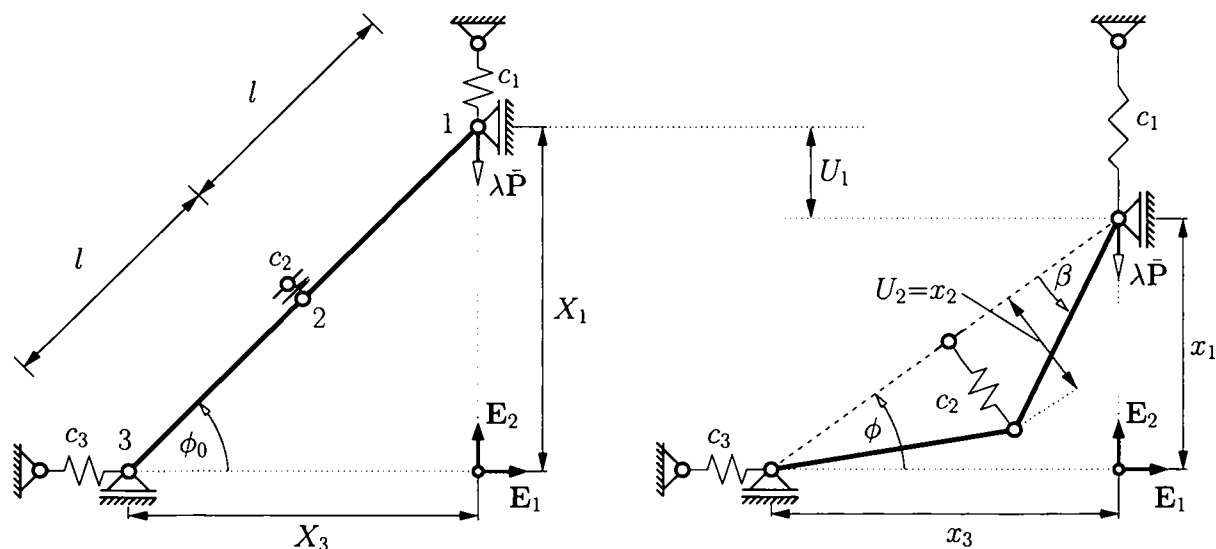


Fig. 1. Geometric properties of a pin-jointed bar with two rigid rods

The displacements of the three joints, \mathbf{U}_1 , U_2 , \mathbf{U}_3 , are expressed in terms of the two angles ϕ and β (see Fig. 1). For joint 2, only the displacement normal to the line connecting joints 1 and 3 is considered. (Therefore, \mathbf{U}_2 is treated as a scalar.) \mathbf{U}_1 , U_2 , and \mathbf{U}_3 are given as follows:

$$\begin{aligned} \mathbf{U}_1 &= (x_1 - X_1) \mathbf{E}_2 = (2l \sin \phi \cos \beta - 2l \sin \phi_0) \mathbf{E}_2 = U_1 \mathbf{E}_2, \\ U_2 &= x_2 = l \sin \beta, \\ \mathbf{U}_3 &= (x_3 - X_3) (-\mathbf{E}_1) = (2l \cos \phi \cos \beta - 2l \cos \phi_0) (-\mathbf{E}_1) = U_2 (-\mathbf{E}_1). \end{aligned} \quad (2)$$

The total potential energy of the structure is obtained as

$$\Pi = \Pi(\phi, \beta, \lambda) = U(\phi, \beta, \lambda) + W(\phi, \beta, \lambda), \quad (3)$$

where

$$U(\phi, \beta, \lambda) = \frac{1}{2} c_1 \mathbf{U}_1^T \cdot \mathbf{U}_1 + \frac{1}{2} c_2 (U_2)^2 + \frac{1}{2} c_3 \mathbf{U}_3^T \cdot \mathbf{U}_3 \quad (4)$$

is the strain energy and

$$W(\phi, \beta, \lambda) = -\lambda \bar{\mathbf{P}}^T \cdot \mathbf{U}_1 = -\lambda (-\mathbf{E}_2)^T \cdot \mathbf{U}_1 = \lambda U_1 \quad (5)$$

is the potential of the external load. With the notation of Eq. (1) in Part I of this work [5], the equilibrium equations of the considered discrete mechanical system are given as

$$\mathbf{G}(\phi, \beta, \lambda) = \begin{bmatrix} G_1(\phi, \beta, \lambda) \\ G_2(\phi, \beta, \lambda) \end{bmatrix} = \begin{bmatrix} \frac{\partial \Pi}{\partial \phi} \\ \frac{\partial \Pi}{\partial \beta} \end{bmatrix} = \mathbf{0}. \quad (6)$$

The displacements and the load-displacement functions of the primary and secondary solution path satisfy (6). They are obtained as

$$\begin{aligned} \beta^I(\phi) &= 0, \\ \lambda^I(\phi) &= -2lc_1 (\sin \phi - \sin \phi_0) + 2lc_3 (\cos \phi - \cos \phi_0) \frac{\sin \phi}{\cos \phi}, \end{aligned} \quad (7)$$

and

$$\begin{aligned} \beta^{II}(\phi) &= \pm \arccos \left[\frac{4c_3}{(4c_3 - c_2) \cos \phi} \cos \phi_0 \right], \\ \lambda^{II}(\phi) &= \frac{8lc_3}{4c_3 - c_2} \left(\frac{c_2}{4} - c_1 \right) \frac{\sin \phi}{\cos \phi} \cos \phi_0 + 2lc_1 \sin \phi_0, \end{aligned} \quad (8)$$

respectively.

The angle associated with bifurcation of equilibrium or snap-through is obtained as

$$\phi_{bif} = \pm \arccos\left(\frac{4c_3}{4c_3 - c_2} \cos \phi_0\right) \quad \text{and} \quad \phi_{st} = \pm \arccos\left(\sqrt[3]{\frac{c_3 \cos \phi_0}{c_3 - c_1}}\right), \quad (9)$$

respectively. Based on (6), the initial postbuckling analysis can be performed analytically and the linearized eigenproblem (see Appendix D in Part I of this work [5]) can be solved analytically.

2.1.1 Increase of spring stiffness c_1

This situation refers to Fig. 4(a) in the companion paper [5]. The design parameter κ is the stiffness c_1 of the spring attached to joint 1. Three different values of c_1 , referring to points S , T , and I in Fig. 4(a) in Part I of this work [5], are considered. The geometric properties, the spring stiffnesses, and the resulting values for λ_2 , λ_4 , and a_1 are listed in Table 1. Load-displacement paths and corresponding eigenvalue curves are shown in Fig. 2.

Table 1

Geometric properties (dimensionless), spring stiffnesses (dimensionless), and results (λ_2 , λ_4 , a_1) from initial postbuckling analysis

geometric properties	spring stiffnesses	point	S	T	I
$l = 10$	$\kappa = c_1$	$\kappa = c_1$	0.0	1.5	5.6
$\phi_0 = 0.9$ [rad]	$c_2 = 6$	λ_2	-21.99253	0	60.06497
	$c_3 = 10$	λ_4	-4.48822	0	12.25802
		a_1	-0.02131	-0.009915	0

The main parts of interest are the stretch of the primary path before the stability limit and the (projection of the) secondary path (into the U_1 - λ plane). These parts are shown as solid lines. The dashed parts of the curves refer to the stretch of the primary path between the stability limit and the return of the secondary to the primary path. The stability limit is denoted as C , and the snap-through point as D . Fig. 2(b) shows the corresponding eigenvalue curves $\lambda_1^*(\lambda)$ and $\lambda_2^*(\lambda)$, where $\lambda_1^*(\lambda)$ refers to the bifurcation mode and $\lambda_2^*(\lambda)$ to the snap-through mode.

The slope of the eigenvalue curve $\lambda_1^*(\lambda)$ at the bifurcation point C is zero (see Eq. (D.15) in Part I of this work [5]), whereas the slope of $\lambda_2^*(\lambda)$ at the snap-through point D is -1 (Helnwein [3]). For $c_1 = 0$, the structure is imperfection sensitive ($\lambda_2 < 0$). An increase of the spring stiffness improves the postbuckling behavior and the structure eventually becomes imperfection insensitive.

The condition $c_1 = c_2/4$ represents the so-called *borderline case* (transition point T in Fig. 4(a) in Part I of this work [5]), i.e. $\lambda_2 = 0, \lambda_4 = 0, \lambda_6 = 0, \dots$ (see Eq. (95) in Part I of this work [5]). For $c_1 \approx 5.6$, a_1 becomes zero (see Eq. (96) in Part I of this work [5]), i.e. the eigenvalue curve has a saddle point at the bifurcation point (see Eq. (D.26) in Part I of this work [5]). This situation refers to point I in Fig. 4(a) in Part I of this

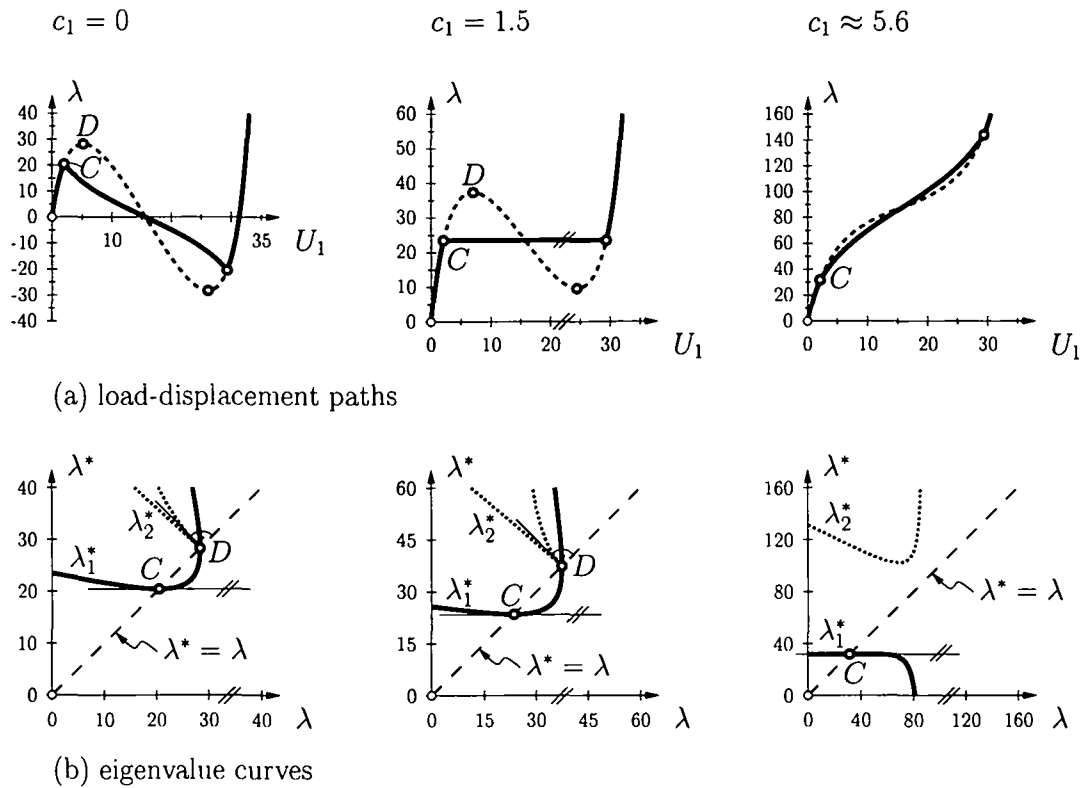


Fig. 2. (a) Load-displacement paths and (b) corresponding eigenvalue curves of a pin-jointed bar for three different values of the spring stiffness c_1

work [5]. Hence, for this example, the change of the sign of the curvature of the eigenvalue curve is not associated with the transition of the structure from imperfection sensitivity into insensitivity.

2.1.2 Reduction of initial rise of the structure

In the following, the influence of a reduction of the rise of the undeformed truss on the initial postbuckling behavior will be investigated. This example refers to Fig. 4(f) in the companion paper. The design parameter κ is the initial angle ϕ_0 of the structure. Geometric properties, spring stiffnesses, and resulting values for λ_2 , λ_4 , and a_1 for three different values of ϕ_0 , referring to points $S=T$ and $F=N=T$ in Fig. 4(f) in Part I of this work [5], are listed in Table 2.

Table 2

Geometric properties (dimensionless), spring stiffnesses (dimensionless), and results (λ_2 , λ_4 , a_1) from initial postbuckling analysis

geometric properties	spring stiffnesses	point	$S=T$	$F=N=T$
$l = 10$	$c_1 = 1.5$	$\kappa = \phi_0$	0.90	0.55
$\kappa = \phi_0$ [rad]	$c_2 = 6.0$	λ_2, λ_4	0	0
	$c_3 = 10.0$	a_1	-0.009915	-0.057356
				$-\infty$

The degeneration of the horizontal secondary path (*borderline case*) to a single point on the primary path is of interest. The condition for this degeneration is obtained as

$$4c_3(1 - \cos \phi_0) = c_2. \quad (10)$$

Load-displacement paths and corresponding eigenvalue curves for the considered values of ϕ_0 are shown in Fig. 3. As the initial rise of the structure decreases, the buckling load is decreasing.

The slope of the corresponding eigenvalue curve $\lambda_1^*(\lambda)$ at the bifurcation point is equal to -1 (see Eq. (D.48) in Part I of this work [5]) and the curvature is infinite (see Eq. (D.49) in Part I of this work [5]). The notation $C=D$ in Fig. 3 could be misleading insofar as this point, which represents the transition to no loss of stability, is neither a bifurcation point nor a snap-through point. For $\phi_0 = 0.50$, the load-displacement path is monotonous and does not contain a bifurcation point.

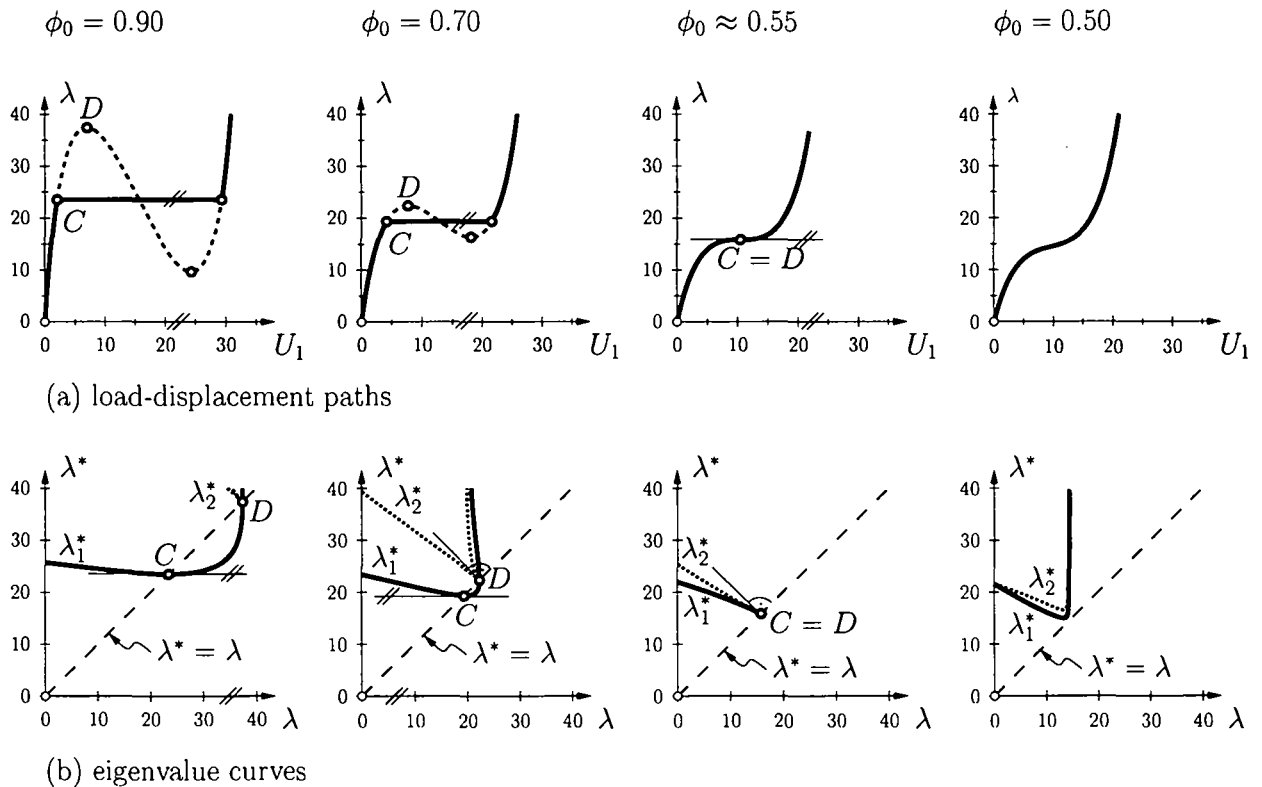
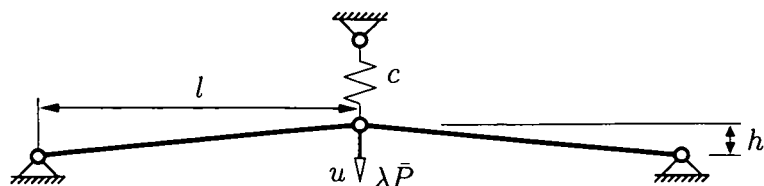


Fig. 3. (a) Load-displacement paths and (b) corresponding eigenvalue curves of a pin-jointed bar for four different values of the angle ϕ_0

2.2 Example 2: von Mises truss

The second example is a *von Mises* truss with an elastic spring attached to the load point. This example refers to Fig. 4(b) in Part I of this work [5]. Fig. 4 contains the geometric data, the values of the cross-sectional area A , the moment of inertia I , the

modulus of elasticity E , the shear modulus G , and the value of the reference load \bar{P} . u indicates the vertical displacement at the load point and λ is a dimensionless load factor.



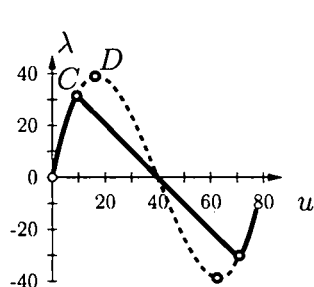
h	$=$	40 cm
l	$=$	400 cm
A	$=$	396 cm ²
I	$=$	12 982 cm ⁴
E	$=$	3102.75 kN/cm ²
G	$=$	1193.37 kN/cm ²
\bar{P}	$=$	40.0 kN

Fig. 4. Geometric properties of a *von Mises* truss with an attached spring

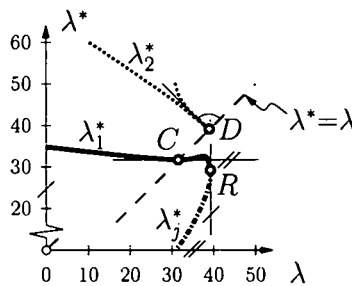
Fig. 5(a) contains load-displacement paths for a *von Mises* truss without a spring. The slope of the postbuckling path at the stability limit is negative ($\lambda_2 < 0$). Hence, the structure is imperfection sensitive.

Fig. 5(b) shows the corresponding eigenvalue curves $\lambda_1^*(\lambda)$ and $\lambda_2^*(\lambda)$, referring to the bifurcation mode and the snap-through mode, respectively. The slope of the eigenvalue curve $\lambda_1^*(\lambda)$ at the bifurcation point C is zero (see Eq. (D.15) in Part I of this work [5]), whereas the slope of $\lambda_2^*(\lambda)$ at the snap-through point D is -1 (Helnwein [3]). The curvature of the eigenvalue curve $\lambda_1^*(\lambda)$ at the bifurcation point is positive. Hence, the nonlinearity coefficient a_1 is negative (see Eq. (D.21) in Part I of this work [5]).

In the following, the eigenvalue curve $\lambda_2^*(\lambda)$ will only be shown for the case that the bifurcation point C coincides with the snap-through point D (hilltop buckling) or if snap-through is the relevant mode of loss of stability. Fig. 5(b) also contains the eigenvalue curve $\lambda_j^*(\lambda)$. For $\lambda > \lambda_R$, where λ_R refers to point R , $\lambda_1^*(\lambda)$ and $\lambda_j^*(\lambda)$ are conjugate complex functions (see also Figs. D.1 and D.2 in Part I of this work [5]).



(a) load-displacement paths



(b) eigenvalue curves

Fig. 5. (a) Load-displacement paths and (b) corresponding eigenvalue curves of a *von Mises* truss without a spring

2.2.1 Increase of spring stiffness c

The original *von Mises* truss is imperfection sensitive. In order to achieve a conversion into an imperfection-insensitive structure, a spring is attached to the hinge. Fig. 6(a) contains load-displacement paths of the *von Mises* truss for three different values of the spring

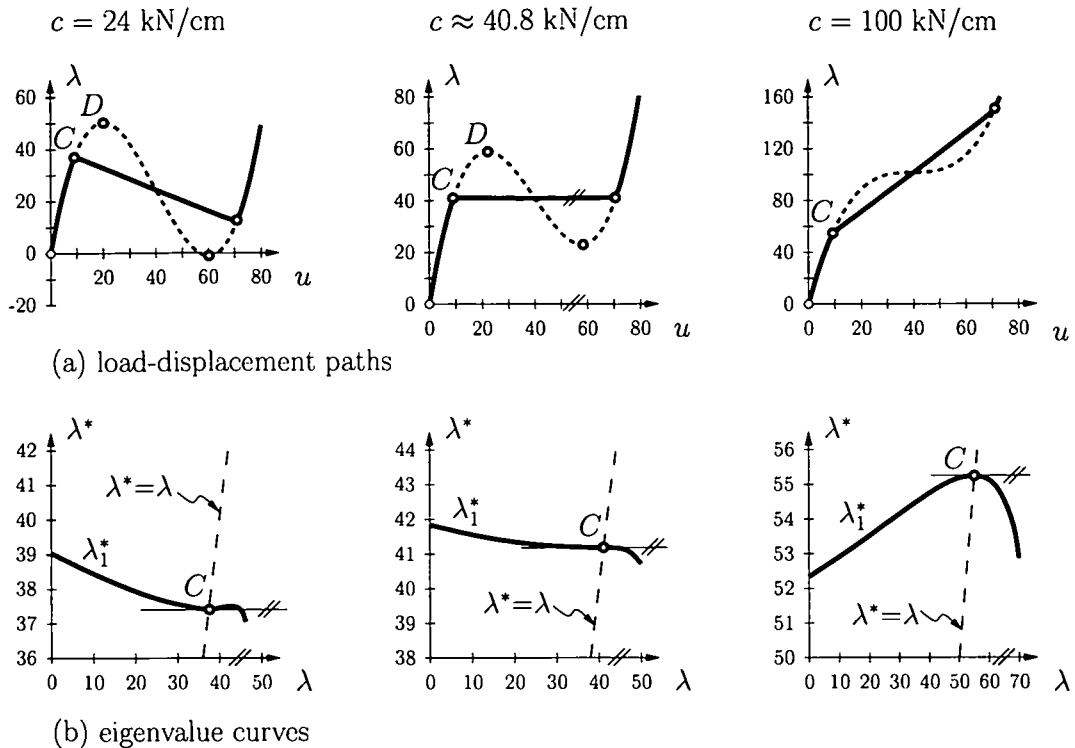


Fig. 6. (a) Load-displacement paths and (b) corresponding eigenvalue curves of a *von Mises* truss for three different values of the spring stiffness c

stiffness c . Fig. 6(b) shows the corresponding eigenvalue curves $\lambda_1^*(\lambda)$. For $c = 24 \text{ kN/cm}$, the structure is still imperfection sensitive ($\lambda_2 < 0$). For $c \approx 40.8 \text{ kN/cm}$, $\lambda_2 = 0$, $\lambda_4 = 0$, $\lambda_6 = 0, \dots$, representing the previously mentioned *borderline case* (see Eq. (97) in Part I of this work [5]). Hence, the postbuckling path is horizontal. For a larger spring stiffness, the structure is imperfection insensitive ($\lambda_2 > 0$). Thus, the increase of the spring stiffness leads to an improvement of the postbuckling behavior.

Fig. 6(b) shows that the *borderline case* is associated with a saddle point of the eigenvalue curve $\lambda_1^*(\lambda)$ at the stability limit. Hence, in contrast to the previous example, the nonlinearity coefficient a_1 vanishes nontrivially at the point of transition from imperfection sensitivity to insensitivity (see Eq. (D.22) in Part I of this work [5]). For the imperfection-sensitive truss ($c < 40.8 \text{ kN/cm}$), the curvature of this curve is positive ($a_1 < 0$), whereas it is negative ($a_1 > 0$) for the imperfection-insensitive truss ($c > 40.8 \text{ kN/cm}$).

2.2.2 Reduction of initial rise of the *von Mises* truss

In the following, the influence of a reduction of the initial rise on the initial postbuckling behavior will be investigated. This will be done for two different values of the spring stiffness c . One value is associated with the *borderline case*, i.e. with imperfection sensitivity, and the other one with imperfection insensitivity.

- $c \approx 40.8 \text{ kN/cm}$. The spring stiffness of a *von Mises* truss with a horizontal postbuckling path (*borderline case*) is kept constant, whereas the initial rise of the truss is reduced. This example refers to Fig. 4(g) in Part I of this work [5]. Figs. 7(a) and 7(b) show load-

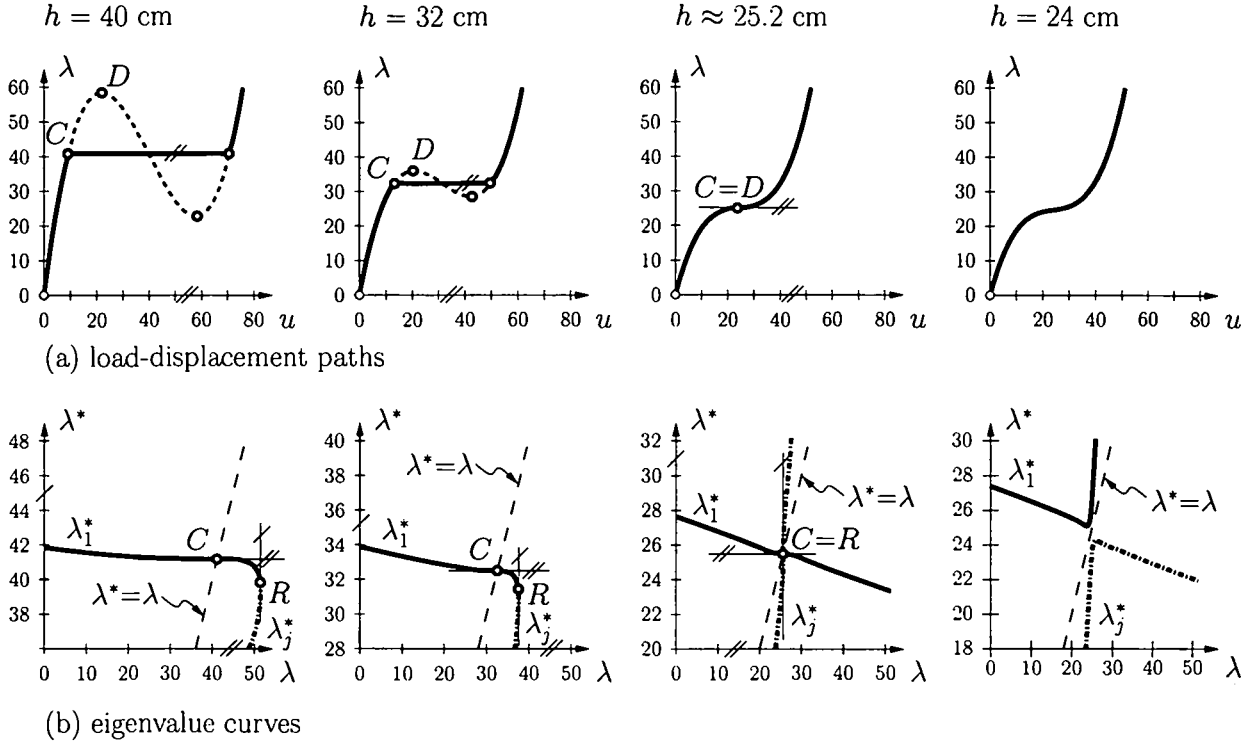


Fig. 7. (a) Load-displacement paths and (b) corresponding eigenvalue curves of a *von Mises* truss with $c \approx 40.8$ kN/cm for four different values of the initial rise h of the truss

displacement paths and corresponding eigenvalue curves, respectively, for four different values of the initial rise h of the truss.

As mentioned previously, the original *von Mises* truss is imperfection sensitive. At first, the postbuckling behavior does not change when the initial rise of the truss is reduced. For $h \approx 25.2$ cm, however, the postbuckling path degenerates to a point on the primary path, which is a saddle point (see Eq. (121) in Part I of this work [5]). Hence, a transition to no loss of stability occurs, as was found to be the case for example 1. (Again, point $C=D$ is neither a bifurcation point nor a snap-through point.) For $h = 24$ cm, the load-displacement path is monotonous and does not contain a bifurcation point.

Irrespective of the rise of the structure, the eigenvalue curve $\lambda_1^*(\lambda)$ has a saddle point at the stability limit (see Eqs. (D.74) in Part I of this work [5]). For $\lambda > \lambda_R$, where R refers to the respective points in Fig. 7(b), $\lambda_1^*(\lambda)$ and $\lambda_j^*(\lambda)$ are conjugate complex functions. For the truss with $h \approx 25.2$ cm, $C=R$, indicating a saddle point of higher order (see Eqs. (D.75) in Part I of this work [5]). Hence, a_1 is always zero (see Eq. (D.21) in Part I of this work [5]). For $h = 24$ cm, the eigenvalue curves $\lambda_1^*(\lambda)$ and $\lambda_j^*(\lambda)$ do not intersect the line $\lambda^* = \lambda$, which is consistent with the absence of a stability limit.

- $c = 60$ kN/cm. This *von Mises* truss is imperfection insensitive. Figs. 8(a) and 8(b) contain load-displacement paths and corresponding eigenvalue curves $\lambda_1^*(\lambda)$, respectively, for three different values of the initial rise h of the *von Mises* truss.

When h is reduced, the originally nonmonotonous primary path eventually becomes monotonous. However, analogous to the situation illustrated in Figs. 3(a) and 7(a), the

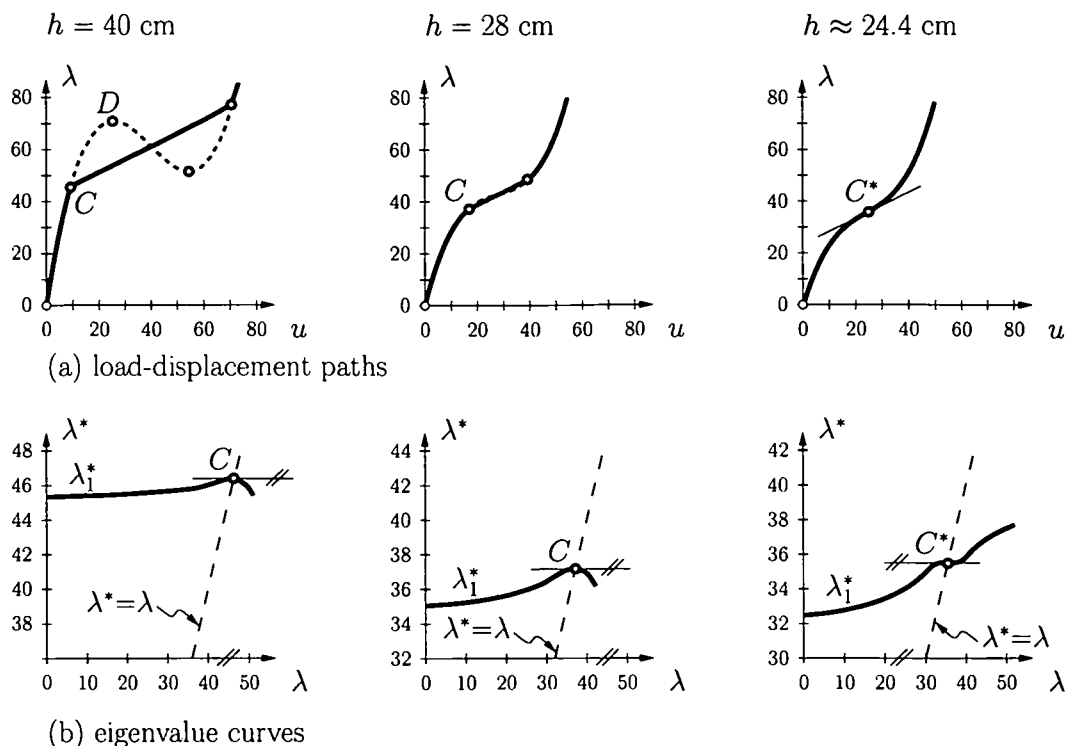


Fig. 8. (a) Load-displacement paths and (b) corresponding eigenvalue curves of a *von Mises* truss with $c = 60$ kN/cm, for three different values of the initial rise h of the truss

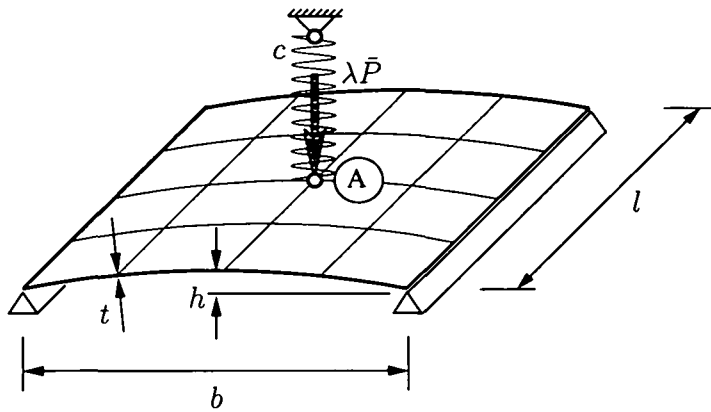
postbuckling response does not change in the sense that the slope of the postbuckling path at the bifurcation point C remains the same if h is reduced. For $h \approx 24.4$ cm, a transition from bifurcation buckling to no loss of stability occurs. The postbuckling path degenerates to a point on the monotonous primary path (see also Fig. 5(b) in Part I of this work [5]). In contrast to the situation at point $C=D$ in Figs. 3(a) and 7(a), where $\tilde{\mathbf{K}}_T$ is just still singular, at point C^* in Fig. 8(a), $\tilde{\mathbf{K}}_T$ has just become regular (see comment on Fig. 5(b) in Part I of this work [5]).

The curvature of the eigenvalue curve $\lambda_1^*(\lambda)$ at the stability limit is negative as long as bifurcation buckling occurs. Hence, a_1 is positive (see Eq. (D.21) in Part I of this work [5]). For $h \approx 24.4$ cm, $a_1 = 0$. The situation at C is analogous to the one at point $C=R$ in Fig. 7(b). (In contrast to Fig. 7(b), the eigenvalue curve $\lambda_2^*(\lambda)$ has been omitted in Fig. 8(b).)

2.3 Example 3: Shallow cylindrical shell

The third example is a shallow cylindrical shell with an elastic spring attached to the load point. Fig. 9 contains the geometric data and the values of the rise of the shell, h , the modulus of elasticity E , the shear modulus G , and the reference load \bar{P} . u indicates the vertical displacement of the load point A of the shell and λ is a dimensionless load factor.

Fig. 10(a) contains load-displacement paths of the shell without the spring, for a thickness of 6.35 cm. This structure is imperfection sensitive. Fig. 10(b) shows the corresponding eigenvalue curves $\lambda_1^*(\lambda)$ and $\lambda_2^*(\lambda)$, where $\lambda_1^*(\lambda)$ refers to the bifurcation mode and $\lambda_2^*(\lambda)$ to



$$\begin{aligned}
 l &= 508 \text{ cm} \\
 b &= 506.45 \text{ cm} \\
 h &= 12.7 \text{ cm} \\
 E &= 3102.75 \text{ kN/cm}^2 \\
 G &= 1193.37 \text{ kN/cm}^2 \\
 \bar{P} &= 52.65 \text{ kN}
 \end{aligned}$$

Fig. 9. Geometric properties of a shallow cylindrical shell with an attached spring

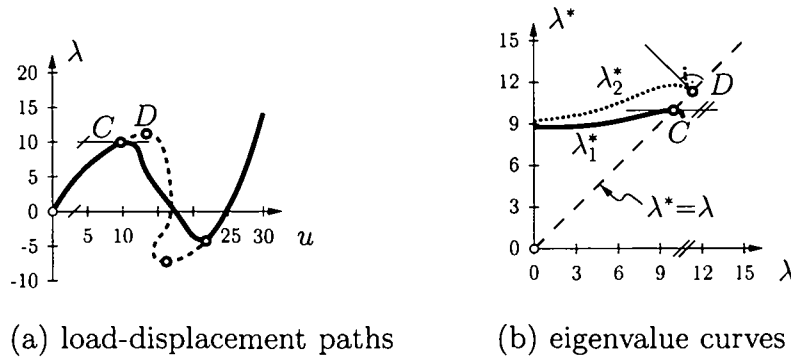


Fig. 10. (a) Load-displacement paths and (b) eigenvalue curves of a shallow cylindrical shell without a spring

the snap-through mode. The curvature of the eigenvalue curve $\lambda_1^*(\lambda)$ at the stability limit C is negative. Hence, the nonlinearity coefficient a_1 is positive (see Eq. (D.21) in Part I of this work [5]).

In the following, the eigenvalue curve $\lambda_2^*(\lambda)$ will only be shown for the case of hilltop buckling or if snap-through is the relevant mode of loss of stability.

2.3.1 Increase of thickness of shell

At first, the influence of an increase of the thickness of the shell, t , on the initial postbuckling behavior is investigated. The starting value of t is 3.35 cm; the final value is approximately 13.3 cm. This example refers to Fig. 4(c) in the companion paper [5]. Figs. 11(a) and 12(a) contain load-displacement paths for altogether five different values of t . Figs. 11(b) and 11(c) contain details of load-displacement paths and corresponding eigenvalue curves $\lambda_1^*(\lambda)$, respectively, in the vicinity of the stability limit for the first three values of t . Fig. 12(b) shows the eigenvalue curves $\lambda_1^*(\lambda)$ and $\lambda_2^*(\lambda)$ for the remaining two values of t .

Each one of the five investigated shells is imperfection sensitive. For the thinnest shell ($t = 3.35$ cm), for which $\lambda_2 < 0$, $\lambda_4 > 0$, the slope of the postbuckling path at the stability limit is negative, whereas the curvature is positive. The secondary path has a snap-through point (point D'). For the shell with $t \approx 6.35$ cm, the slope of the postbuckling path at the

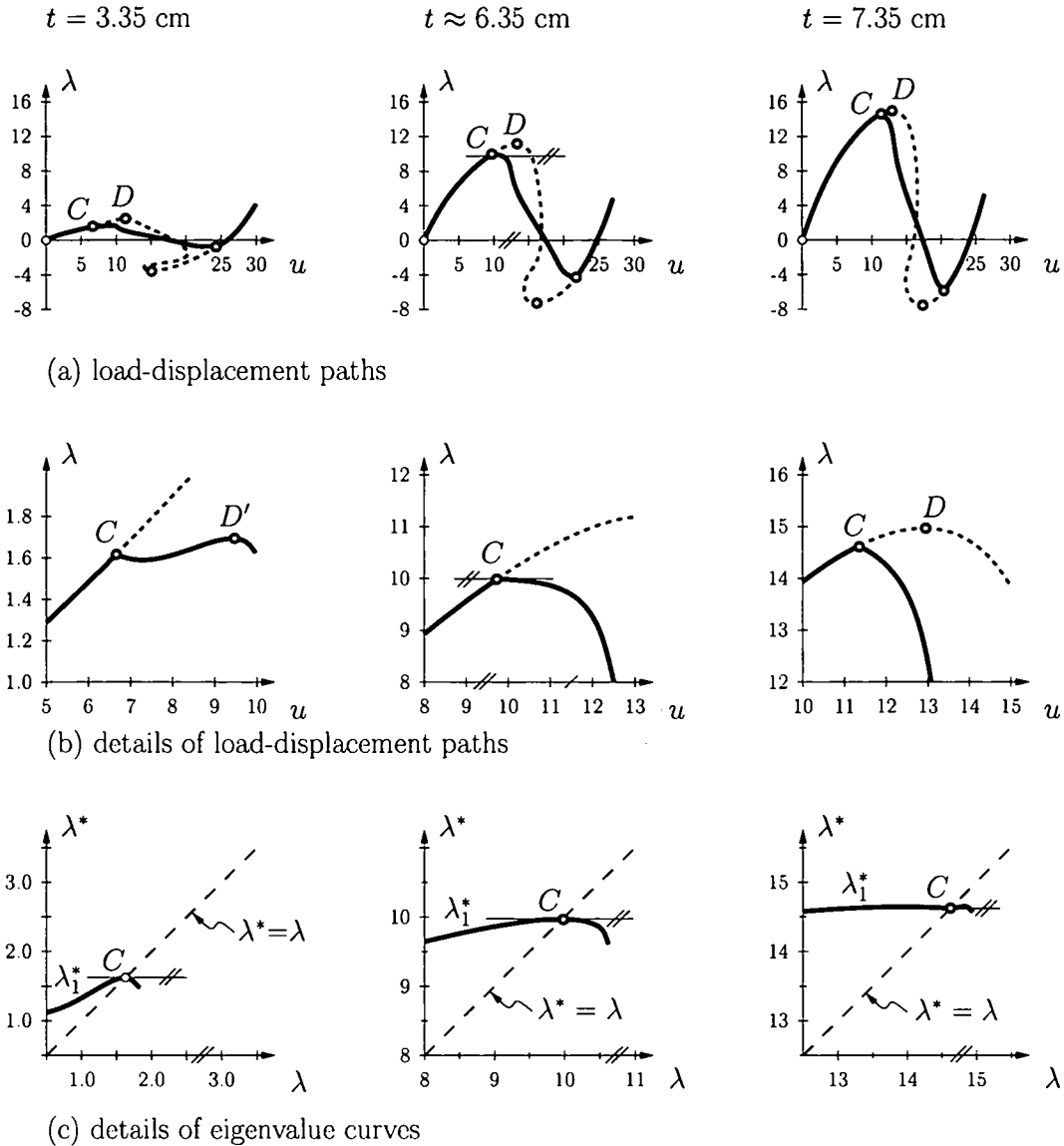


Fig. 11. (a) Load-displacement paths, (b) details of these paths and (c) of the corresponding eigenvalue curves in the vicinity of the stability limit C of a shallow cylindrical shell for three different values of the shell thickness

stability limit is zero ($\lambda_2 = 0$). For shells with $t > 6.35$ cm, this slope is again negative ($\lambda_2 < 0$). However, for these shells, for which $\lambda_4 < 0$, the curvature of the postbuckling path at the stability limit is negative. Thus, $\lambda_2 = 0$, $\lambda_4 = 0$, associated with $\lambda_6 < 0$, represents a maximum of the slope of the postbuckling path at the stability limit. It is characterized by a negative curvature.

For the shell with $t \approx 8.1$ cm, hilltop buckling occurs (see Fig. 12(a)). If the thickness is further increased, loss of stability occurs by snap-through. For $t \approx 13.3$ cm, the postbuckling path degenerates to a point on the primary path, which coincides with a point of inflection. In contrast to the situation at point $C=D$ in Figs. 3(a) and 7(a), where $\tilde{\mathbf{K}}_T$ is just still singular, at point C^* in Fig. 12(a), $\tilde{\mathbf{K}}_T$ has just become regular (see comment on Fig. 5(c) in Part I of this work [5]).

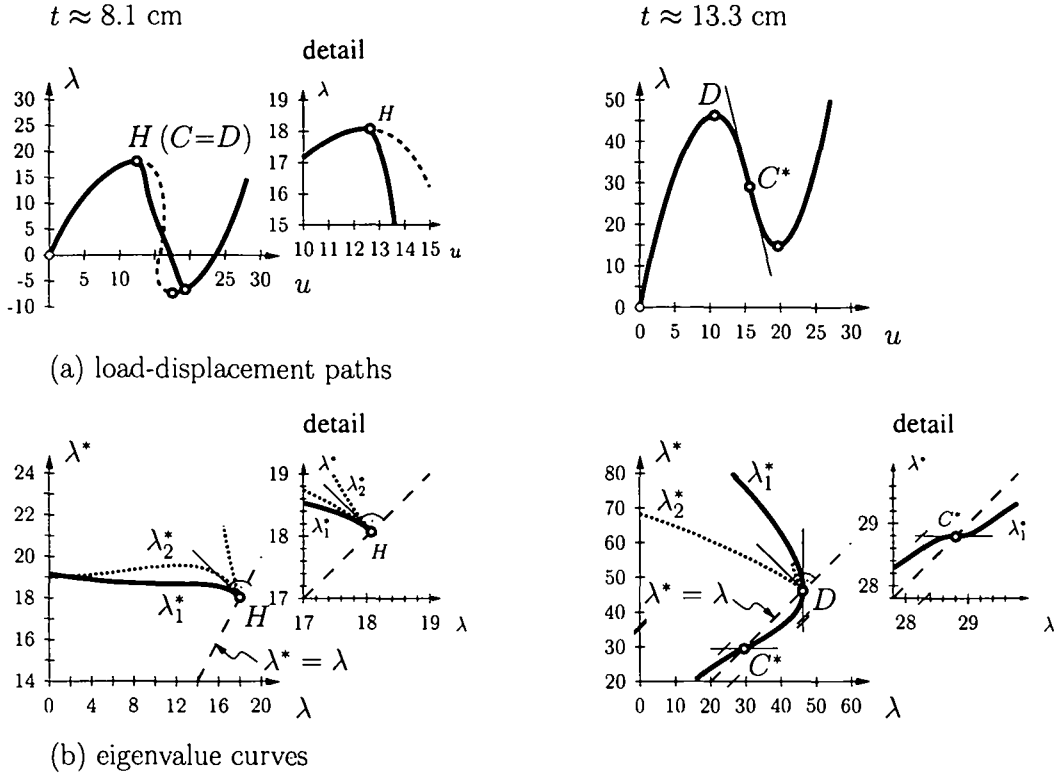


Fig. 12. (a) Load-displacement paths and (b) corresponding eigenvalue curves of a shallow cylindrical shell for two different values of the shell thickness

The curvature of the eigenvalue curves $\lambda_1^*(\lambda)$ has an extreme value at the bifurcation point C , characterized by $\lambda_1^*(\lambda) = \lambda$, $\lambda_{1,\lambda}^* = 0$, and $\lambda_{1,\lambda\lambda\lambda}^* = 0$ ^{(D.34) in [5]} $a_1^* = 0$ (see Eq. (D.27) in Part I of this work [5]). For $t \approx 6.35$ cm, the eigenvalue curve $\lambda_1^*(\lambda)$ has a planar point at C . Hence, in addition to $a_1^* = 0$, $a_1 = 0$ (see Eqs. (D.28) and (D.34) in Part I of this work [5]). For the thinnest shell, the curvature is negative ($a_1 > 0$), whereas it is positive ($a_1 < 0$) for the shell with $t = 7.35$ cm. A further increase of the thickness leads to a change of the mode of loss of stability from bifurcation buckling via hilltop buckling to snap-through. For hilltop buckling, the slope of the eigenvalue curve $\lambda_1^*(\lambda)$ at $H(C=D)$ is equal to -1 and the curvature becomes infinite ($a_1 = -\infty$) (see Eq. (102) in Part I of this work [5]). The eigenvalue curve $\lambda_1^*(\lambda)$ associated with the thickest shell has a saddle point at C ($a_1 = 0$).

Figs. 11 and 12 show that stiffening of the structure by means of a uniform increase of the thickness results in an increase of the stability limit but not in the desired conversion from imperfection sensitivity into imperfection insensitivity.

2.3.2 Increase of spring stiffness c

A spring is attached to the load point (point A in Fig. 9). The stiffness of the spring, c , represents the design parameter. The investigation is performed for two different values of the shell thickness t .

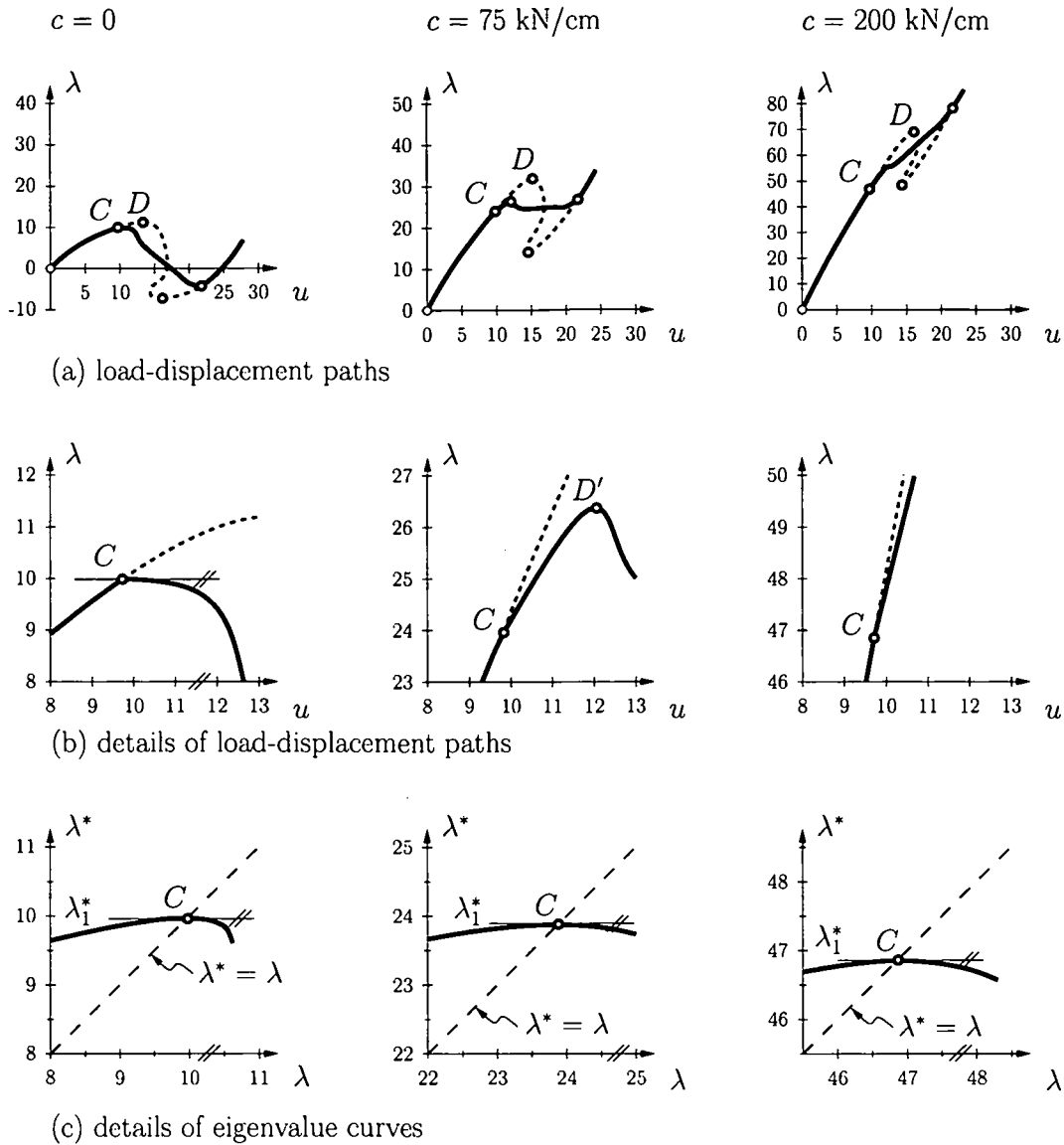


Fig. 13. (a) Load-displacement paths, (b) details of these paths and (c) of the corresponding eigenvalue curves in the vicinity of the stability limit C of a shallow cylindrical shell with $t \approx 6.35$ cm, for three different values of the spring stiffness

• $t \approx 6.35$ cm. This example refers to Fig. 4(e) in the companion paper [5]. Figs. 13(a) and 13(b) contain load-displacement paths and details of these paths in the vicinity of the stability limit, respectively, for three different values of the spring stiffness c . Fig. 13(c) shows details of the corresponding eigenvalue curves $\lambda_1^*(\lambda)$ at the stability limit C . For the shell without the spring ($c = 0$), the slope of the postbuckling path at the stability limit vanishes ($\lambda_2 = 0$). Moreover, $\lambda_4 = 0$ (see comments on Fig. 11(a)). Since λ_6 is negative, the structure is imperfection sensitive. Increasing the stiffness of the spring, leads to an increase of the slope of the postbuckling path at the stability limit. Hence, λ_2 becomes positive. However, λ_4 remains zero (see Eq. (105) in Part I of this work [5]), whereas λ_6 remains negative. This explains why the postbuckling path has a snap-through point, D' .

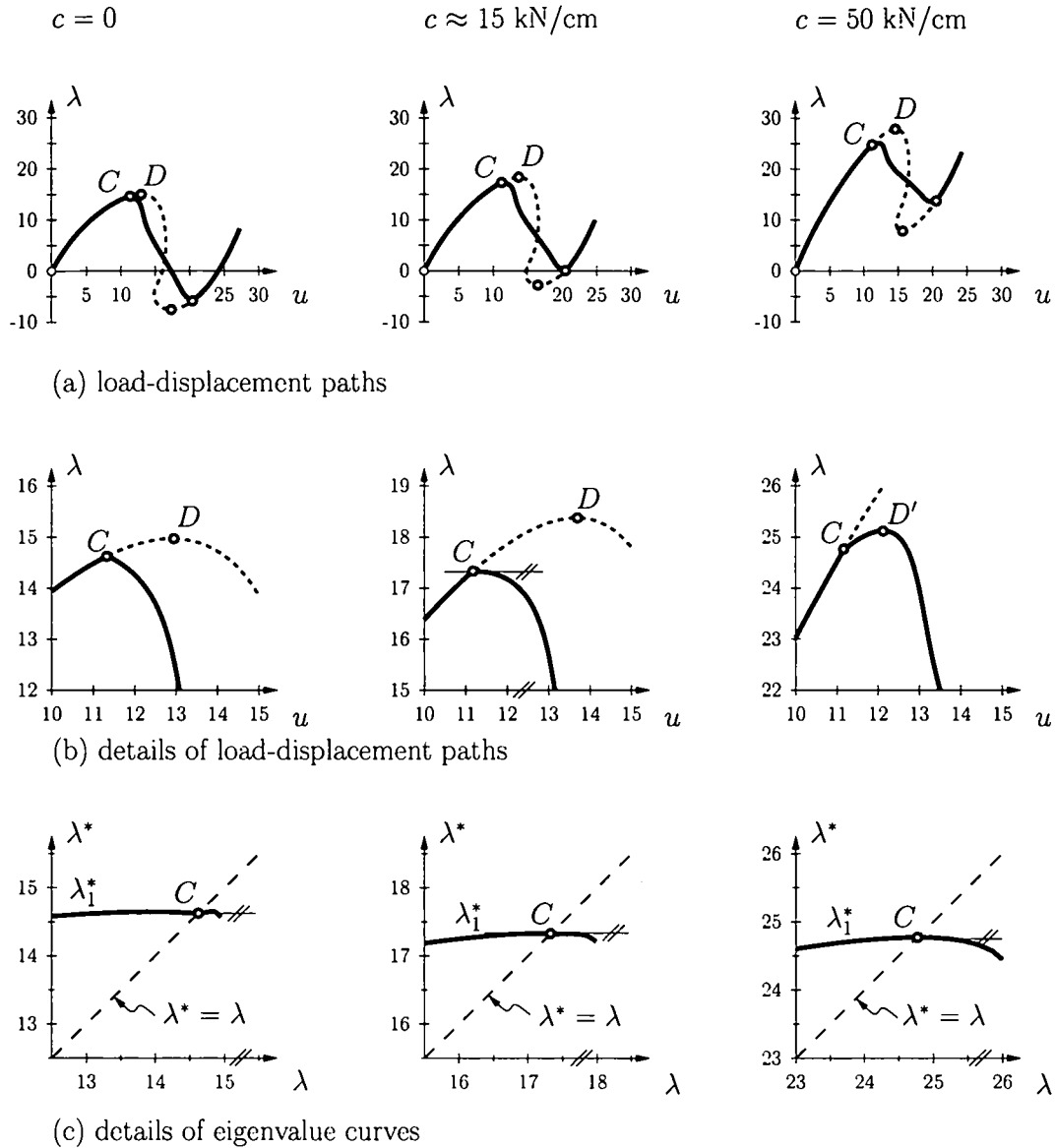


Fig. 14. (a) Load-displacement paths, (b) details of these paths and (c) of the corresponding eigenvalue curves in the vicinity of the stability limit C of a shallow cylindrical shell with $t = 7.35$ cm, for three different values of the spring stiffness c

This point disappears after a further increase of the spring stiffness.

• $t = 7.35 \text{ cm}$. This example refers to Fig. 4(d) in the companion paper [5]. Figs. 14(a) and 14(b) contain the load-displacement paths and details of these paths in the vicinity of the stability limit, respectively, for three different values of the spring stiffness c . Fig. 14(c) shows details of the corresponding eigenvalue curves $\lambda_1^*(\lambda)$ at the stability limit C . The slope of the postbuckling path at the stability limit is negative ($\lambda_2 < 0$). Hence, the unstiffened shell ($c = 0$) is imperfection sensitive. For $c \approx 15 \text{ kN/cm}$, the slope of the initial postbuckling path becomes zero ($\lambda_2 = 0$). Since $\lambda_4 < 0$, the shell is still imperfection sensitive. If c is further increased, the structure becomes imperfection insensitive ($\lambda_2 > 0$).

Hence, for a spring stiffness of $c \approx 15$ kN/cm a conversion from an imperfection-sensitive into an imperfection-insensitive structure occurs. Since λ_4 stays negative, the curvature of the postbuckling path at C remains negative. This is the reason for the existence of a snap-through point on the secondary path (point D'). A further increase of the spring stiffness eventually leads to a monotonous secondary path, similar to the previous example (see Fig. 13).

The curvature of the eigenvalue curve $\lambda_1^*(\lambda)$ has an extreme value at C , characterized by $\lambda_1^* = \lambda$, $\lambda_{1,\lambda}^* = 0$, and $\lambda_{1,\lambda\lambda}^* = 0 \xrightarrow{(D.34) \text{ in } [5]} a_1^* = 0$ (see Eq. (D.27) in Part I of this work [5]). It is positive for the unstiffened shell, zero for $c \approx 15$ kN/cm, and negative for larger values of c . Hence, for the point of transition, in addition to $a_1^* = 0$, $a_1 = 0$ (see Eqs. (D.28) and (D.34) in Part I of this work [5]), indicating that the eigenvalue curve $\lambda_1^*(\lambda)$ has a planar point at the stability limit.

2.3.3 Reduction of the initial rise of the shell

In the following, the influence of a change of the initial rise of the shell on the initial postbuckling behavior will be investigated. This will be done for two different pairs of values of the shell thickness t and the spring stiffness c .

- $t \approx 6.35$ cm, $c = 0$. This pair of values refers to point T in Fig. 4(c) in Part I of this work [5]. Because of $\lambda_2 = 0$, $\lambda_4 = 0$, and $\lambda_6 < 0$, the respective structure is imperfection sensitive. The thickness of the shell and the stiffness of the spring are kept constant, whereas the initial rise of the structure is reduced. This example refers to Fig. 4(g) in Part I of this work [5]. Figs. 15(a) and 15(b) contain load-displacement paths and details of these paths in the vicinity of the stability limit C , respectively, for three different values of the initial rise h of the shell. Fig. 15(c) shows details of the corresponding eigenvalue curves $\lambda_1^*(\lambda)$ in the vicinity of C . At first, the postbuckling behavior at C does not change when the initial rise of the shell is reduced. For $h \approx 4.0$ cm, however, the postbuckling path degenerates to a point on the primary path, which is a saddle point (see Eq. (121) in Part I of this work [5]). Hence, a transition to no loss of stability occurs.

For the shell with $h = 8$ cm and 6 cm, respectively, the eigenvalue curve $\lambda_1^*(\lambda)$ has a planar point at the stability limit (see Eqs. (D.76) in Part I of this work [5]). For the shell with $h \approx 4.0$ cm, the eigenvalue curve $\lambda_1^*(\lambda)$ has a saddle point of higher order at C (see Eqs. (D.77) in Part I of this work [5] and comments on Fig. 7(b)). Hence, a_1 and a_1^* are always zero (see Eqs. (D.21) and (D.28) together with (D.34) in Part I of this work [5]).

- $t = 7.35$ cm, $c \approx 15$ kN/cm. The shell with a thickness of $t = 7.35$ cm and a spring stiffness of $c \approx 15$ kN/cm refers to point T in Fig. 4(d) in Part I of this work [5]. The thickness of the shell and the stiffness of the spring are kept constant, whereas the initial rise of the shell is reduced. This example refers to Fig. 4(h) in Part I of this work [5]. Figs. 16(a) and 16(b) contain load-displacement paths and details of these paths in the vicinity of the stability limit C , respectively, for three different values of the initial rise h of the shell. Fig. 16(c) shows details of the corresponding eigenvalue curves $\lambda_1^*(\lambda)$ in the vicinity of C . Because of $\lambda_2 = 0$ and $\lambda_4 < 0$, the respective structure is originally imperfection sensitive. When the initial rise of the shell is reduced, the slope of the postbuckling path at C remains horizontal, whereas the curvature increases. For $h \approx 6.0$ cm, the postbuckling path degenerates to a

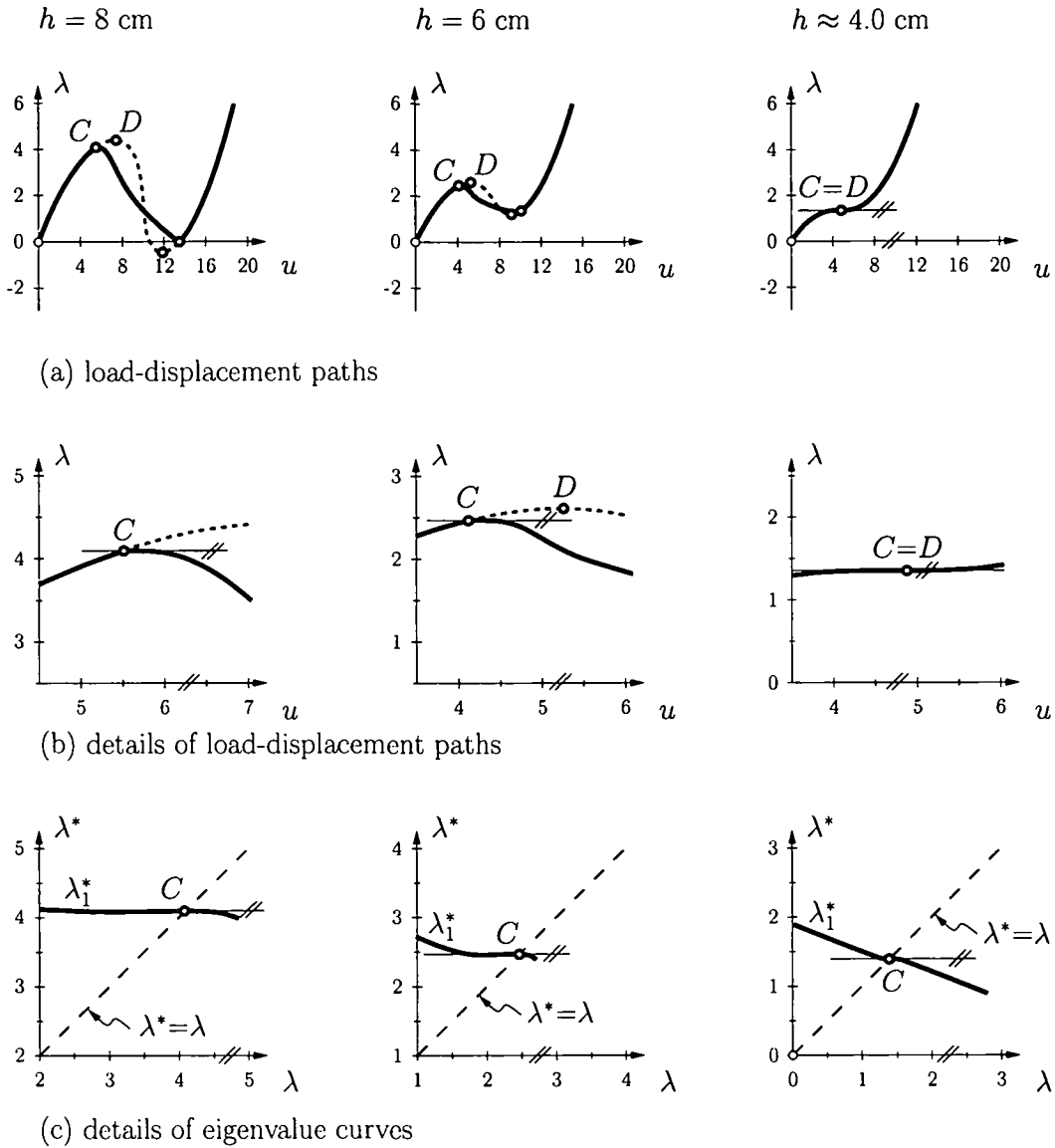


Fig. 15. (a) Load-displacement paths, (b) details of these paths and (c) of the corresponding eigenvalue curves in the vicinity of the stability limit C of a shallow cylindrical shell with $t = 6.35$ cm, for three different values of the initial rise h of the shell

point on the primary path, which is a saddle point (see Eqs. (121) in Part I of this work [5]). Hence, a transition to no loss of stability occurs.

For the shell with $h = 9$ cm and 7 cm, respectively, the eigenvalue curve $\lambda_1^*(\lambda)$ has a planar point at the stability limit (see Eqs. (D.76) in Part I of this work [5]). For the shell with $h \approx 6.0$ cm, the eigenvalue curve $\lambda_1^*(\lambda)$ has a saddle point of higher order at C (see Eqs. (D.77) in Part I of this work [5] and comments on Fig. 7(b)). Hence, a_1 and a_1^* are always zero (see Eqs. (D.21) and (D.28) together with (D.34) in Part I of this work [5]).

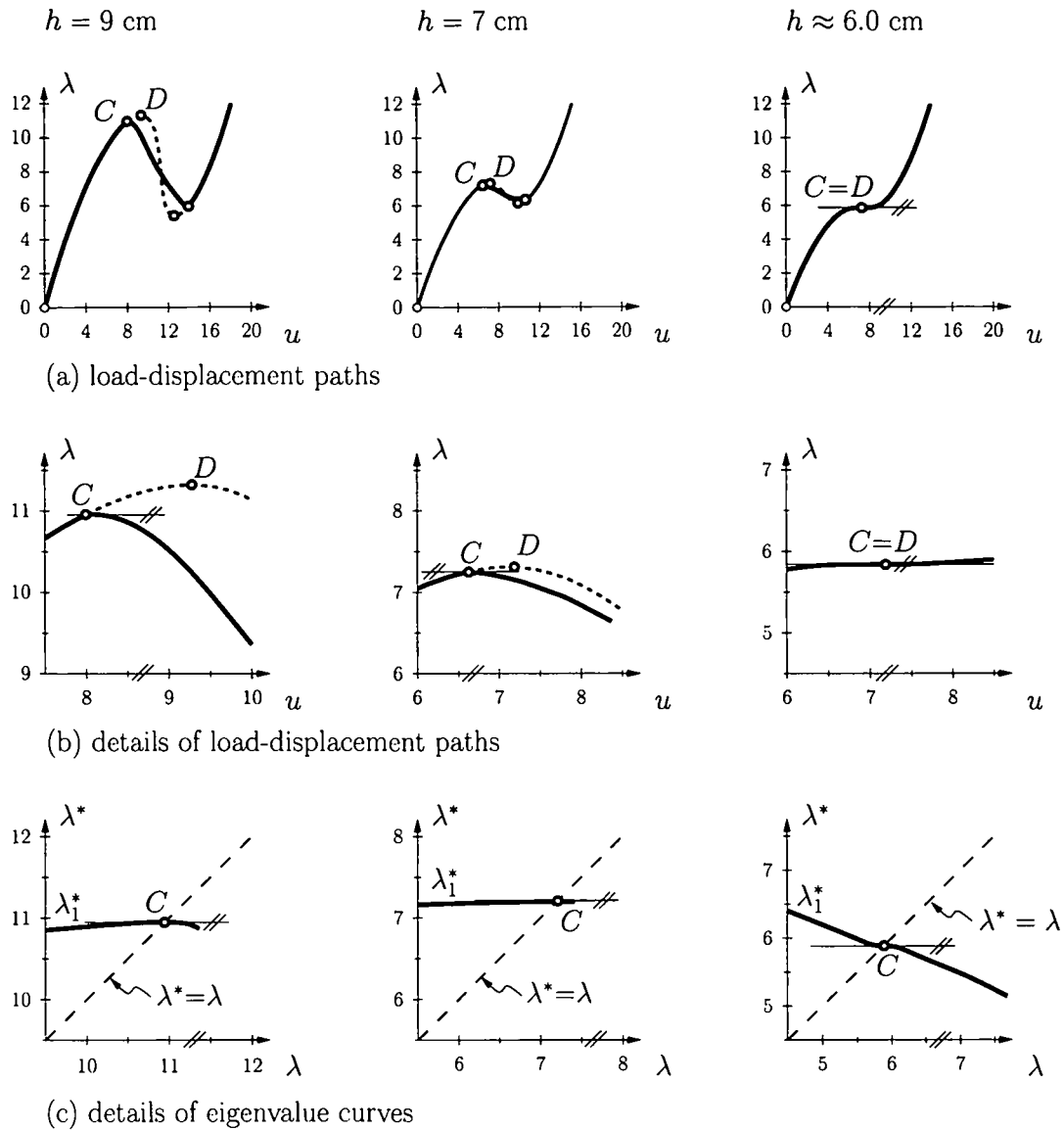


Fig. 16. (a) Load-displacement paths, (b) details of these paths and (c) of the corresponding eigenvalue curves in the vicinity of the stability limit C of a shallow cylindrical shell with $t = 7.35$ cm and $c \approx 15$ kN/cm, for three different values of the initial rise h of the shell

2.4 Example 4: Pin-jointed bar with linear prebuckling paths

For structures with linear prebuckling paths,

$$\tilde{\mathbf{K}}_{T,\lambda\lambda} = \mathbf{0} \Rightarrow a_1 = 0, \quad \tilde{\mathbf{K}}_{T,\lambda\lambda\lambda} = \mathbf{0} \Rightarrow a_1^* = 0, \quad \dots \quad (11)$$

(see Eqs. (129) of Part I of this work [5]). The eigenvalue curves degenerate to horizontal straight lines. In contrast to the situation for nonlinear prebuckling paths, no information can be extracted from $\lambda^*(\lambda) = \text{const}$.

Consider the plane pin-jointed bar in Fig. 17, composed of two rigid members of length l , one rigid member of length $k \cdot l$, one linear-elastic spring with the stiffness c_1 and one with

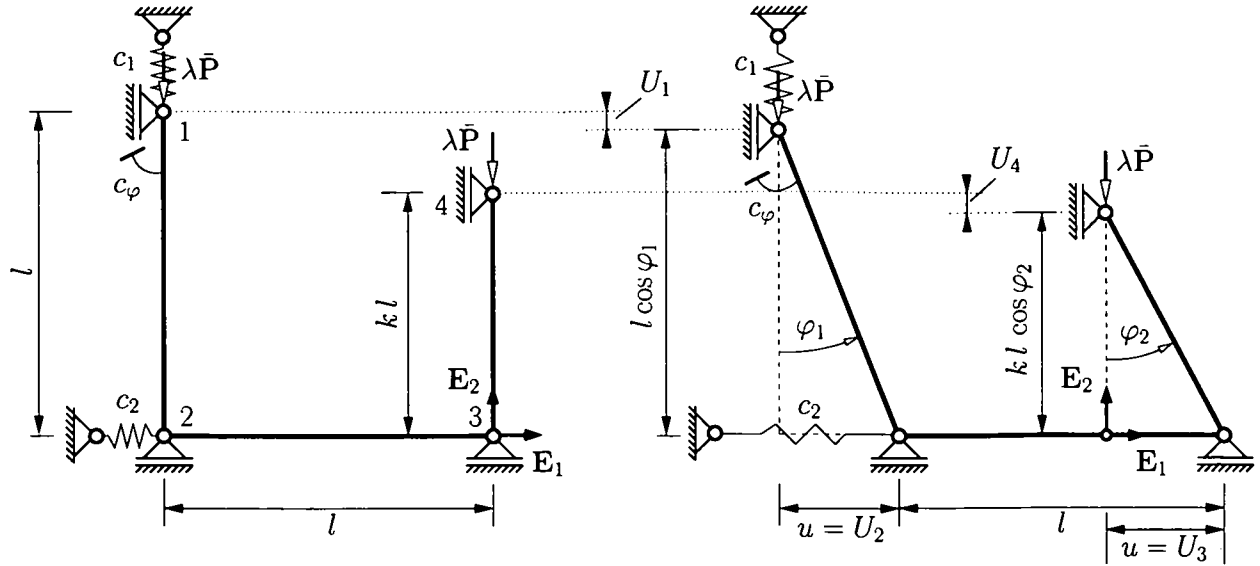


Fig. 17. Geometric properties of a pin-jointed bar with three rigid rods

the stiffness c_2 , and one linear-elastic rotational spring with the stiffness c_φ . The structure is loaded by two vertical nodal forces $\lambda \bar{\mathbf{P}}$ at joints 1 and 4; $\bar{\mathbf{P}} = -\mathbf{E}_2$ is the reference force and λ is a dimensionless load factor. The angles φ_1 and φ_2 of the deformed system are expressed in terms of the horizontal displacements of joints 2 and 3, u :

$$\varphi_1 = \arcsin\left(\frac{u}{l}\right) \quad \text{and} \quad \varphi_2 = \arcsin\left(\frac{u}{kl}\right). \quad (12)$$

The displacements of the three joints 1, 2, and 4 can also be expressed in terms of u :

$$\begin{aligned} \mathbf{U}_1 &= (l - l \cos \varphi_1) (-\mathbf{E}_2) = l \left\{ 1 - \cos \left[\arcsin \left(\frac{u}{l} \right) \right] \right\} (-\mathbf{E}_2) = U_1 (-\mathbf{E}_2), \\ \mathbf{U}_2 &= u \mathbf{E}_1 = U_2 \mathbf{E}_1, \\ \mathbf{U}_4 &= (l - l \cos \varphi_2) (-\mathbf{E}_2) = l \left\{ 1 - \cos \left[\arcsin \left(\frac{u}{kl} \right) \right] \right\} (-\mathbf{E}_2) = U_4 (-\mathbf{E}_2), \end{aligned} \quad (13)$$

where use of (12) was made. The total potential energy of the structure is obtained as

$$\Pi = \Pi(u, \lambda) = U(u, \lambda) + W(u, \lambda), \quad (14)$$

where

$$U(u, \lambda) = \frac{1}{2} c_1 \mathbf{U}_1^T \cdot \mathbf{U}_1 + \frac{1}{2} c_2 \mathbf{U}_2^T \cdot \mathbf{U}_2 + \frac{1}{2} c_\varphi \varphi_1^2 \quad (15)$$

is the strain energy and

$$W(u, \lambda) = -\lambda (\bar{\mathbf{P}}^T \cdot \mathbf{U}_1 + \bar{\mathbf{P}}^T \cdot \mathbf{U}_4) = -\lambda (-\mathbf{E}_2)^T \cdot (\mathbf{U}_1 + \mathbf{U}_4) = -\lambda (U_1 + U_4) \quad (16)$$

is the potential of the external loads. With the notation of Eq. (1) in Part I of this work [5], the equilibrium equation of the considered discrete mechanical system is given as

$$G(u, \lambda) = \frac{\partial \Pi}{\partial u} = 0. \quad (17)$$

From (17), the function $\lambda(u)$ describing the load-displacement behavior is obtained as

$$\lambda(u) = \frac{\frac{c_\varphi}{l} \frac{\arcsin\left(\frac{u}{l}\right)}{\left(\frac{u}{l}\right)} + c_1 l \left[1 - \sqrt{1 - \left(\frac{u}{l}\right)^2}\right] + c_2 l \sqrt{1 - \left(\frac{u}{l}\right)^2}}{1 + \frac{1}{k} \frac{\sqrt{1 - \left(\frac{u}{l}\right)^2}}{\sqrt{1 - \frac{1}{k^2} \left(\frac{u}{l}\right)^2}}}. \quad (18)$$

Setting $u = 0$ in (18), yields the stability limit as

$$\lambda_C = \lambda_{bif} = \frac{1}{l} (c_\varphi + c_2 l^2) \frac{k}{1+k}. \quad (19)$$

The function $\lambda(u)$ can be expanded as a series (see Eq. (6) in Part I of this work [5]):

$$\lambda(u) = \lambda_C + \lambda_2 u^2 + \lambda_4 u^4 + \lambda_6 u^6 + \dots, \quad (20)$$

where the first three nonvanishing load coefficients are obtained as

$$\lambda_2 = \frac{1}{6k(1+k)l^3} \left[(-3 + 3k + k^2) c_\varphi - 3l^2 (1 - k + k^2) c_2 + 3k^2 l^2 c_1 \right], \quad (21)$$

$$\lambda_4 = \frac{1}{120k^3(1+k)l^5} \left[(-15 - 15k + 5k^2 + 25k^3 + 9k^4) c_\varphi - 15l^2 (1 + k - 3k^2 + k^3 + k^4) c_2 + 15k^2 l^2 (-2 + 2k + k^2) c_1 \right], \quad (22)$$

$$\lambda_6 = \frac{1}{1680k^5(1+k)l^7} \left[(-105 - 105k - 35k^2 - 35k^3 + 77k^4 + 203k^5 + 75k^6) c_\varphi - 105l^2 (1 + k - k^2 - k^3 - k^4 + k^5 + k^6) c_2 + 105k^2 l^2 (1 + k - 2k^3 - k^4) c_1 \right]. \quad (23)$$

The load parameters λ_2 , λ_4 , and λ_6 depend on the stiffnesses of the two extensional springs, c_2 and c_1 , the stiffness of the rotational spring, c_φ , and on the ratio of the length of the right and the left column, k .

In the following, these parameters will be varied. For all examples, $l = 2$ m. Fig. 18 contains λ_2 - λ_4 curves, where $T = T(\lambda_2 = 0, \lambda_4)$ and $Q = Q(\lambda_2, \lambda_4 = 0)$. S denotes an arbitrary starting point and F an arbitrary final point (see Fig. 4 in Part I of this work [5]).

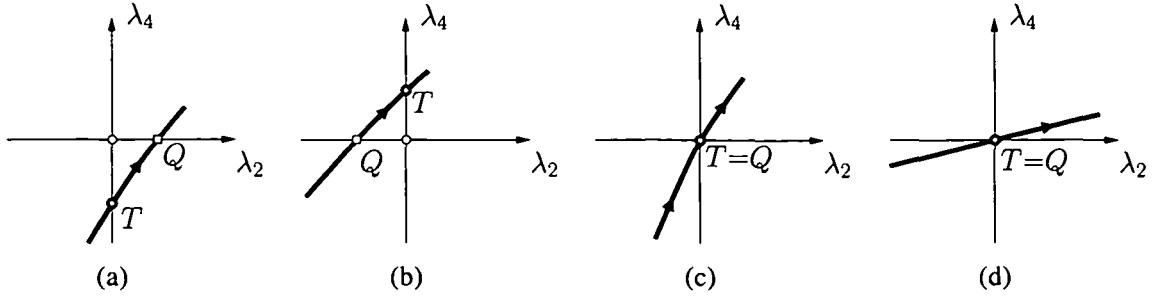


Fig. 18. Plots of curves $\lambda_2 = \lambda_2(\kappa)$, $\lambda_4 = \lambda_4(\kappa)$, with one point $T(\lambda_2 = 0, \lambda_4)$ and one point $Q(\lambda_2, \lambda_4 = 0)$ each

• $c_\varphi = 5 \text{ kNm/rad}$, $c_1 = c_2 = 0$. The factor k is chosen as the design parameter, i.e. $\kappa = k$. Table 3 contains the values of λ_2 and λ_4 for five different values of k . The respective λ_2 - λ_4 diagram is shown in Fig. 18(a).

Table 3

Results (λ_2, λ_4) for $c_\varphi = 5 \text{ kNm/rad}$ and $c_1 = c_2 = 0$, for five different values of $\kappa = k$

point		T		Q	
$\kappa = k$	0.700	0.791	0.850	0.904	1.000
λ_2	-0.144	0.000	0.072	0.128	0.208
λ_4	-0.440	-0.184	-0.075	0.000	0.094

With increasing value of k , the length of the right column of the pin-jointed bar in Fig. 17 is increasing. The conversion from an imperfection-sensitive into an imperfection-insensitive structure (point T) occurs before the transition from $\lambda_4 < 0$ to $\lambda_4 > 0$ (point Q).

• $c_\varphi = 10 \text{ kNm/rad}$, $c_1 = 0$, $c_2 = 1 \text{ kN/m}$. Again, the factor k is chosen as the design parameter, i.e. $\kappa = k$. Table 4 contains the values of λ_2 and λ_4 for five different values of k . The respective λ_2 - λ_4 diagram is shown in Fig. 18(b).

Table 4

Results (λ_2, λ_4) for $c_\varphi = 10 \text{ kNm/rad}$, $c_1 = 0$, and $c_2 = 1 \text{ kN/m}$, for five different values of $\kappa = k$

point		Q		T	
$\kappa = k$	0.900	0.967	1.000	1.053	1.100
λ_2	-0.284	-0.143	-0.083	0.000	0.064
λ_4	-0.164	0.000	0.063	0.143	0.199

For this example, the transition from $\lambda_4 < 0$ to $\lambda_4 > 0$ (point Q) occurs before the conversion from an imperfection-sensitive into an imperfection-insensitive structure (point T).

In the following, the parameters will be modified such that the conversion from imperfection sensitivity into imperfection insensitivity occurs simultaneously with the transition

from $\lambda_4 < 0$ to $\lambda_4 > 0$, and, hence, results in $T=Q$. If $\lambda_2 = 0$ and $\lambda_4 = 0$, the sign of λ_6 indicates whether the structure is imperfection sensitive or not. Therefore, also the value of λ_6 will be listed.

- $c_\varphi = 10 \text{ kNm/rad}$, $c_1 = 0.366636 \text{ kN/m}$, $c_2 = 1 \text{ kN/m}$. Again, the factor k is chosen as the design parameter, i.e. $\kappa = k$. The values of c_φ and c_2 are the same as in the preceding example. The value of c_1 is chosen such that $\lambda_2 = \lambda_4 = 0$. Table 5 contains the values of λ_2 and λ_4 for three different values of k . The respective λ_2 - λ_4 diagram is shown in Fig. 18(c).

Table 5

Results (λ_2, λ_4) for $c_\varphi = 10 \text{ kNm/rad}$, $c_1 = 0.366636 \text{ kN/m}$, and $c_2 = 1 \text{ kN/m}$, for three different values of $\kappa = k$

point		$T=Q$	
$\kappa = k$	0.930	0.948589	0.960
λ_2	-0.040	0.000	0.024
λ_4	-0.046	0.000	0.026
λ_6	-0.097	-0.044	-0.015

At point $T=Q$, $\lambda_6 < 0$. Hence, the structure is still imperfection sensitive.

- $c_\varphi = 0$, $c_2 = 1 \text{ kN/m}$, $k = 1$. Instead of k , the stiffness of the vertical spring, c_1 , is now chosen as the design parameter, i.e. $\kappa = c_1$. The resulting λ_2 - λ_4 diagram is shown in Fig. 18(d). In this case, the parameters $\lambda_2, \lambda_4, \lambda_6, \dots$ are obtained as

$$\lambda_2 = \frac{c_1 - 1}{4l}, \quad \lambda_4 = \frac{c_1 - 1}{16l^3}, \quad \lambda_6 = \frac{c_1 - 1}{32l^5}, \quad \dots \quad (24)$$

Specializing the system for $c_1 = c_2 = 1 \text{ kN/m}$, yields a horizontal postbuckling path:

$$\lambda_2 = 0, \quad \lambda_4 = 0, \quad \lambda_6 = 0, \quad \dots \quad (25)$$

Following from (25.1) and (25.2), $T=Q$. Tarnai [9] has studied a structure with such a postbuckling behavior in the framework of an investigation of “zero stiffness structures”.

3 Conclusions

Three structures with nonlinear and one with linear prebuckling paths were chosen to verify the theoretical findings presented in Part I of this work [5].

Nonlinear prebuckling paths. Depending on the kind of modification of the original structure, for symmetric bifurcation a conversion of the original structure from imperfection sensitivity into insensitivity is possible.

- Increasing the stiffness of the structure by means of a uniform increase of its thickness does not result in the desired conversion from imperfection sensitivity into imperfection

insensitivity. Expectedly, such an increase yields an increase of the stability limit. The limiting case $\lambda_2 = 0$, $\lambda_4 = 0$, $\lambda_6 < 0$ is associated with a change of the sign of λ_4 but not with one of λ_2 . Hence, $\lambda_{2,\kappa} = 0$ and $\lambda_{2,\kappa\kappa} \neq 0$ (see Table 1 in Part I of this work [5]).

- Increasing the stiffness of an elastic spring, suitably attached to the structure, enables its conversion from an imperfection-sensitive into an imperfection-insensitive structure. Two different modes of transition from imperfection sensitivity to imperfection insensitivity were found to exist: (a) $\lambda_2 = 0$, $\lambda_4 < 0$, and (b) $\lambda_2 = 0$, $\lambda_4 = 0$, $\lambda_6 = 0$,

Re (a): If the spring stiffness is further increased, $\lambda_2 > 0$, $\lambda_4 < 0$. This situation is characterized by a snap-through point on the postbuckling path.

Re (b): This mode is characterized by horizontal postbuckling paths.

- Reducing the initial rise of an imperfection-sensitive structure eventually results in the transition from bifurcation buckling to no loss of stability. This transition is characterized by the degeneration of the secondary paths to one point each, which coincides with a saddle point on the respective primary path. The reduction of the initial rise of the structure is associated with a decrease of the stability limit. Hence, from a practical viewpoint, the aforementioned transition from bifurcation buckling to no loss of stability is counterproductive.

Linear prebuckling paths. Irrespective of whether the prebuckling paths are nonlinear or linear, the condition for $\lambda_2 = 0$, for the case of symmetric bifurcation, is $d_1 = 0$ (see Part I of this work [5]). For nonlinear prebuckling paths, additional conditions were shown to exist (see Part I of this work [5]). They involve the matrices $\tilde{\mathbf{K}}_{T,\lambda\lambda}$ and $\tilde{\mathbf{K}}_{T,\lambda\lambda\lambda}$, which vanish trivially for the special case of linear prebuckling paths. Hence, for this special case the aforementioned additional conditions do not exist. Consequently, the restrictions on the modes of conversion from imperfection-sensitive into imperfection-insensitive structures (see the projections of the curves $\lambda_2 = \lambda_2(\kappa)$, $\lambda_4 = \lambda_4(\kappa)$, $a_1 = a_1(\kappa)$ onto the λ_2 - λ_4 plane in Fig. 4 in Part I of this work [5]) do not exist. This could explain why Figs. 18(a) and 18(b) seem to have no counterpart in the general case of symmetric bifurcation from nonlinear prebuckling paths.

Acknowledgement

The first author thankfully acknowledges partial financial support by the Austrian Science Fund under the contract P14808.

References

- [1] B. Bochenek and J. Kruzelecki. A new concept of optimization for postbuckling behaviour. *Engineering Optimization*, 33:503–522, 2001.
- [2] F. Fujii. Multiple hill-top branching. In L. G. Wang, C.M. and K. Ang, editors, *Proceedings of the 2nd International Conference on Structural Stability and Dynamics*. Singapore, December 16–18, 2002, World Scientific, 2002.

- [3] P. Helnwein. Zur initialen Abschätzbarkeit von Stabilitätsgrenzen auf nichtlinearen Last-Verschiebungspfaden elastischer Strukturen mittels der Methode der Finiten Elemente [On ab initio estimates of stability limits on nonlinear load-displacement paths of elastic structures using the finite element method], volume 79 of Dissertationen an der Technischen Universität Wien. Österreichischer Kunst- und Kulturverlag, Wien, 1997. In German.
- [4] W. Koiter. On the stability of elastic equilibrium. translation of ‘Over de Stabiteit van het Elastisch Evenwicht’ (1945). In NASA TT F-10833. Polytechnic Institute Delft, H.J. Paris Publisher, Amsterdam, 1967.
- [5] H. Mang, C. Schranz, and P. Mackenzie-Helnwein. Conversion of imperfection sensitive to -insensitive elastic structures I: Theory. Accepted for publication to Computer Methods in Applied Mechanics and Engineering.
- [6] R. Reitinger. Stabilität und Optimierung imperfektionsempfindlicher Tragwerke [Stability and optimization of imperfection-sensitive structures]. Dr.-Ing. dissertation, Universität Stuttgart, Institut für Baustatik, 1994. Bericht Nr. 17. In German.
- [7] J.C. Simo, D.D. Fox, and M.S. Rifai. On a stress resultant geometrically exact shell model. Part II: The linear theory; computational aspects. structures. Computer Methods in Applied Mechanics and Engineering, 73:53–92, 1990.
- [8] J.C. Simo, D.D. Fox, and M.S. Rifai. On a stress resultant geometrically exact shell model. Part III: Computational aspects of the nonlinear theory. structures. Computer Methods in Applied Mechanics and Engineering, 79:1–62, 1990.
- [9] T. Tarnai. Zero stiffness elastic structures. International Journal of Mechanical Sciences, 45:425–431, 2003.
- [10] O. Zienkiewicz and R. Taylor. The Finite Element Method, volume 1. McGraw-Hill, London, England, 4. edition, 1994.

List of Tables

1	Geometric properties (dimensionless), spring stiffnesses (dimensionless), and results $(\lambda_2, \lambda_4, a_1)$ from initial postbuckling analysis	50
2	Geometric properties (dimensionless), spring stiffnesses (dimensionless), and results $(\lambda_2, \lambda_4, a_1)$ from initial postbuckling analysis	51
3	Results (λ_2, λ_4) for $c_\varphi = 5 \text{ kNm/rad}$ and $c_1 = c_2 = 0$, for five different values of $\kappa = k$	67
4	Results (λ_2, λ_4) for $c_\varphi = 10 \text{ kNm/rad}$, $c_1 = 0$, and $c_2 = 1 \text{ kN/m}$, for five different values of $\kappa = k$	67
5	Results (λ_2, λ_4) for $c_\varphi = 10 \text{ kNm/rad}$, $c_1 = 0.366636 \text{ kN/m}$, and $c_2 = 1 \text{ kN/m}$, for three different values of $\kappa = k$	68

List of Figures

1	Geometric properties of a pin-jointed bar with two rigid rods	48
2	(a) Load-displacement paths and (b) corresponding eigenvalue curves of a pin-jointed bar for three different values of the spring stiffness c_1	51
3	(a) Load-displacement paths and (b) corresponding eigenvalue curves of a pin-jointed bar for four different values of the angle ϕ_0	52
4	Geometric properties of a <i>von Mises</i> truss with an attached spring	53
5	(a) Load-displacement paths and (b) corresponding eigenvalue curves of a <i>von Mises</i> truss without a spring	53
6	(a) Load-displacement paths and (b) corresponding eigenvalue curves of a <i>von Mises</i> truss for three different values of the spring stiffness c	54
7	(a) Load-displacement paths and (b) corresponding eigenvalue curves of a <i>von Mises</i> truss with $c \approx 40.8 \text{ kN/cm}$ for four different values of the initial rise h of the truss	55
8	(a) Load-displacement paths and (b) corresponding eigenvalue curves of a <i>von Mises</i> truss with $c = 60 \text{ kN/cm}$, for three different values of the initial rise h of the truss	56
9	Geometric properties of a shallow cylindrical shell with an attached spring	57
10	(a) Load-displacement paths and (b) eigenvalue curves of a shallow cylindrical shell without a spring	57
11	(a) Load-displacement paths, (b) details of these paths and (c) of the corresponding eigenvalue curves in the vicinity of the stability limit C of a shallow cylindrical shell for three different values of the shell thickness	58
12	(a) Load-displacement paths and (b) corresponding eigenvalue curves of a shallow cylindrical shell for two different values of the shell thickness	59
13	(a) Load-displacement paths, (b) details of these paths and (c) of the corresponding eigenvalue curves in the vicinity of the stability limit C of a shallow cylindrical shell with $t \approx 6.35 \text{ cm}$, for three different values of the spring stiffness	60

14	(a) Load-displacement paths, (b) details of these paths and (c) of the corresponding eigenvalue curves in the vicinity of the stability limit C of a shallow cylindrical shell with $t = 7.35$ cm, for three different values of the spring stiffness c	61
15	(a) Load-displacement paths, (b) details of these paths and (c) of the corresponding eigenvalue curves in the vicinity of the stability limit C of a shallow cylindrical shell with $t = 6.35$ cm, for three different values of the initial rise h of the shell	63
16	(a) Load-displacement paths, (b) details of these paths and (c) of the corresponding eigenvalue curves in the vicinity of the stability limit C of a shallow cylindrical shell with $t = 7.35$ cm and $c \approx 15$ kN/cm, for three different values of the initial rise h of the shell	64
17	Geometric properties of a pin-jointed bar with three rigid rods	65
18	Plots of curves $\lambda_2 = \lambda_2(\kappa)$, $\lambda_4 = \lambda_4(\kappa)$, with one point $T(\lambda_2 = 0, \lambda_4)$ and one point $Q(\lambda_2, \lambda_4 = 0)$ each	67

Curriculum Vitae

Dipl.-Ing. Christian Schranz, M.Sc.

Personal Details

Date of Birth: 26.12.1973
Place of Birth: Linz, Austria
Nationality: Austria
Postal Address: Dempschergasse 9, 1180 Wien, Austria
E-mail address: Christian.Schranz@tuwien.ac.at

Education and Qualifications

9/1988–6/1993 Technical High school (civil engineering)
Final exam with distinction

10/1993–11/1999 Diploma studies of Civil Engineering
at Vienna University of Technology
Graduation with distinction

10/1997–05/1999 Post graduate studies of Civil Engineering
at University of Illinois at Urbana-Champaign, USA
Graduation with distinction

01/2000–02/2005 Doctoral studies,
Institute for Mechanics of Materials and Structures
at Vienna University of Technology

01/2000–01/2005 Research Assistant,
Institute for Mechanics of Materials and Structures
at Vienna University of Technology

01/2005–present University Assistant,
Institute for Building Construction and Rehabilitation
at Vienna University of Technology